Developing coherent optical wavelength conversion systems for reconfigurable photonic networks

Yi Lin

B. Sc., M.Eng.

A Thesis Submitted in Fulfilment of the Requirements for the

Award of

Doctor of Philosophy (PhD)

to the

Dublin City University

Faculty of Engineering and Computing

School of Electronic Engineering

Supervisor: Prof. Liam P. Barry

January 2020

Declaration

I hereby certify that this material, which I now submit for assessment on the programme of study leading to the award of Doctor of Philosophy is entirely my own work, and that I have exercised reasonable care to ensure that the work is original, and does not to the best of my knowledge breach any law of copyright, and has not been taken from the work of others save and to the extent that such work has been cited and acknowledged within the text of my work.

Signed: _____ (Yi Lin)
ID No.: _____

Date: _____

Acknowledgements

Firstly, I would like to thank my supervisor Prof. Liam P. Barry for his continuous support of my PhD study at Dublin City University, for his patience, motivation, and immense knowledge. His guidance helped me in all the time of research and writing of this thesis. I could not have imagined having a better advisor for my PhD study.

Apart from my supervisor, I would like to express the gratitude to Prof. Yonglin Yu, from Wuhan National Lab for Optoelectronics (WNLO) in China, for supervising me during my master's study in China, for her continuous encouragement and suggestions during my PhD study.

I am also pleased to say thank you to Dr. Aravind P. Anthur, Dr. Seán Ó Dúill, Dr. Elias Giacoumidis and Dr. Colm Browning, who made my access simpler to the laboratory and research facilities. It wouldn't have been possible to conduct my research without their precious support.

I would like to thank Science Foundation Ireland for funding my research. I would like to thank Dublin City University for providing me with a world-class environment to conduct my research.

I would always remember all the past and present colleagues of the Radio and Optical Communication Lab, for the stimulating discussions, the sleepless nights we were working together before deadlines, and for all the fun time we spent together.

Finally, but by no means least, I am grateful to my parents and friends for their unbelievable support. I consider myself nothing without them. They are the most important people in my world and I dedicate this thesis to them.

Contents

List of figures

Acronyms

ASE	Amplified Spontaneous Emission
ASK	Amplitude Shift Keying
AWG	Array Waveguide Grating or Arbitrary Waveform Generator
BER	Bit Error Rate
CMA	Constant Modulus Algorithm
CPR	Carrier Phase Recovery
CD	Chromatic Dispersion
CE	Conversion Efficiency
Coh.Rx	Coherent Receiver
DBP	Digital Backpropagation
DBR	Distributed Bragg Reflector
DBSCAN	Density Based Spatial Clustering of Applications with Noise
DD-PLL	Decision-Directed Phase Locked Loop
DFB	Distributed Feedback
DS-DBR	Digital Super-mode Distributed Bragg Grating
DSH	Delayed Self Heterodyne
DSP	Digital Signal Processing
DWDM	Dense Wavelength Division Multiplexing
ECLs	External Cavity Lasers
EDFAs	Erbium Doped Fiber Amplifiers
ESA	Electrical Spectrum Analyzer
FEC	Forward Error Correction
FSK	Frequency Shift Keying
FSR	Free Spectral Range
FWM	Four Wave Mixing
GCSR	Grating assisted Co-directional coupler with Sampled Reflector
HR	High Reflective
I	In-phase

IM/DD	Intensity Modulation with Direct Detection
IP	Internet Protocol
ISO	Isolator,
LO	Local Oscillator
MGY	Modulated Grating Y-branch
MLL	Mode-locked Laser
MMA	Multi Modulus Algorithm
MPN	Mode Partition Noise
M-QAM	Multilevel Quadrature Amplitude Modulation
MRR	Micro Ring Resonators
MZI	Mach Zehnder Interferometer
NLC	Nonlinearity Compensation
OBPF	Optical Band Pass Filter
OBS	Optical Burst Switching
OEO	Optical-to-Electrical-to-Optical
OOK	On–Off Keying
OPS	Optical Packet Switching
OSA	Optical Spectrum Analyzer
OSNR	Optical Signal to Noise Ratio
OXCs	Optical Cross-Connects
PBS	Polarization Beam Splitter
PC	Polarization Controller
PDM	Polarization Division Multiplexed
PICs	Photonic Integrated Circuits
PM	Polarization Multiplexer or Polarization Maintaining
PMD	Polarisation Mode Dispersion
PolarSK	Polarization Shift Keying
PRBS	Pseudo Random Bit Sequences
PSK	Phase Shift Keying

Q	Quadrature-phase
QAM	Quadrature Amplitude Modulation
QD-PMLL	Quantum Dash Passively Mode Locked Laser
QPSK	Quadrature Phase Shift Keying
RBW	Resolution Bandwidth
RIN	Relative Intensity Noise
ROADMs	Reconfigurable Optical Add Drop Multiplexers
RoF	Radio Over Fiber
SE	Spectral Efficienecy
SGDBR	Sampled Grating Distributed Bragg Reflector
SMSR	Side Mode Suppression Ratio
SOA	Semiconductor Optical Amplifier
SSB-SC	Single Side Band Suppressed Carrier
SSG-DBR	Super Structure Grating Distributed Bragg Reflector
TEC	Thermoelectric Cooler
TIAs	Transimpedance Amplifiers
TMM	Transfer Matrix Method
TOF	Tunable Optical Filter
TRBER	Time Resolved Bit Error Rate
VOA	Variable Optical Attenuator
WC	Wavelength Conversion
WDM	Wavelength Division Multiplexing
XGM	Cross Gain Modulation
XPM	Cross Phase Modulation

Abstract

In future optical networks that employ wavelength division multiplexing (WDM), the use of optical switching technologies on a burst or packet level, combined with advanced modulation formats would achieve greater spectral efficiency and utilize the existing bandwidth more efficiently. All-optical wavelength converters are expected to be one of the key components in these broadband networks. They can be used at the network nodes to avoid contention and to dynamically allocate wavelengths to ensure optimum use of fiber bandwidth.

In this work, a reconfigurable wavelength converter comprising of a Semiconductor Optical Amplifier (SOA) as the nonlinear element and a fast-switching sampled grating distributed Bragg reflector (SG-DBR) tunable laser as one of the pumps is developed. The wavelength conversion of 12.5-Gbaud quadrature phase shift keying (QPSK) and Pol-Mul QPSK signals with switching time of tens of nanoseconds is experimentally achieved. Although the tunable DBR lasers can achieve ns tuning time, they present relatively large phase noise. The phase noise transfer from the pump to the converted signal can have a deleterious effect on signal quality and cause a performance penalty with phase modulated signals. To overcome the phase noise transfer issue, a wavelength converter using tunable dual-correlated pumps provided by the combination of a single-section quantum dash passively mode-locked laser (QD-PMLL) and a programmable tunable optical filter is designed and the wavelength conversion of QPSK and 16-quadrature amplitude modulation (16-QAM) signals at 12.5 GBaud is experimentally investigated. Nonlinear distortion of the wavelength converted signal caused by gain saturation effects in the SOA can significantly degrade the signal quality and cause difficulties for the practical wavelength conversion of signal data with advanced modulation formats. In this work, the machine learning clustering based nonlinearity compensation method is proposed to improve the tolerance to nonlinear distortion in an SOA-based wavelength conversion system with 16-QAM and 64-QAM signals.

Introduction

The desire for multi-media content and richly interactive data services is shaping a new era for telecommunications networks. Future networks will need to be capable of offering Triple Play, IPTV, Video-on-Demand, Voice-over-IP and High-Speed Internet Access, combined with guaranteed Quality of Service. These networks will employ wavelength division multiplexing (WDM) technology, and advanced modulation formats, in order to achieve the high capacities required [1]. In addition, given the bursty nature of this data it is expected that dynamic allocation of the bandwidth will be implemented to efficiently use the available capacity. The key components in these networks will be the tunable laser transmitters that generate the different wavelength packets, and also all-optical wavelength convertors (comprising tunable lasers) that allow optical information packets on a certain wavelength to be converted to a different wavelength. A semiconductor optical amplifier (SOA) with high non-linearity and short carrier lifetime has the potential to achieve all-optical wavelength conversion.

The clear trend in order to increase the bit rate in modern optical communication systems that use WDM is the use of advanced modulation formats that exploit a mix of intensity and phase modulation, such as quadrature phase shift keying (QPSK) and 16-quadrature amplitude modulation (16-QAM). In addition, there is also a drive to develop WDM networks that can reconfigure quickly to make the most efficient use of the available capacity of WDM channels. These optically switched networks require wavelength conversion devices at the network nodes to resolve contention for access to a given channel at a node. These contentions occur in packet/burst switched WDM networks whenever two or more packets are trying to leave the switch from the same output port on the same wavelength channel [2]. One approach to perform all-optical wavelength conversion (WC) is to employ the four-wave mixing (FWM) process within semiconductor optical amplifiers or other nonlinear media [3-4]. Using this approach the data signal and a pump signal (or signals) at a different wavelength are injected into the SOA. Through the FWM process a replica of the data signal at a different wavelength is generated and can be filtered out after the SOA. The wavelength of the

converted signal can be altered by tuning the wavelength of the pump lasers.

This work will investigate the use of SOA-based wavelength converters using tunable laser pump sources, for use in practical reconfigurable optical networks. The thesis will investigate how the tunable lasers can be controlled precisely and quickly to ensure that the incoming data packets can be converted to the required wavelength channel at the right time, and without degradation in signal performance. The main aim of this work is be to demonstrate the successful all-optical wavelength conversion of data, employing QPSK or 16-QAM modulation formats, using four-wave mixing in SOAs.

The main contributions of this work can be summarized as follows:

- First implementation of fast reconfigurable WC system for advanced modulation formats using a sampled-grating distributed Bragg reflector (SGDBR) laser as the pump. The wavelength conversion of QPSK and Pol-Mul-QPSK signals at 12.5-Gbaud are experimentally investigated. Reconfiguration times below 50 ns and 160 ns are achieved for the reconfigurable wavelength conversion system for 12.5 Gbaud QPSK and PM-QPSK signals, respectively.
- Demonstration of all-optical SOA-based WC system using lines from a single-section quantum dash passively mode-locked laser and detailed investigation of how the correlation between comb lines effects WC performance. The tunable pumps are generated by the combination of the mode locked laser and a tunable optical filter. Wavelength conversion of 12.5 Gbaud QPSK and 16-QAM data over a range of pump spacing exceeding 300 GHz using the proposed scheme is demonstrated.
- First demonstration of clustering based machine learning algorithms to reduce the nonlinear distortion effect in SOA-based WC system for the wavelength conversion of 16-QAM and 64-QAM signals. Machine learning clustering based nonlinearity compensation (NLC) is performed using K-means and Density-based spatial clustering of applications with

noise (DBSCAN). Results reveal that the machine learning clustering based NLC has a clear benefit due to its ability of tackling the combination of non-circularly-symmetric Gaussian noise and nonlinearity.

- Detailed characterization of a novel tunable laser based on silicon nitride micro ring resonators structure. The tunable laser is employed in coherent transmission systems using advanced modulation formats such as QPSK, 16-QAM and 64-QAM, and shows similar performance compare to commercial external cavity lasers (ECLs). The laser can be potentially integrated with SOA and micro ring resonators based optical tunable filters, make it suitable for a photonics integrated WC chip.

The structure of the thesis is as follows:

In Chapter 1, a short review of the evolution of optical networks trend is presented, followed by an introduction to tunable lasers, the all-optical wavelength conversion, and main techniques in coherent optical communications system is given. It can be seen that an all-optical wavelength converter with rapid re-configurability is highly desirable in the next generation optical networks such as optical packet switching (OPS) and optical burst switching (OBS) networks. The different wavelength conversion techniques are then explained and the concept of a fast reconfigurable all-optical wavelength conversion scheme employing switching tunable pump lasers is introduced. The chapter continues by taking a look at the applications and solutions of tunable lasers. Finally, techniques for coherent transmission systems such as modulation formats, coherent homodyne detection, and the necessary digital signal processing (DSP) algorithms are discussed.

In Chapter 2, a dynamic theoretical model for a SOA-based FWM wavelength conversion system using a fast switching tunable SGDBR laser as the pump is demonstrated. The time-resolved BER is introduced, and the results show that the wavelength conversion system can achieve a BER of $<10^{-5}$ in several nanoseconds after the switching event. The primary characteristics (the tuning map, the phase noise, and

the switching performance) of different types of tunable lasers including the SGDBR laser, and the Modulated-Grating Y-branch (MGY) laser are investigated. After laser characterization, an SOA-based FWM wavelength conversion system using a fast switching tunable SGDBR laser and a narrow linewidth ECL as the pumps is demonstrated. The wavelength conversion of QPSK and Pol-Mul (PM) -QPSK signals at 12.5-Gbaud with total data rates of 25 Gbps and 50 Gbps, respectively, are experimentally studied, using the proposed scheme. Under 50 ns and 160 ns reconfiguration time is achieved for the proposed reconfigurable wavelength conversion system for QPSK and PM-QPSK signals, respectively.

An all-optical SOA-based coherent wavelength conversion system with QPSK and 16-QAM signals using tunable dual-correlated pumps provided by the combination of a quantum dash passively mode-locked laser (QD-PMLL) and a programmable tunable optical filter (TOF) is demonstrated in chapter 3. The effects of additional phase noise transfer to the wavelength converted idler due to non-ideal correlation between the comb lines of the QD-PMLL is investigated. The properties of the QD-PMLL are analyzed by characterizing the phase noise and the relative intensity noise (RIN). Then the performance of wavelength conversion of QPSK and 16-QAM signals at 12.5 GBaud using the proposed scheme is investigated, with total data rates of 25 Gbps and 50 Gbps, respectively. The experimental results show that the bit error rate (BER) performance is below the 7% forward error correction (FEC) limit over a range of pump spacing exceeding 300 GHz for QPSK signals, and conversion of 16-QAM signals is limited by the wavelength conversion scheme though is nonetheless below the 20% FEC limit.

In Chapter 4, the nonlinear distortion effect in the SOA-based wavelength conversion system is discussed. Two unsupervised machine learning clustering based algorithms, K-means method and DBSCAN method are proposed to improve the tolerance to nonlinear distortion. The wavelength conversion of 10 GBaud 16-QAM and 5 GBaud 64-QAM signals in an SOA-based single pump configuration that

incorporates the proposed machine learning clustering based blind NLC algorithms is presented.

Chapter 5 presents a hybrid InP-TriPleX integrated tunable laser based on silicon nitride micro ring resonators. This narrow linewidth tunable laser can be potentially used in all-optical wavelength convertors based on FWM in SOA's, in which the wavelength conversion of the advanced modulation formats will require very narrow linewidth tunable lasers. Detailed characterization of the laser is presented, including the wavelength tuning map, side mode suppression ratio (SMSR) tuning map, the relative intensity noise, phase noise, and switching speed. The performance of the micro ring resonators (MRR)-ECL laser is also investigated in the coherent transmission system for 12.5 Gbaud 16-QAM and 5 Gbaud 64-QAM signals, and the presented laser exhibits comparable performance with a commercial ECL laser.

Chapter 6 presents a brief conclusion and proposes the future research plan for this work.

References

1. Winzer, Peter J., and Ren-Jean Essiambre, "Advanced modulation formats for high-capacity optical transport networks," *J. Lightw. Technol.*, vol. 24, no. 12, pp. 4711-4728, 2006.

2. Yoo, SJ Ben, "Optical packet and burst switching technologies for the future photonic internet," *J. Lightw. Technol.*, vol. 24, no.12, pp. 4468-4492, 2006.

3. Sepideh T. Naimi, Seán P. Ó Dúill, and Liam P. Barry, "Detailed Investigation of the Pump Phase Noise Tolerance for Wavelength Conversion of 16-QAM Signals Using FWM," *J. Opt. Commun. Netw*. vol. 6, no. 9, pp. 793-800, 2014.

4. S. Diez, C. Schmidt, R. Ludwig, H. G. Weber, K. Obermann, S. Kindt, I. Koltchanov, K. Petermann, "Four-wave mixing in semiconductor optical amplifiers for frequency conversion and fast optical switching", *IEEE J. Sel. Topics Quantum Electron.*, vol. 3, no. 5, pp. 1131-1144, Oct. 1997.

Chapter 1

Tunable lasers and reconfigurable all-optical wavelength conversion

1.1 Introduction

Future optical networks will need to be agile and reconfigurable in order to achieve the high capacities and low latencies required for mission-critical Internet of things applications such as autonomous vehicles, automated manufacturing and augmented or virtual reality. Wavelength conversion is a key technology in reconfigurable optical networks due to the potential to increase the capacity of a communication system by assigning dynamic links between channels. All-optical wavelength converters typically comprise the tunable pump laser, the nonlinear media and the tunable optical filter. The wavelength converter allows optical information packets on a certain wavelength to be converted to a different wavelength precisely and quickly, and is highly desirable in order to reduce the number of power-hungry high-speed optical-electronic-optical conversions at networks nodes.

In this chapter, a simple review of the evolution of optical networks is presented. Different wavelength conversion mechanisms such as four-wave mixing and cross-modulation are then studied, and a fast reconfigurable all-optical wavelength conversion scheme employing switching tunable pump lasers is introduced. The chapter will subsequently explore different applications and solutions for wavelength tunable lasers. Finally, some of main technologies required for optical coherent transmission systems including the advanced modulation formats and digital signal processing algorithms are discussed.

1.2 Optical networks evolution trend

Modern lightwave communications had its origin in the first demonstration of the semiconductor laser in 1960 [1], then the development of the low loss fibers in the early

1970s made the first fiber optic communication system possible in 1978 [2]. Over the years, tremendous technical progress has been made since the days of short distance multimode transmission at 0.8 μm [3]. Single-channel transmission at 10 Gb/s across over 8000 km was achieved with the advent of erbium-doped fiber amplifiers (EDFAs) [4].

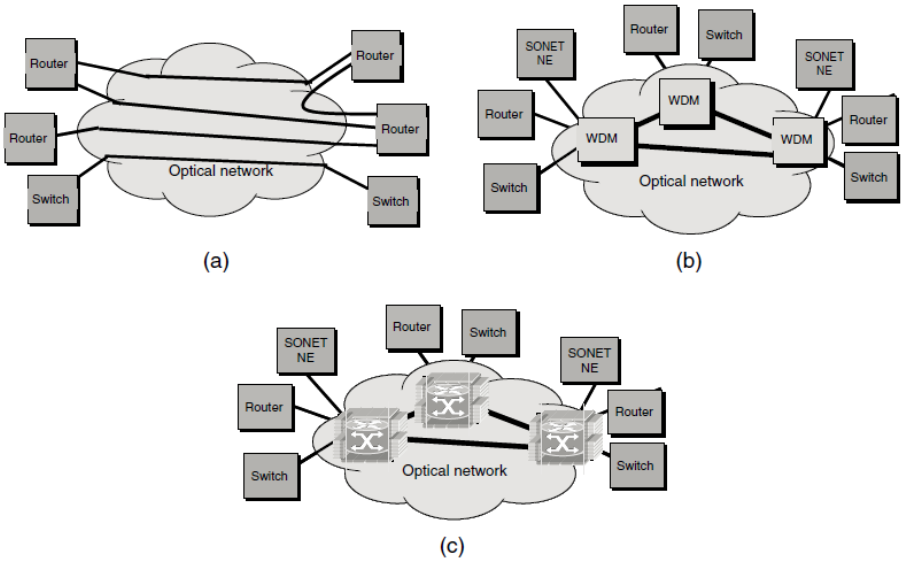

Fig.1-1 Evolution of optical Internetworking from (a) first-generation optical networking involving point-to-point static optical networking, (b) second-generation optical networking involving wavelength routed optical cross-connects (OXCs), and (c) third-generation optical networking involving OPS and OBS routers interfacing with other network elements.

Fig.1-1 shows the network evolution trend from the first-generation optical networking to the second- and the third-generation optical networking employing reconfigurable optical network elements such as reconfigurable optical add drop multiplexers (ROADMs), optical cross-connects (OXCs) and optical routers. In the first-generation optical networking system, although single-channel point-to-point link deployment can provide various solutions to the rapidly growing network capacity demands, they have disadvantages such as the use of a small fraction of the enormous bandwidth available in an optical fiber, and not allowing for a multiuser environment. Reconfigurations must take place using electronic switches or routers because the optical networking supports only point-to-point connectivity. By employing the WDM

technology, a simple multiuser system may be a point-to-point link with many simultaneous channels, and a more complicated system can take the form of a local, metropolitan, or wide-area network with either high bidirectional connectivity or simple unidirectional distribution [5]. In the WDM system, each end-user's equipment will operate at the electronic rate, however, multiple WDM channels from different end-users can be multiplexed on the same fiber. Second-generation optical networking systems can achieve reconfigurations of optical wavelength circuit paths by properly configuring the optical devices in the optical networking elements such as ROADMs and OXCs.

Third-generation optical networking systems will be capable of switching data packets or bursts directly in the optical layer. The optical packet switching (OPS) and optical burst switching (OBS) technologies are particularly attractive from the viewpoint of a true IP-over-WDM architecture, where the IP packets are switched or forwarded over the all-optical WDM network without excessive electronic processing in the data plane [6]. The optical network is currently evolving from traditional point-to-point static WDM networking to dynamically reconfigurable optical networking. Its continuing evolution is likely to lead to optical networking capable of dynamic switching of optical bursts and packets.

1.3 Wavelength conversion

The desire for multi-media content and richly interactive data services is shaping a new era for telecommunications networks. Future networks will need to be capable of offering IPTV, Voice-over-IP, Video-on-Demand and High-Speed Internet Access, combined with guaranteed Quality of Service [7]. These networks will employ WDM technology and advanced modulation formats, in order to achieve the high capacities required. In addition, given the bursty nature of this data it is expected that dynamic allocation of the bandwidth will be implemented to efficiently use the available capacity by employing the OPS and OBS technologies.

To solve the wavelength contention problems at the connecting nodes, it is necessary to be able to perform wavelength conversion. All-optical wavelength

conversion is required to reduce significant power consumption associated with multiple optical-to-electrical-to-optical (OEO) conversions [8]. The level of power consumption required by OEO convertors becomes significant as we move to advanced modulation formats (due to the required DSP), making all-optical wavelength conversion a vital technology for future optical networks. All-optical wavelength converters will be key components in OPS and OBS networks due to their potential to increase the capacity of a communication system by assigning dynamic links between channels [9]. The wavelength converters will be required in network nodes to avoid contention and to dynamically allocate wavelengths to ensure optimum use of fiber bandwidth [10]. One key component in the wavelength converters will be the tunable laser transmitters that generate the different wavelength packets.

There are two different techniques that have primarily been used for wavelength conversion. One is optoelectronic conversion, in which the signal has to be converted from optical to electrical format before being transmitted at a new optical wavelength. This technique is presently good up to bit rates of 10 Gbit/s [11], however as discussed earlier the move to DSP intensive advanced modulation formats will make OEO conversion techniques impractical due to the large power consumption required. The second method is all-optical, and it can be further be divided into two different approaches: nonlinear optical parametric processes and cross-modulation using a nonlinear media.

1.3.1 Four-wave mixing

The most common nonlinear optical technique that can be used for all-optical wavelength conversion is four-wave mixing (FWM) [12]. FWM is a third-order optical nonlinearity that can be achieved in optical fibers, and is also achievable in other passive waveguides such as semiconductor waveguides and in an active medium such as semiconductor optical amplifier (SOA). FWM in SOA is attracting a lot of interest for all optical wavelength conversion of advanced modulation formats due to the transparency of FWM in SOA's to modulation format and baud rate. Fig.1-2 shows the basic principle of all-optical wavelength conversion using four-wave mixing in a

semiconductor optical amplifier. When the signal beam is mixed with a pump beam, if we have a signal at frequency F_s and a pump at frequency at F_p, two frequencies are generated at frequencies $2F_p - F_s$ and $2F_s - F_p$ according to the phase-matching condition. An optical tunable filter used at the output, filters out the converted idler, as shown in Fig. 1-2. The FWM process is polarization sensitive and generates additional frequencies, which reduces the conversion efficiency and contributes to inter-channel crosstalk. Another drawback of the FWM-based wavelength conversion system is that there is phase noise transfer effect between the pump(s) and the converted idlers. The issue is of crucial importance when advanced modulation formats are used in the wavelength conversion system because the increased phase uncertainty at the receiver degrades the overall system performance.

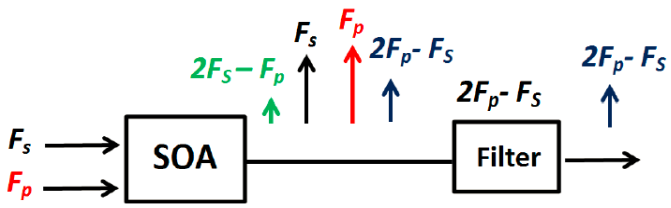

Fig.1-2. FWM in a semiconductor optical amplifier, F_s represents the signal frequency, F_p represents the pump frequency.

1.3.2 Cross-modulation

Another promising method for wavelength conversion is cross-modulation in an SOA in which either the gain or the phase can be modulated (XGM and XPM, respectively) [13]. A basic XGM converter is shown in Fig. 1-3(a). The idea behind XGM is to mix the input signal with a CW beam at the new desired wavelength in the SOA. Due to gain saturation, the CW beam will be intensity modulated so that after the SOA it carries the same information as the input signal. A filter is placed after the SOA to eliminate the original wavelength λs. The signal and the CW beam can be either co- or counter propagating. A counter propagation approach has the advantage of not requiring the filter. A typical XGM based converter is polarization independent but

suffers from an inverted output signal and low extinction ratio. Using an SOA in XPM mode for wavelength conversion makes it possible to generate a non-inverted output signal with improved extinction ratio. The XPM relies on the fact that the refractive index in the active region of an SOA depends on the carrier density. Therefore, when an intensity-modulated signal propagates through the active region of an SOA it depletes the carrier density, thereby modulating the refractive index, which results in phase modulation of a CW beam propagating through the SOA simultaneously [14]. The converted signal can be either inverted or non-inverted in the XPM-based wavelength conversion scheme. The XPM-based conversion converter is more power efficient than XGM-based converter. Fig. 1-3(b) shows a Mach-Zehnder interferometer setup. Two SOAs are used in the asymmetric configuration setup, the splitters are used to make sure the phase change in two SOAs is different, so that the phase modulation can be transformed into an intensity modulated signal. The XPM converter can also be setup by using one SOA in one of the interferometer arms, but it is less power efficient and polarization sensitive to the input CW signal [15].

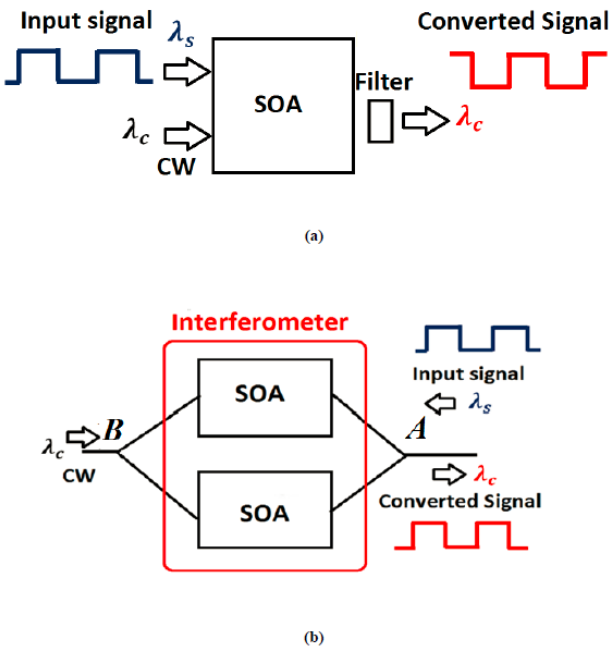

Fig.1-3 Different types of wavelength converters (a) Cross gain modulation (XGM) (b) Cross phase modulation (XPM)

1.4 Fast reconfigurable all-optical wavelength converter

An optical wavelength converter for next generation optical networks should have the following characteristics [16]:

- Fast setup time of output wavelength
- Transparency to bit rates and coding schemes
- Conversion to both shorter and longer wavelengths
- Moderate input power levels
- Possibility for no wavelength conversion
- Polarization independence
- Small chirp
- High extinction ratio
- Large ratio of signal power to the noise power (SNR)

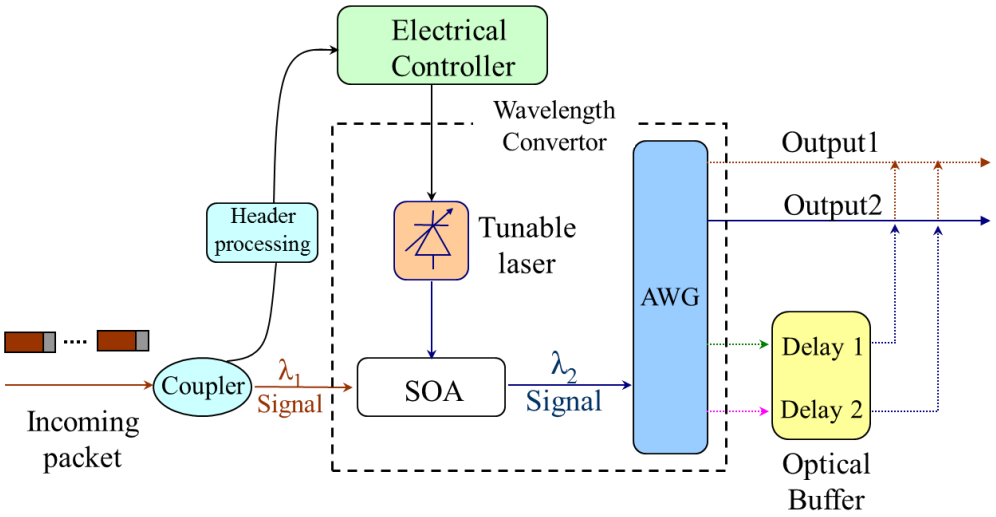

Fig.1-4 A simple schematic of wavelength converter with tunable lasers.

Fig.1-4 shows a simple schematic of a wavelength converter with tunable lasers used to control the wavelength that the incoming signal is converted to. The described all-optical wavelength converter consists of an SOA as the nonlinear media, a tunable laser as the pump and an array waveguide grating (AWG) used for filtering out the wavelength converted idler. The optical label of the incoming packet is first recovered by the receiver (detection followed by electrical header processing), then the control signals are generated and used to switch the fast-tunable lasers. After the nonlinear

wavelength conversion process in the SOA, the converted signal is then filtered out using an AWG and sent to the next network node.

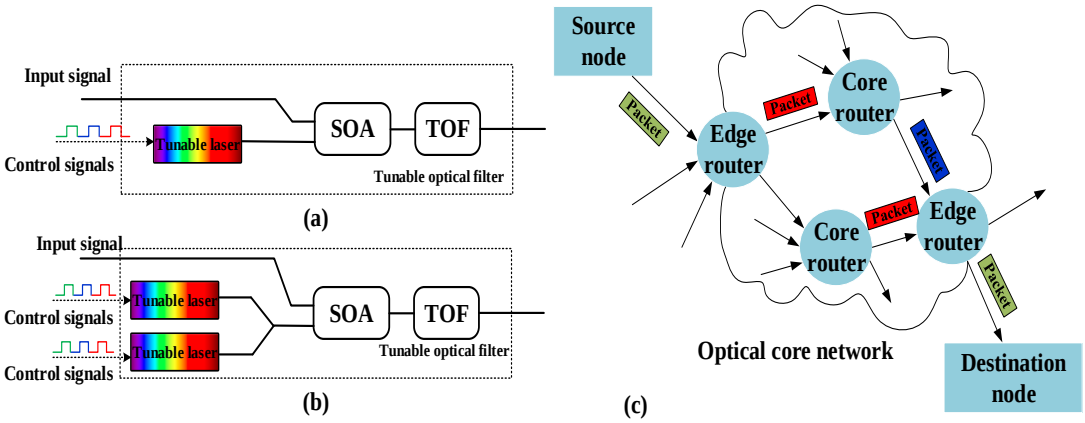

Fig. 1-5 (a) A single pump SOA-based wavelength converter employing one fast tunable pump laser. (b) A dual-pump SOA-based wavelength converter employing fast tunable pump lasers where the output wavelengths can be chosen by appropriately selecting the wavelength of the tunable lasers. The wavelengths of the tunable lasers are adjusted by the control signals to the tunable lasers (c) Schematic of an all-optical packet-switched network.

An example of a typical all-optical packet-switched network which employs wavelength conversion is illustrated in Fig. 1-5. The structure of the single pump and dual-pump SOA-based wavelength converter employing fast tunable pump lasers are shown in Fig. 1-5 (a) and Fig. 1-5 (b), respectively. Fig. 1-5(c) shows the schematic of an all-optical packet-switched network. IP packets enter the network through the edge router where they are retransmitted on a new wavelength to avoid contention. By employing the all-optical wavelength converter in this network, it can enable rapid routing of the same wavelength channel from any direction to any direction, and easily avoid the contention in which different packets with the same wavelengths are trying to leave the edge router. The wavelength converter consists of fast tuning tunable lasers as the pumps, an SOA and a tunable optical filter. The wavelength of the wavelength converted signal through FWM can be precisely altered by tuning the wavelength of the pump sources, and after the nonlinear wavelength conversion process in the SOA, the converted signal is then filtered out by using a tunable optical filter and sent to the next network node. The switching speed of this SOA-based wavelength converter

mainly depends on the tunable pump lasers and the tunable optical filter. All the components in the wavelength converter (lasers and SOA) can be integrated and these results motivate the construction of a compact, optically-integrated, and rapidly reconfigurable all-optical wavelength converter.

As previously discussed, fast switching widely tunable semiconductor lasers will be used as the pump lasers in the wavelength converters to provide the re-configurability. There are a number of tunable lasers technolgies that can be employed:

(a) External cavity lasers (ECLs)

ECLs are very suitable to be used as optical sources in coherent communication system as they provide wide range wavelength tuning (>35 nm), high power (> 10 dBm), narrow linewidth (<100 kHz), and high stability. ECLs have a resonant cavity external to the active semiconductor section. The active section is a simple Fabry-Perot structure. The wavelength can be tuned by mechanically changing the length of the laser cavity. However, it is not impossible to use them in OPS/OBS networks due to their slow tuning speed of several milliseconds. Fig.1-6 shows the simple structure of a Littman-cavity based ECL [17,18]. A grating and a reflector are used to achieve high level of side mode suppression (>50 dB).

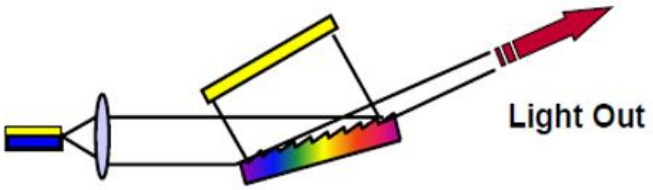

Fig.1-6 Littman Cavity based ECL

(b) Distributed Bragg Reflector (DBR) lasers

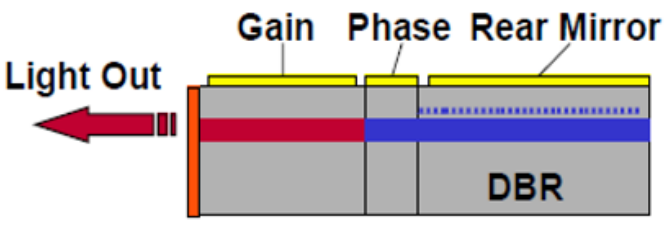

Fig.1-7 Three-section DBR laser

Fig.1-7 shows the structure of a 3-section distributed Bragg reflector (DBR) laser. It consists of the gain section, the phase section and the grating section. The laser structure is fabricated with surface features that define a monolithic, single mode ridge waveguide that runs the entire length of the device. A resonant cavity is defined by a highly reflective DBR mirror on one end, and a low reflectivity cleaved exit facet on the other end. Within the cavity is a gain ridge portion, where current is injected to produce a single spatial lasing mode. The DBR mirror is designed to reflect only a single longitudinal mode. As a result, the laser operates on a single spatial and longitudinal mode. The laser emits from the exit facet opposite the DBR end. The DBR is continuously tunable over approximately a 2 nm range by changing current or temperature.

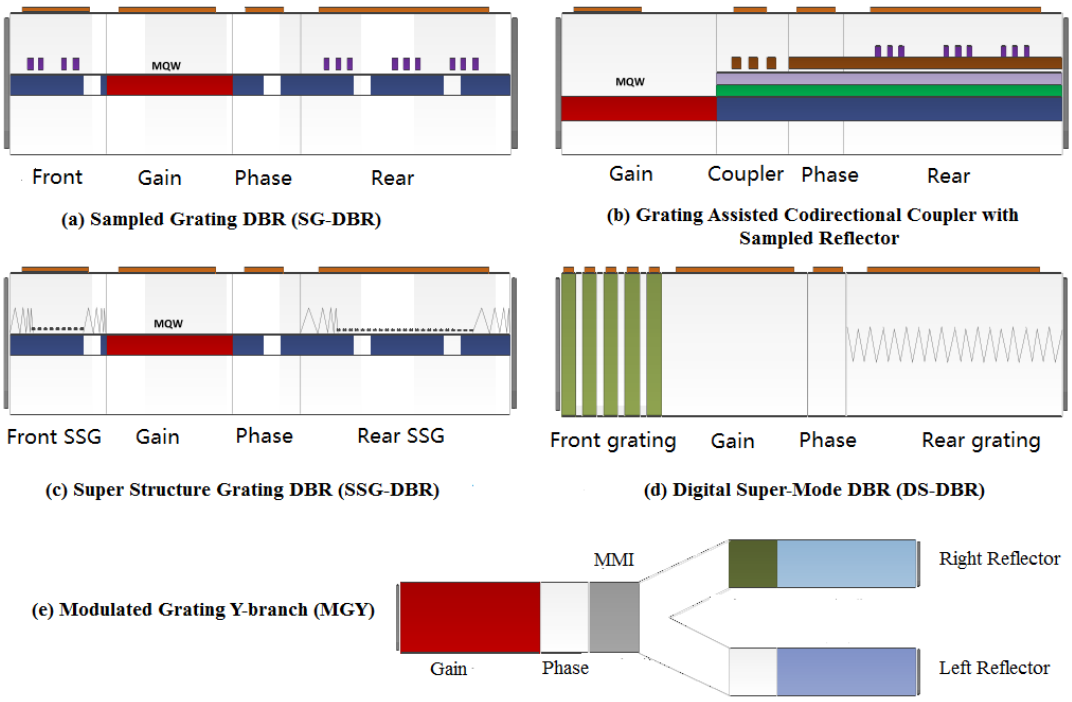

Fig. 1-8 Different kinds of widely tunable lasers

The application of three section DBR lasers is limited by their narrow wavelength tuning range. In order to extend the tuning range of DBR lasers, the Vernier effect has been used and many new DBR-based tunable lasers with different structures have been reported. Fig. 1-8 shows the structures of different kinds of tunable lasers including (a) the sampled grating distributed Bragg reflector (SG-DBR) lasers [19-20], (b) the

grating assisted co-directional coupler with sampled reflector (GCSR) lasers [21], (c) the super structure grating DBR (SSG-DBR) lasers [22], (d) the digital super-mode distributed Bragg grating (DS-DBR) lasers [23], and (e) the modulated grating Y-branch (MGY) lasers [24]. These tunable lasers can achieve large wavelength tuning range (>40 nm) owing to the Vernier effect. And they can be tuned quickly on the nanosecond timescale.

1.5 Coherent transmission system

Coherent transmission techniques have been widely investigated and discussed since the 1980's [25-29]. The motivation for using the coherent transmission techniques is that they can increase the spectral efficienecy (SE) of the WDM system and make more efficient use of the available fiber. In comparison to the intensity modulation with direct detection (IM/DD) system, the coherent transmission techniques can greatly improve the receiver sensitivity, restore the amplitude, frequency, and phase information from the carrier, thus can achieve higher capacity. Another advantage of using the coherent transmission system is that the DSP algorithms can be used to compensate the chromatic and polarization mode dispersion due to optical fibers.

1.5.1 Digital modulation formats

In coherent transmission systems, the information can be sent by modulating the amplitude, the phase or the frequency of an optical carrier. The optical signal field can be expressed by,

$$E_s = E_p A_m \cos(wt + \varphi) \tag{1.1}$$

Where E_p, A_m, w, φ represent the polarizaion coefficient, the signal amplitude, the optical angular frequency and the phase. Depending on the modulation item of the optical carrier, different modulation formats can be categorized as follows:

(a) Amplitude-shift keying (ASK)

The amplitude A_m is modulated while other values such as the angular frequency and the phase are kept unchanged for one-bit duration. The binary

symbol 1 represents transmitting a waveform with a fixed amplitude signal and fixed frequency for a but duratuon of T seconds. If $A_m = 0$, a signal value of 0 will be transmitted. The ASK format is also called on–off keying (OOK) which is normally employed in IM/DD system.

(b) Phase-shift keying (PSK)

In the case of PSK, the phase φ is modulated while other values E_p, A_m, w are kept unchanged. For binary PSK format, there are two phase states, and the phase values can be assigned to 0 and π. As the phase states increase, the values of the phase will be changed accordingly. To implement PSK, an external modulator which is capable of changing the optical phase by changing the applied voltages is needed. A LiNbO3-based phase modulator is a common option as a Mach-zehnder interferometer (MZI) design is not needed for pure phase modulation. The number of phase states for PSK format cannot be very high, as the requirement for the linewidths of the laser sources and the local oscillator is stringent in order to recovery the phase information at the receiver side without ambiguity.

(c) Frequency-shift keying (FSK)

FSK is a frequency modulation scheme in which signal waveform is transmitted through discrete frequency changes of a carrier wave. Only the frequency w is modulated while the values E_p, A_m, φ remain unchanged.

(d) Polarization-shift keying (PolarSK)

For the case of PolarSK, the polarization field E_p takes one polarization for the binary symbol 1 and the other for the symbol 0. By using the PolarSK scheme in conjunction with other modulation formats, the transmission capacity of the modulated signal can be doubled.

The M-ary QAM formats are widely used in today's commercial telecommunications system to transmit information. In order to increase the transmission capacity, the use of the M-ary QAM such as 16-QAM or 64-QAM can

increase the number of bits per symbol. However, as the value of M increases, the requirement for the optical signal to noise ratio (OSNR) would be more stringent.

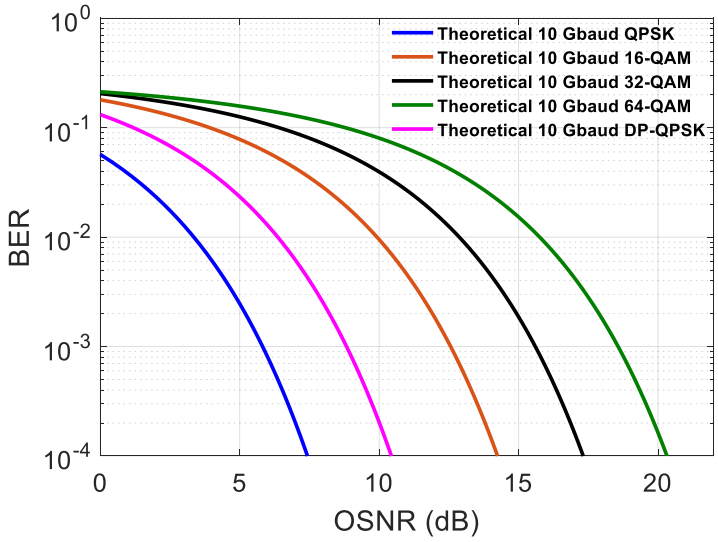

Fig. 1-9 Theoretical BER versus OSNR curves for 10 Gbaud optical signals with QPSK, 16-QAM, 32QAM, 64-QAM and DP-QPSK.

Fig.1-9 shows the theoretical BER versus OSNR curves for optical signals at 10 Gbaud with different M-ary QAM formats including QPSK, 16-QAM, 32-QAM, 64-QAM and dual-polarization QPSK. The relation between OSNR and BER can be calculated by $BER = \frac{\sqrt{M}-1}{\sqrt{M} \times log_2\left(\sqrt{M}\right)} \cdot erfc\left(\sqrt{\frac{3}{M-1} \cdot \frac{BW_{ref}}{B}}\right)$ [30]. Where M is the order of the QAM modulation formats, BW_{ref} is 12.5 GHz that OSNR is usually measured against, B is the bandwidth of signal. It can be observed that at a BER of 1e-3, the required OSNR of 16-QAM is about 6.8 dB above that required for QPSK. For 64-QAM, an extra 6 dB OSNR is needed compared to 16-QAM to achieve a BER of 1e-3. It also shows that the dual-polarization QPSK would require 3 dB more OSNR to achieve the same BER performance compared to single-polarization QPSK. Clearly, more carrier signal power would be required to get enough OSNR for higher level modulation formats, however this could hit the threshold of nonlinear distortion effects. Therefore, there is a trade-off between the fiber nonlinearity at high launch power levels and the Amplified spontaneous emission (ASE) noise at low launch power levels [31].

Therefore the optimum launch power of the optical transmission system with different modulation formats would be different.

1.5.2 I-Q modulator

Although I-Q modulators can be used to generate many different modulation formats, they are commonly designed for QAM signal generation and single side-band suppressed carrier (SSB-SC) transmission [32]. A typical I-Q modulator consists of two parallel MZIs for intensity modulation and a phase modulator to control the phase of the optical signal as shown in Fig.1-10. There are DC bias controls designed for the parallel MZIs to allow the users to change the bias conditions. This provides the ability to generate different QAM signals by using different operation conditions.

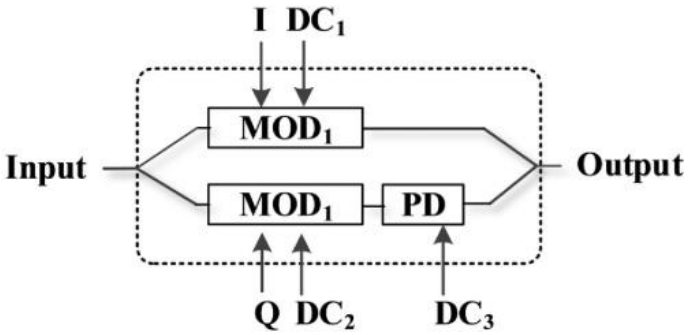

Fig.1-10 I-Q modulator

The common operation processes to generate QAM signals by using I-Q modulators are summarized as follows:

(a) Select one MZI from the two parallel MZIs, and change the bias voltage between $\frac{V_\pi}{2}$ and $-\frac{V_\pi}{2}$ to make the modulator operate at the null point. The RF signals should be off during optimization.

(b) The RF signals which are the I (in-phase) and Q (quadrature-phase) signals are then applied to the two MZI's. It should be noted that the amplitude of the applied RF signals should be operated at appropriate levels to make sure that the modulator works in the linear region. Otherwise, the signal waveforms could be strongly distorted that would degrade the signal quality at the output.

(c) Change the bias voltage on the phase section. The optical sampling oscilloscope can be used to monitor the eye-diagram of the QAM signals from the output

while optimizing the bias on the phase section.

The method demonstrated above can be used to generate different QAM signals such as QPSK, 16-QAM and 64-QAM.

1.5.3 Coherent detection

In order to extract the full information including the amplitude, the phase, and the state of the polarization from the received signals, the coherent receiver can be used. In this section, the discussion is focus on the homodyne receiver where the frequency offset between the signal and local oscillator is zero [33]. A schematic of a phase diverse coherent homodyne receiver is shown in Fig. 1-11.

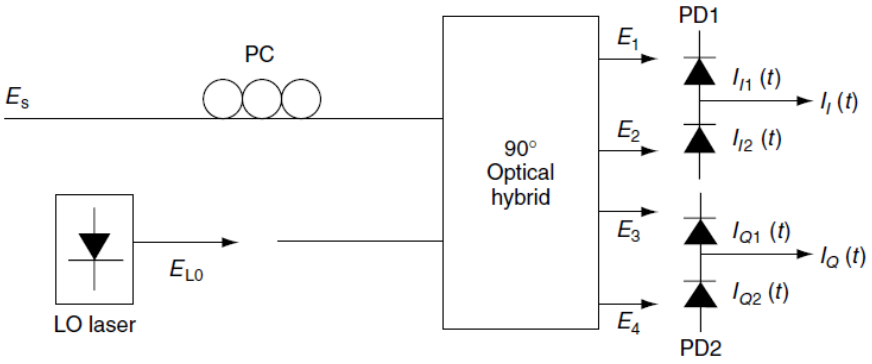

Fig. 1-11 A schematic of a phase diverse coherent homodyne receiver.

The receiver consists of a 90-degree optical hybrid coupler which mixes the received data signal ($E_s(t)$) and the local oscillator (E_{LO}). A π/2 optical delay is used in the optical hybrid coupler to recovery the quadrature part of the signal. The obtained optical outputs are sent to two balanced photo-detectors and can be given by,

$$E_1 = \frac{1}{2}(E_s + E_{LO}) \tag{1.2}$$

$$E_2 = \frac{1}{2}(E_s - E_{LO}) \tag{1.3}$$

$$E_3 = \frac{1}{2}(E_s + jE_{LO}) \tag{1.4}$$

$$E_4 = \frac{1}{2}(E_s - jE_{LO}) \tag{1.5}$$

The output current from the balanced photo-detectors can then be given by [34],

$$I_I(t) = I_{I1}(t) - I_{I2}(t) = R\sqrt{P_s P_{LO}}\cos\{\theta_s(t) - \theta_{LO}(t)\} \tag{1.6}$$

$$I_Q(t) = I_{Q1}(t) - I_{Q2}(t) = R\sqrt{P_s P_{LO}}\sin\{\theta_s(t) - \theta_{LO}(t)\} \tag{1.7}$$

Where R represents the photodiode responsitivity, P_s the power of signal, P_{LO} the power of local oscillator (LO), $\theta_s(t)$ and $\theta_{LO}(t)$ are the phase of the signal and LO. By using the equation (1.6) and equation (1.7), the amplitude information of the optical signal can be restored directly. However, digital signal processing (DSP) is needed to estimate the phase noise of the optical signal and restore the phase information. More details on DSP will be discussed in the next section.

In order to restore the state of the polarization of the optical signal, the coherent receiver with polarization diversity can be used. Fig. 1-12 shows the configuration of a polarization diverse coherent receiver which consists of polarization beam splitters (PBS) and two phase diverse homodyne receivers. The input signal and the LO are both divided into x and y polarization components by using the PBSs. The output after the PBSs can be written by,

$$E_{sx} = \sqrt{\alpha P_s}\cdot e^{j\phi}\cdot e^{jw_s t}\cdot e^{j\theta_s(t)} \tag{1.8}$$

$$E_{sx} = \sqrt{(1-\alpha)P_s}\cdot e^{jw_s t}\cdot e^{j\theta_s(t)} \tag{1.9}$$

$$E_{LO,x} = \sqrt{\frac{P_{LO}}{2}}\cdot e^{jw_{LO} t}\cdot e^{j\theta_{LO}(t)} \tag{1.10}$$

$$E_{LO,y} = E_{LO,x} \tag{1.11}$$

Where α is the proportion of the optical power going into x and y polarization and ϕ is the phase variation between them.

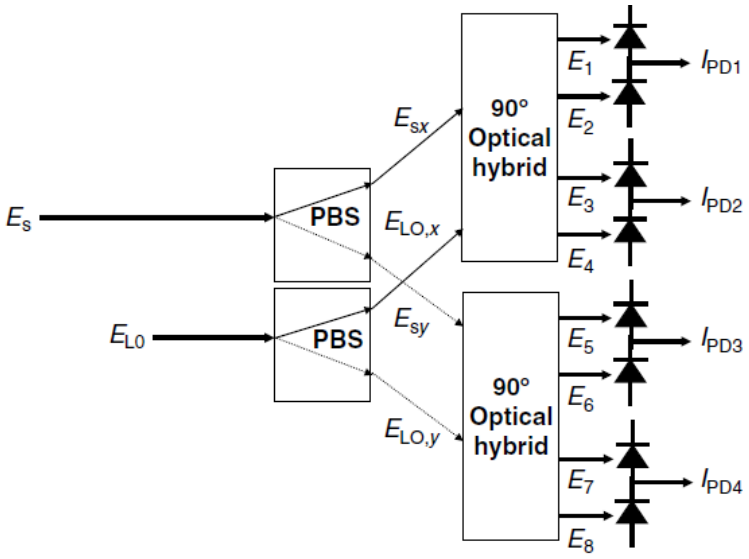

Fig. 1-12 A schematic of polarization diverse coherent receiver [34]

The electric fields of the 8 outputs from the 90-degree optical hybird can be written by [34],

$$E_{1,2} = \frac{1}{2}(E_{sx} \pm \frac{1}{\sqrt{2}} E_{LO,x}) \tag{1.12}$$

$$E_{3,4} = \frac{1}{2}(E_{sx} \pm \frac{j}{\sqrt{2}} E_{LO,x}) \tag{1.13}$$

$$E_{5,6} = \frac{1}{2}(E_{sy} \pm \frac{1}{\sqrt{2}} E_{LO,y}) \tag{1.14}$$

$$E_{7,8} = \frac{1}{2}(E_{sy} \pm \frac{j}{\sqrt{2}} E_{LO,y}) \tag{1.15}$$

The output current from the balanced photo-detectors can then be given by,

$$I_{PD1}(t) = R\sqrt{\frac{\alpha P_s P_{LO}}{2}} \cos\{\theta_s(t) - \theta_{LO}(t) + \phi\} \tag{1.16}$$

$$I_{PD2}(t) = R\sqrt{\frac{\alpha P_s P_{LO}}{2}} \sin\{\theta_s(t) - \theta_{LO}(t) + \phi\} \tag{1.17}$$

$$I_{PD3}(t) = R\sqrt{\frac{(1-\alpha) P_s P_{LO}}{2}} \cos\{\theta_s(t) - \theta_{LO}(t)\} \tag{1.18}$$

$$I_{PD4}(t) = R\sqrt{\frac{(1-\alpha)P_s P_{LO}}{2}}\sin\{\theta_s(t) - \theta_{LO}(t)\} \tag{1.19}$$

It can be observed from equation (1.16) to equation (1.19) that the polarization diverse coherent receiver can be used to restore the full signal information including the amplitude, the phase, and the state of the polarization.

1.5.4 Digital signal processing for back-to-back system

Most of the DSP algorithms for the optical coherent systems are derived from the wireless telecommunication systems. However, these algorithms need to be modified to cope with the nature of the fiber transmission system. The real-time or off-line DSP processes need to be more advanced as the modulation formats evolve from QPSK to multilevel QAM (M-QAM). QPSK data format will be taken as an example in this section to explain the principle of the DSP alogrithms such as the frequency offset compensation, the constant modulus algorithm (CMA), and the carrier phase recovery (CPR) algorithm. DSP algorithms such as chromatic dispersion (CD), polarisation mode dispersion (PMD) [35] and digital backpropagation (DBP) [36] will not be discussed, as they are only required for the long-haul transmission system. This thesis will focus on back-to-back transmission and coherent wavelength conversion system.

A generic flow diagram of the DSP for a back-to-back optical system employing polarization division multiplexed QPSK (PDM-QPSK) or other M-QAM formats is shown in Fig. 1-13. The signals from the coherent receiver are amplified by transimpedance amplifiers (TIAs) and then captured by using the real-time digital scope. Due to the optical and electronic propagation in the back-to-back system, there are different delay times between the four-channel signals (I and Q signals from both x and y polarizations) which need to be compensated. The skew estimation can be undertaken before the transmission experiments. Otherwise, deskew needs to be done after the capture to align the I and Q signals from both polarizations.

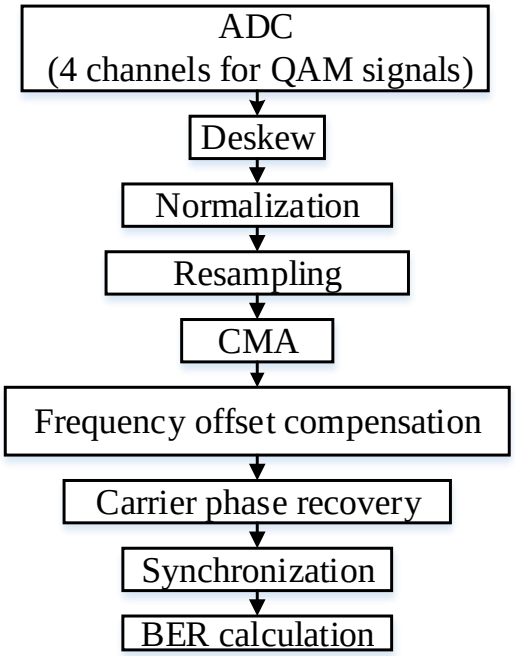

Fig. 1-13 A flow diagram of the DSP for a back-to-back optical system

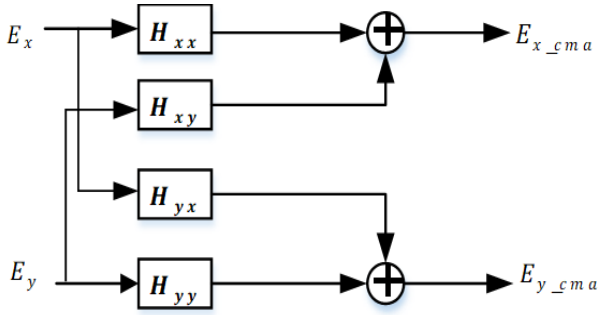

Fig. 1-14 Configuration of the CMA filter

After the I-Q deskew and the amplitude normalization, the next step is to resample the signals to 2 samples per symbol. The CMA can be considered as an adaptive N tap FIR filter and can be used for polarization demultiplexing and channel equalization for PDM-QPSK. Fig 1-14 shows the configuration of the CMA filter. H_{xx}, H_{xy}, H_{yx} and H_{yy} represent the tap weights and each has N coefficients. For simplicity, we consider that $E(n)=[E_x(n);E_y(n)]$, $H_x(n)=[H_{xx}(n);H_{xy}(n)]$ and $H_y(n)=[H_{yx}(n);H_{yy}(n)]$. Thus, the outputs from the fulters can be written by,

$$E_{x\_cma}(n)=H_x^T(n)\cdot E(n) \tag{1.20}$$

$$E_{y\_cma}(n) = H_y^T(n) \cdot E(n) \tag{1.21}$$

The cost function can be given by [37],

$$\varepsilon_x(n) = 1 - \left| E_{x\_cma}(n) \right|^2 \tag{1.22}$$

$$\varepsilon_y(n) = 1 - \left| E_{y\_cma}(n) \right|^2 \tag{1.23}$$

Correspondingly, the update equations can be given by [38],

$$H_x(n+1) = H_x(n) + \mu \cdot \varepsilon_x(n) \cdot E^*_{x\_cma}(n) \cdot E(n) \tag{1.24}$$

$$H_y(n+1) = H_y(n) + \mu \cdot \varepsilon_y(n) \cdot E^*_{y\_cma}(n) \cdot E(n) \tag{1.25}$$

Where μ is the step size coefficient. The CMA can perform well for QPSK signals, however, as the modulation formats evolve to more advanced modulation formats such as PDM-16QAM, the cost function of CMA can never converge. In this case, multi-modulus algorithm (MMA) can be employed [39].

In a coherent receiver, the free running local oscillator and the transmitter lasers are not frequency locked. This results in some residual frequency offset in the received signal that needs to be estimated and compensated for. The widely used method to compensate the frequency offset is called the 4th power method [40]. Consider E_{cma} as the frequency offset between the received signal and LO. Since the spectrum of E_{cma}^4 exhibits a peak at the frequency of four times of the frequency offset, Δf is then estimated from the spectrum. The implementation complexity of this method increases for high-order modulation formats. Note that the complexity is for high order square QAM by considering only outmost four constellation points combined with the use of linear interpolation and down sampling-based methods [41].

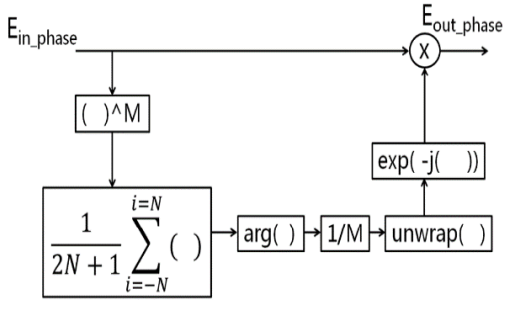

Fig. 1-15 Mth power phase estimation

After frequency offset compensation, it is necessary to perform phase estimation. This is by performing M[th] power phase estimation (Viterbi and Viterbi) [42] as shown in Fig.1-15. For QPSK the carrier phase is estimated using a fourth-order nonlinearity in order to remove the phase modulation, giving the estimate of the phase as follows,

$$\theta_{est}(n) = \frac{1}{4}\arg\{\frac{1}{2N+1}\sum_{i=-N}^{i=N} E_{in\_phase}^{4}(i+n)\} \tag{1.26}$$

E_{in_phase} represents the input signal after frequency offset compensation. The phase estimation method is very similar to the frequency-offset estimation algorithm. And after the $\theta_{est}(n)$ is obtained, it can be removed from E_{in_phase} in order to mitigate the Wiener phase noise. After the carrier phase recovery process, the synchronization [43] should be carried out before calculating the Bit error rate (BER).

1.6 Conclusion

In this chapter, the optical network evolution has been presented. Optical networks are experiencing a shift towards greater re-configurability in order to increase the switching efficiency and reduce the network latency. Wavelength converters play an important role in the next generation optical networks, and wavelength conversion based four-wave mixing and cross-modulation are presented. Four-wave mixing in semiconductor optical amplifiers optical amplifiers is considered to be the key technology for all optical wavelength converting signals with advanced modulation formats due to the transparency of FWM to modulation format and baud rate. The wavelength tunable laser is the key component to build a wavelength converter. The different applications and solutions of tunable lasers were discussed. Initially deployed for sparing and inventory management in WDM networks, tunable lasers also enable functionality such as dynamic bandwidth provisioning, protection, restoration, OBS and OPS. Depending on the required application, the required switching time can range from seconds to nanoseconds. In this chapter, the main techniques for coherent transmission systems were also introduced, including the advanced modulation formats, QAM signals generation by using I-Q modulator, the principle of the polarization diverse coherent receiver and necessary DSP algorithms for a back-to-back system.

References

[1] G. Keiser, Optical Fiber Communications, 4th ed. New York: Mc-Graw Hill, 2010.

[2] G. Agrawal, Long-wavelength semiconductor lasers, New York: Van Nostrand Reinhold, 1986.

[3] F. P. Kapron, Fiber-Optic System Tradeoffs, IEEE Spectrum Magazine, pp. 60–75, 1985.

[4] Y. K. Park, T. V. Nguyen, O. Mizuhara, C. D. Chen, L. D. Tzeng, P. D. Yeates, F. Heismann, Y. C. Chen, D. G. Ehrenbergh, and J. C. Feggeler, Field Demonstration of 10-Gb/s Line-Rate Transmission on an Installed Transoceanic Submarine Lightwave Cable, IEEE Photon. Tech. Lett. , vol. 8, pp. 425–427, 1996.

[5] D. P. Berztsekas and R. G. Gallager, Data Networks, Prentice Hall, Englewood Cliffs, New Jersey, 1987.

[6] Yoo, SJ Ben. "Optical packet and burst switching technologies for the future photonic internet." J. Lightwave Technol., vol.24, no. 12, pp. 4468-4492, 2006.

[7] Chang, Gee-Kung, Jianjun Yu, Yong-Kee Yeo, Arshad Chowdhury, and Zhensheng Jia. "Enabling technologies for next-generation optical packet-switching networks." Proceedings of the IEEE 94, no. 5, pp.892-910, 2006.

[8] S. J. B. Yoo, Wavelength conversion technologies for WDM network applications, J. Lightwave Technol. Vol.14, no.6, pp. 955-966, 1996.

[9] Bhopalwala, Mariya, Houman Rastegarfar, Daniel C. Kilper, Michael Wang, and Keren Bergman, Energy efficiency of optical grooming of QAM optical transmission channels, Opt. express 24, no. 3, pp. 2749-2764, 2016.

[10] Bayvel, P., Wavelength routing and optical burst switching in the design of future optical network architectures, Opt. Commun., vol. 4, pp. 616–619, 2001.

[11] C. A. Brackett, “Dense wavelength division multiplexing networks: Principles and applications,” IEEE J. Select. Areas Commun., vol. 8, pp. 948, 1990.

[12] Agrawal, Govind P. ,Population pulsations and nondegenerate four-wave mixing in semiconductor lasers and amplifiers, JOSA B vol.5, no. 1, pp. 147-159, 1988.

[13] H. Lee, H. Yoon, Y. Kim, J. Jeong, Theoretical study of frequency chirping and

extinction ratio of wavelength-converted optical signals by XGM and XPM using SOA's, IEEE J. Quantum Electron., vol. 35, no. 8, pp. 1213-1219, Aug. 1999.

[14] Allard, Frederick C. Fiber optics handbook: for engineers and scientists. McGraw-Hill Companies, 1990.

[15] Kaur, Anupjeet, Kulwinder Singh and Bhawna Utreja., Wavelength Converters in Optical Communication Systems, Material Science, 2013.

[16] Durhuus, Terji, et al. All-optical wavelength conversion by semiconductor optical amplifiers, J. Lightwave Technol., vol.14, no.6, pp.942-954, 1996.

[17] Souhaite, G., et al., 16 channels, switchable external cavity-based multi-wavelength laser for DWDM applications, ECOC. 27th European Conference on. Vol. 2. IEEE, 2001.

[18] Precision, M. E. M. S., Flexure mount for a Littman tunable external cavity laser-W Huang, RRA Syms, J., Stagg and A. A Lohmann, IEEE Prc-Sci Meas. Technol, vol.151, no.2, pp.67-75, 2004.

[19] Simsarian, John E., et al., Less than 5-ns wavelength switching with an SG-DBR laser, IEEE Photon. Tech. Lett., vol.18, no.4, pp. 565-567, 2006.

[20] Larry A. Coldren, G. A. Fish, Y. Akulova, J. S. Barton, L. Johansson, and C. W. Coldren, Tunable Semiconductor Lasers: A Tutorial, IEEE J. Lightwave Technol., vol.22, pp.193, 2004.

[21] Rigole, P-J., et al., Wavelength coverage over 67 nm with a GCSR laser: tuning characteristics and switching speed, Semiconductor Laser Conference,15th IEEE, 1996.

[22] Sarlet, Gert, Geert Morthier, and Roel Baets., Control of widely tunable SSG-DBR lasers for dense wavelength division multiplexing, IEEE J. Lightwave Technol., vol.18, no.8, pp.1128, 2000.

[23] A. J. Ward, D. J. Robbins, G. Busico, E. Barton, L. Ponnampalam, J. P. Duck, et al., Widely tunable DS-DBR laser with monolithically integrated SOA: design and performance, IEEE J. Quantum Electron., vol. 11, pp. 149-156, 2005.

[24] J.-O. Wesström, S. Hammerfeldt, J. Buus, R. Siljan, R. Laroy, and H. De Vries, Design of a widely tunable modulated grating Y-branch laser using the additive Vernier

effect for improved super-mode selection, in Proc. of 18th Int. Semiconductor Laser Conf.(ISLC), Garmisch, Germany, 2002.

[25] T. Okoshi, Recent advances in coherent optical fiber communication systems, J. Lightw. Technol., vol. LT-5, no. 1, pp. 44-52, Jan. 1987.

[26] T. Kimura, Coherent optical fiber transmission, J. Lightwave Technol., vol. LT-15, pp. 414-428, 1987.

[27] R. A. Linke, A. H. Gnauck, High-capacity coherent lightwave systems, J. Lightwave Technol., vol. 6, pp. 1750-1769, 1988.

[28] Y. Yamamoto, T. Kimura, Coherent optical fiber transmission systems, IEEE J. Quantum Electron., vol. QE-17, pp. 919-935, 1981.

[29] J. Salz, Coherent lightwave communications, AT&T Tech. J., vol. 64, no. 10, pp. 2153-2209, Dec. 1985.

[30] Ali Grami, Introduction to Digital Communications, Academic Press, 2015.

[31] V. E. Perlin, H. G. Winful, On trade-off between noise and nonlinearity in WDM systems with distributed Raman amplification, Proc. Opt. Fiber Commun. Conf. (OFC), pp. 178-180, 2002.

[32] S. Shimotsu, S. Oikawa, T. Saitou, N. Mitsugi, K. Kubodera, T. Kawanishi, M. Izutsu, Single side-band modulation performance of a $LiNbO_3$ integrated modulator consisting of four-phase modulator waveguides , IEEE Photon. Technol. Lett., vol. 13, no. 4, pp. 364-366, Apr. 2001.

[33] J. Crols, M. Steyaert, Low-IF Topologies for High-Performance Analog Front Ends of Fully Integrated Receivers, IEEE Trans. Circuits and Sys. II, vol. 45, no. 3, pp. 269-282, 1998.

[34] K. Kikuchi, Coherent optical communication systems, in Optical Fiber Telecommunications VB: Systems and Networks, I. P. Kaminow, T. Li, and A. E. Willner, eds. (Academic Press, Oxford), pp. 95-130, 2008.

[35] E. Ip, J. Kahn, Digital equalization of chromatic dispersion and polarization mode dispersion, J. Lightw. Technol., vol. 25, no. 8, pp. 2033-2043, Aug. 2007.

[36] D. Rafique, M. Mussolin, M. Forzati, J. Mårtensson, M. N. Chugtai, A. D. Ellis,

Compensation of intra-channel nonlinear fibre impairments using simplified digital backpropagation algorithm, Proc. OSA Opt. Exp., vol. 19, no. 10, pp. 9453-9460, 2011.

[37] I. Fijalkow, C. Manlove, C. R. Johnson Jr., Adaptive fractionally spaced blind CMA equalization: Excess MSE, IEEE Trans. Signal Processing, vol. 46, pp. 227-231, Jan. 1998.

[38] N. Kaneda, A. Leven, Coherent polarization-division-multiplexed QPSK receiver with fractionally spaced CMA for PMD compensation, Photon. Technol. Lett., vol. 21, no. 4, pp. 203-205, Feb. 2009.

[39] J.-T. Yuan, T.-C. Lin, Equalization and carrier phase recovery of CMA and MMA in blind adaptive receivers, IEEE Trans. Signal Process, vol. 58, no. 6, pp. 3206-3217, 2010.

[40] Y. Gao, A. P. T. Lau, and C. Lu, Residual Carrier-Aided Frequency Offset Estimation for Square 16-QAM Systems, in OptoElectronics and Communications Conference/ International Conference on Photonics in Switching, pp. TuPR-8, 2013.

[41] A. Leven, N. Kaneda, U.-V. Koc, Y.-K. Chen, Frequency estimation in intradyne reception, IEEE Photon. Technol. Lett., vol. 19, no. 6, pp. 366-368, Mar. 2007.

[42] E. Ip, J. Kahn, Feedforward carrier recovery for coherent optical communications, J. Lightw. Technol., vol. 25, no. 9, pp. 2675-2692, Sep. 2007.

[43] Mori, C. Zhang, K. Igarashi, K. Katoh, and K. Kikuchi, Unrepeated 200-km transmission of 40-Gbit/s 16- QAM signals using digital coherent receiver, Opt. Express no.17, pp.1435–1441, 2009.

Chapter 2

All-optical wavelength conversion system based on fast switching tunable lasers

2.1 Introduction

Optical networks are experiencing a shift towards greater re-configurability in order to increase the switching efficiency and reduce the network latency. Wavelength converters will play an important role in next generation optical networks. Four-wave mixing in semiconductor optical amplifiers is considered to be the key technology for all optical wavelength conversion of signals with advanced modulation formats due to the transparency of FWM in SOAs to modulation format and baud rate [1]. The semiconductor tunable laser is another key component to build a wavelength converter. Depending on the application, the required switching time of the tunable lasers can range from seconds to nanoseconds. The application of tunable lasers in wavelength conversion systems will be investigated in this chapter.

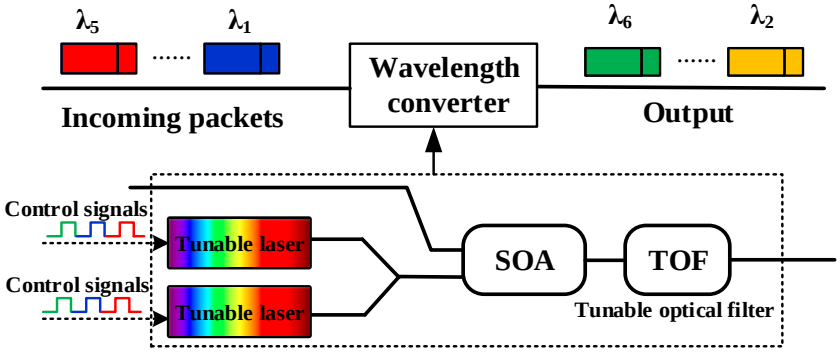

Fig.2-1 A simple scheme to implement wavelength conversion employing fast tunable pump lasers. Incoming data packets need to be converted to new wavelengths, the output wavelengths can be achieved by appropriately selecting the wavelength of the tunable lasers. The wavelengths of the tunable lasers are adjusted by the control signals that can be imbedded in the data packets.

Fig.2-1 displays a simple dual pumping scheme to implement wavelength conversion employing fast switching tunable pump lasers. All the components in the

wavelength converter (lasers and SOA) can be integrated, motivating the construction of a compact, optically-integrated, and rapidly reconfigurable all-optical wavelength converter. The wavelength converter consists of two tunable lasers as the pumps, an SOA and a tunable optical filter. The optical label of the incoming data packet is first recovered by the receiver [2], then the control signals are generated and used to switch the fast-tunable lasers to the required operating wavelengths to convert the incoming packet to the specified wavelength. After the nonlinear wavelength conversion process in the SOA, the converted signal is then filtered out by using a tunable optical filter and sent to the next network node. The switching speed of this wavelength converter mainly depends on the tunable pump lasers and the tunable optical filter, but in this work, we focus on the effect of the tunable laser.

Even though FWM-based wavelength conversion of advanced modulation formats such as QPSK and M-QAM formats have already been demonstrated in a static scenario [3-14], the implementation of wavelength conversion of higher order modulation format in a SOA employing a fast switching tunable laser as the pump, to enable fast reconfigurable wavelength conversion, has not yet been investigated. This chapter will investigate how the tunable lasers can be controlled to ensure that the incoming data packets can be converted to the required wavelength channel, and without degradation in signal performance.

In this chapter, a wavelength converter comprised of an SOA as the nonlinear element and a fast-switching sampled-grating distributed Bragg reflector (SGDBR) tunable laser as one of the pump sources is demonstrated. The performance of the SOA-based wavelength conversion of QPSK signal is investigated by simulation, and rapid wavelength conversion of single polarization QPSK and Pol-Mux-QPSK signals with switching time of 10's of nanoseconds using a fast switching tunable laser as one of the pumps in a dual wavelength pumping scheme is demonstrated experimentally. The simulation and experimental results indicate that the incoming signal can be precisely and quickly converted to the required wavelength channel on a nanosecond timescale. It is found that tracking the frequency offset during the polarization de-multiplexing

digital signal processing stage increases the waiting time from 50 ns for single polarization QPSK to 160 ns for PM-QPSK.

2.2 Simulation model and results for wavelength conversion system

Fig. 2-2 depicts the simulation schematic of SOA-based wavelength conversion of QPSK signals using a four section SGDBR laser as a single pump source. The input 10 Gbaud QPSK signal is created by initially generating a PRBS stream with every two consecutive bits being mapped to the QPSK symbols [1,j,–1,–j]. The generated optical QPSK signal is coupled with the optical output from the SGDBR laser and wavelength converted through degenerate FWM in the SOA. In [15, 16], the details of modelling wavelength conversion using SOAs based on interband carrier density pulsations, intraband carrier heating, and spectral hole burning effects are explained. The wavelength converted signal (idler) is then filtered out by using a Gaussian optical band pass filter and then the QPSK signal is detected using a coherent receiver.

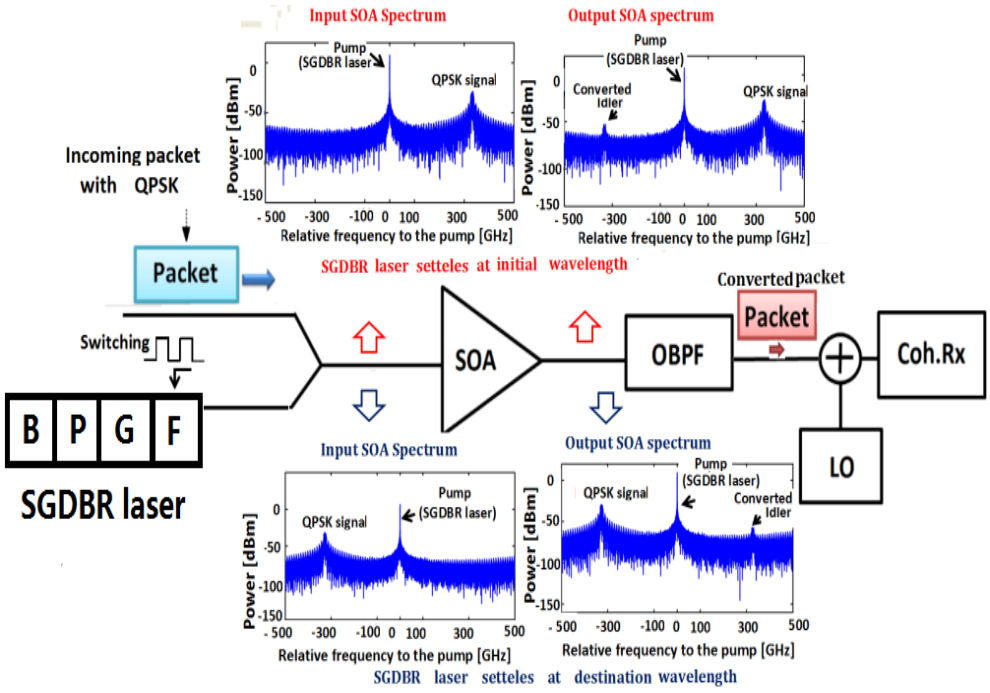

Fig.2-2 Schematic of SOA-based wavelength converter using SGDBR laser. The spectra at the top/bottom show the wavelength converter operating when the SG-DBR laser is at the wavelength of 1534.39/1539.66 nm. OBPF: optical band pass filter, LO: local oscillator, Coh.Rx: coherent receiver.

In [14], the static performance and transient behavior of SGDBR lasers by using the transfer matrix method (TMM) in combination with multimode rate equations were investigated. By solving the multimode rate equations, we can investigate the transient and static characteristics of the SGDBR laser and then combine the dynamic TMM SGDBR laser model with the wavelength convertor model, and hence estimate the performance of the wavelength converter under dynamic wavelength switching conditions. The multimode rate equations used to analyze the dynamic behavior of SGDBR lasers are [14]:

$$\frac{dS_m(t)}{dt} = v_g[\Gamma g(\omega_m, N_a) - \alpha_m] \times S_m(t) + n_{sp} v_g g(\omega_m, N_{ath}) \tag{2.1}$$

$$\frac{dN_a(t)}{dt} = \frac{I_a}{eV_a} - A_a N_a(t) - B_a N_a^2(t) - C_a N_a^3(t) - \sum_m v_g g(\omega_m, N_a) \times \frac{S_m(t)}{V_a} \tag{2.2}$$

$$\frac{dN_j(t)}{dt} = \frac{I_j(t)}{eV_j} - A_j N_j(t) - B_j N_j^2(t) - C_j N_j^3(t), j = f, b, p \tag{2.3}$$

Where $S_m(t)$ is the photon density of the m[th] longitudinal mode with angular frequency ω_m, α_m is the total loss of each mode, n_{sp} is the spontaneous emission coefficient , υ_g is the group velocity, I_a is the injection current on active section, V_a is the volume of the active section, $N_{a,f,b,p}$ are the carrier densities for different sections, $A_{a,f,b,p}$, $B_{a,f,b,p}$, $C_{a,f,b,p}$ stand for the non-radiative linear，the radiative bimolecular, and non-radiative auger recombination coefficient, respectively. The subscript *a*, *f*, *b* and *p* represent the active section, front grating , back grating and phase section respectively. $g(\omega_m, N_a)$ is the gain spectrum, Γ is the optical confinement factor of the gain section. The details about the laser parameters used in this work can be found in [14].

The SOA-based wavelength conversion system simulation platform has already been described in [15, 16] and is applicable for use within a dynamic switching simulation scenario. The only modification needed is to specify the optical field for the tunable pump laser using equation (2.1)-(2.3). In order to significantly reduce the

simulation run-time, a lumped time-domain SOA model operating on the slowly-varying envelope of the input optical field is implemented. The slowly varying envelope of the input optical field is:

$$E_{in} = \sqrt{P_P}\exp[\varphi_P(t)] + \sqrt{P_s}E_s(t)\exp(\Omega_s t) \tag{2.4}$$

Where $\sqrt{P_P}$ is the power of the pump (SGDBR laser), $\sqrt{P_S}$ is the average signal power and $\varphi_P(t)$ is the phase information of the pumps. The pump phase noise is modeled as a random Weiner process [17]. The detuning is defined as $\Omega_S = 2\pi(\omega_S - \omega_P)$ where ω is the optical frequency. The input optical field E_{in} is created using equation (2.4) and then the output field E_{out} is thus given by [18]:

$$E_{out}(t) = \exp\left\{\frac{1}{2}\left[-\alpha_{loss}L + (1+j\alpha_{cdp})h_{cdp}(t) + (1+j\alpha_{ch})h_{ch}(t) + h_{shb}\right]\right\}E_{in}(t) \tag{2.5}$$

With α_{loss} being the internal SOA losses, the gain phase coupling (linewidth-enhancement) factors for the carrier density, pulsations and carrier heating are given by $\alpha_{cdp}, \alpha_{ch}$. Further details about the simulator and parameters can be found in [15,16].

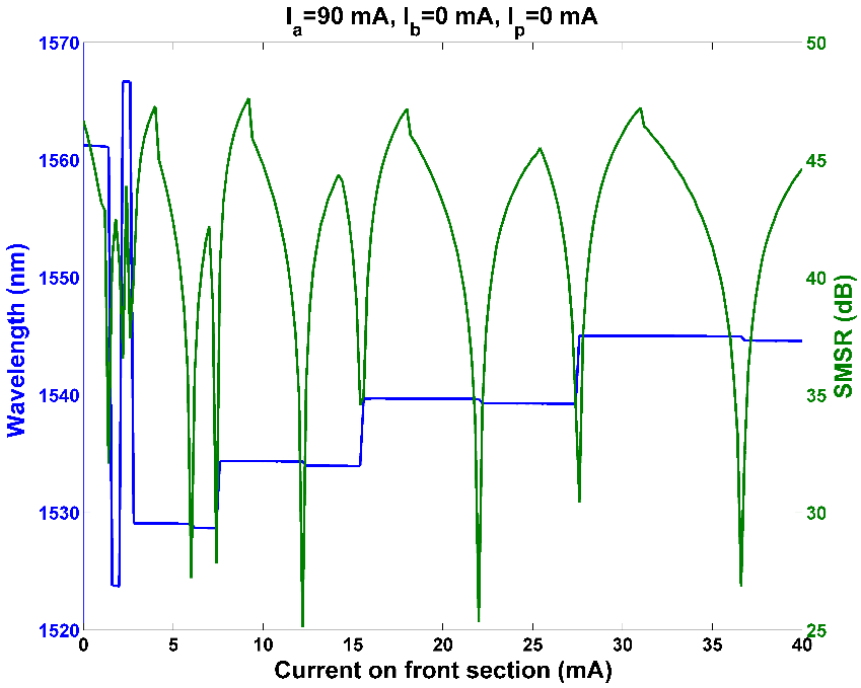

Fig. 2-3 Static wavelength tuning curves of the SGDBR laser as a function of current on front section

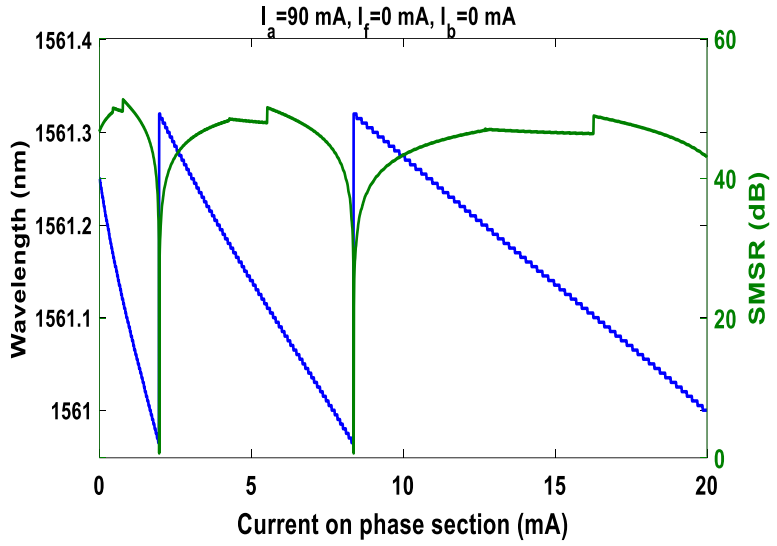

Fig. 2-4 Static side mode suppression ratio (SMSR) of four sections SGDBR laser as a function of current on phase section

In this simulation work, the switching signal applied to the front section or the phase section of the SGDBR laser was selected so that the laser was switched back and forth between two channels. The typical input and output spectra of the degenerate wavelength conversion scheme based on the fast switching tunable laser (SGDBR laser) at initial and destination wavelengths are shown in Fig.2-2. The input pump (SGDBR laser) power and linewidth are 10 mW and 5 MHz when the SGDBR laser is operating in static mode, and the average power of the QPSK signal is 100 μW at 10 Gbaud.

The static characteristics of the SGDBR laser were initially investigated with the model described in the simulator. Wavelength (blue line) and SMSR (green line) tuning curves as a function of the current on the front section and phase section are shown in Fig.2-3 and Fig.2-4. The currents applied to other sections are given on the top of each figure. As shown in Fig. 2-3, the current on the front section was changed from 0 mA to 40 mA, the laser wavelength can be changed roughly and it can provide a large wavelength tuning range by changing the current on the front grating section. By changing the current on the phase section, the laser wavelength can be tuned finely and continuously in a small wavelength tuning range. The wavelength tuning range using the phase section is ~0.4 nm, as shown in Fig.2-4.

In order to investigate the switching performance in the simulations, a square wave

with frequency of 5 MHz was applied to the front and phase sections. During the switching, the currents on the other sections were kept constant. The switching signal applied on the front section is shown in Fig. 2-5 by the green line. It switches the laser wavelength between 1534.39 nm and 1539.66 nm with current on the front section of If1=7.6 mA and If2=22 mA. Two super-modes (three different wavelength modes) can be observed from Fig.2-3 as the current on the front section increase from 7.6 mA to 22 mA. The switching time will vary between switching different wavelength channels, it will take a longer period for the switching with more number of modes between the initial and destination wavelength. The backward switching usually takes a longer period compare to the forward switching.

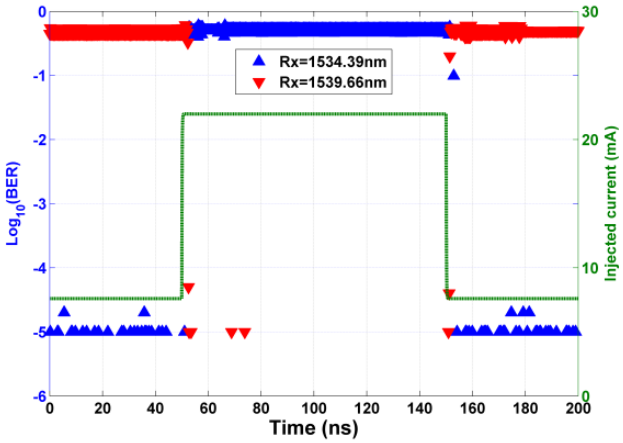

Fig.2-5 Time resolved bit error rate (TRBER) curves when switching signal applied to front section

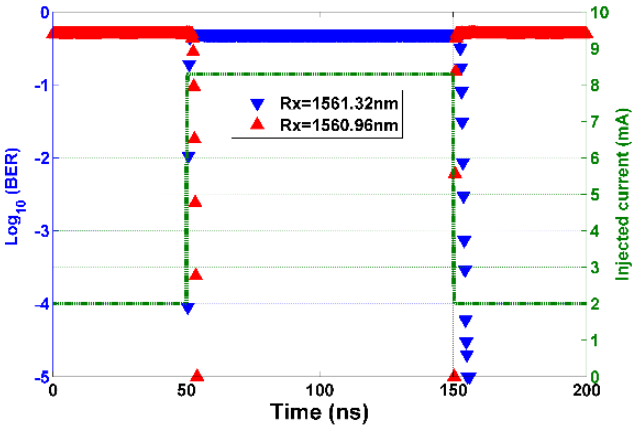

Fig.2-6 Time resolved bit error rate (TRBER) curves when switching signal applied to phase section

Changing the current on the phase section can tune the laser wavelength continuously in a small range. The switching signal applied on the phase section is

shown in Fig. 2-6 by the green line. It switches the laser wavelength between 1561.32 nm and 1560.96 nm with current on the phase section of Ip1=2 mA and Ip2=8.3 mA. To illustrate the time it takes for the wavelength conversion system (consisting of the tuneable SGDBR pump laser and SOA-based wavelength convertor) to transition from error free performance on the initial wavelength channel that the QPSK signal is converted to, to error free performance on the destination wavelength channel that the QPSK signal is converted to, we applied the time-resolved bit error rate (TRBER) measurement through simulation [19]. Fig.2-5 shows the TRBER when the switching signal was applied to the front section. Initially the TRBER measurement was characterized for the initial wavelength channel (1534.39 nm) that the input signal is switched to by fixing the center frequency of the optical filter at the initial wavelength. The optical tunable filter has a bandwidth of 0.1 nm. In this simulation result, each data point in the TRBER curves corresponds to the probability of receiving an error in the 100 ps symbol period, with the data presented being recorded by receiving data for a large number of laser switching events. The process was then repeated for the 1539.66 nm channel. It can be seen that the time taken for the initial and destination wavelength channels to have a BER of better than 10^{-5} is different with the 1534.39 nm and the 1539.66 nm channels taking 2.8 ns and 4.2 ns, respectively. Fig.2-6 shows the TRBER when the switching signal was applied to the phase section. The time taken for the wavelength convertor to reconfigure in this case is 4 ns and 5.4 ns for the initial (1561.32 nm) and destination (1560.96 nm) wavelength channels, respectively.

In this section, we demonstrated a dynamic theoretical model for a SOA-based FWM wavelength conversion system using a fast switching tunable SGDBR laser as the pump. The TRBER simulation results show that the wavelength conversion system can achieve a BER of $<10^{-5}$ in several nanoseconds after the switching event which makes it possible to use the tunable lasers as the pump laser to build fast reconfigurable wavelength convertors for reconfigurable, and bandwidth efficient next generation optical networks.

2.3 Experimental demonstration of reconfigurable wavelength conversion employing tunable SGDBR lasers

To investigate the use of tunable lasers in all-optical wavelength conversion system, static characteristics of the tunable laser including the wavelength tuning range, output power and SMSR will need to be taken into account. The switching speed of the tunable pump laser is also an important parameter, which would limit the reconfiguration time of the all-optical wavelength converter. The phase noise issue of the tunable lasers also needs to be studied in order to achieve the wavelength conversion of advanced modulation formats with the required system performance.

In this section, the characterization of different tunable lasers including the SGDBR laser, and MGY laser were studied. The wavelength change as a function of the current on each section of the tunable lasers was initially presented, and then the phase noise characterization was studied by using a coherent phase noise measurement technique. The linewidths of the MGY laser and SGDBR laser with different grating reflector and phase section currents are measured and presented in the same figures for comparison. Finally, the dynamic characterization results of the MGY laser and SGDBR lasers were presented. The results show that the SGDBR laser present better phase noise performance compare to MGY laser, which makes it more suitable to be used in the wavelength conversion system due to the phase noise transfer that occurs from the pump to the idler in the FWM process.

2.3.1 Tunable laser characterization

The SGDBR laser has four separate sections: gain, front grating, rear grating and phase as shown in Fig.2-7(a). The gain section produces light, whereas the front, rear and phase sections enable wavelength tuning. Course tuning of the wavelength can be realized by changing the current on the front section and back section. The lasing wavelength can be tuned continuously and precisely by changing the current on the phase section. Due to the period of the two gratings being sampled differently, each grating has a different period of reflection maxima as a function of wavelength.

Therefore, the Vernier effect is enabled and enhances the overall tuning range considerably. The function of the phase section is to allow the cavity modes to be shifted independently of the grating's reflection peak, achieving continuous tuning. As the data is modulated on the phase of the laser in the transmission systems employing advanced modulation formats, the phase noise of the lasers becomes an important factor in determining the transmission performance [20]. For the SGDBR laser, both the gain section and the passive tuning sections can contribute to the overall phase noise of the laser [21]. In order to characterize the phase noise of the SGDBR laser, the frequency modulation (FM) noise spectrum, which has been proved to be a very suitable measurement of the phase noise of lasers to be employed in coherent systems [22], can be obtained by the technique using a coherent receiver with a narrow-linewidth LO [23]. Fig. 2-7(b) is the typical frequency modulation (FM) noise spectrum of the SGDBR laser. The phase noise result was measured by using a coherent setup [23], a 3 GHz bandwidth low pass filter was applied to reduce the Gaussian noise in the measurement setup at high frequency. The white noise from the gain section and low frequency carrier noise from the passive tuning sections are observed.

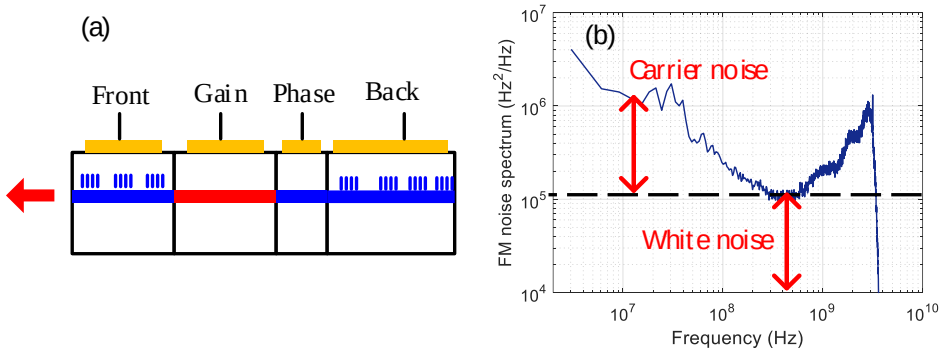

Fig. 2-7 (a) Structure of the SGDBR laser, (b) FM noise spectrum of the SGDBR laser

Due to the advance in digital signal processing (DSP), the low frequency excess phase noise can be compensated. A 2nd-order PLL scheme has been used in the carrier phase estimation to track the excess phase noise [24], which presents the ability to employ fast tunable lasers for coherent communication system with higher order modulation formats.

Fig.2-8 shows the static tuning map of the wavelength and SMSR of the SGDBR laser. The phase current and the gain current are set to 0 mA and 90 mA respectively. The maximum currents on the front and back gratin sections are 30 mA and 40 mA respectively. It can be seen from Fig.2-8 that the SGDBR laser can offer >40 nm wavelength operating range, and the SMSR above 45 dB can be achieved easily.

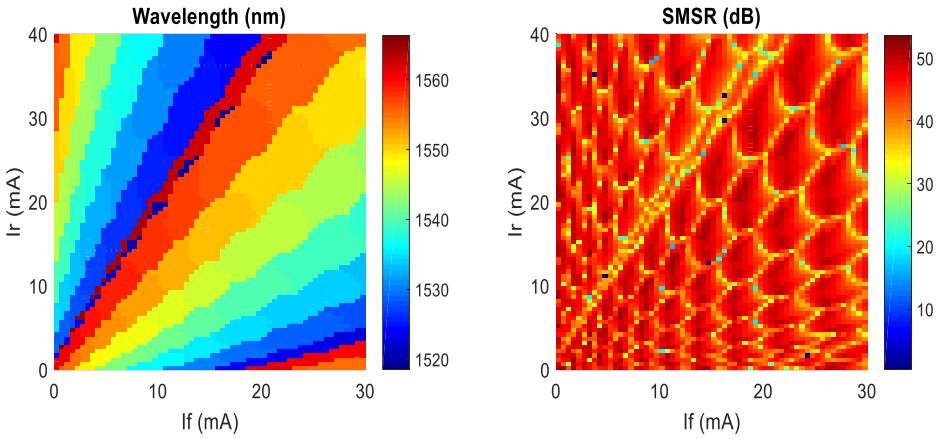

Fig.2-8 Measured static tuning map of SGDBR lasers versus front (If) and back (Ir) grating currents

The tuning mechanism of the MGY is similar to an SG-DBR laser using the Vernier effect. Fig.2-9 shows the wavelength and SMSR tuning map of a five-section MGY laser consisting of gain, front, back, phase and SOA sections. The SOA section is used to amplify the light. The currents on the gain, phase and SOA sections are kept at 90 mA, 0 mA and 100 mA, respectively. From Fig.2-9, it can be observed that similar performance in terms of the wavelength tuning range and SMSR is achieved compare to the SGDBR laser.

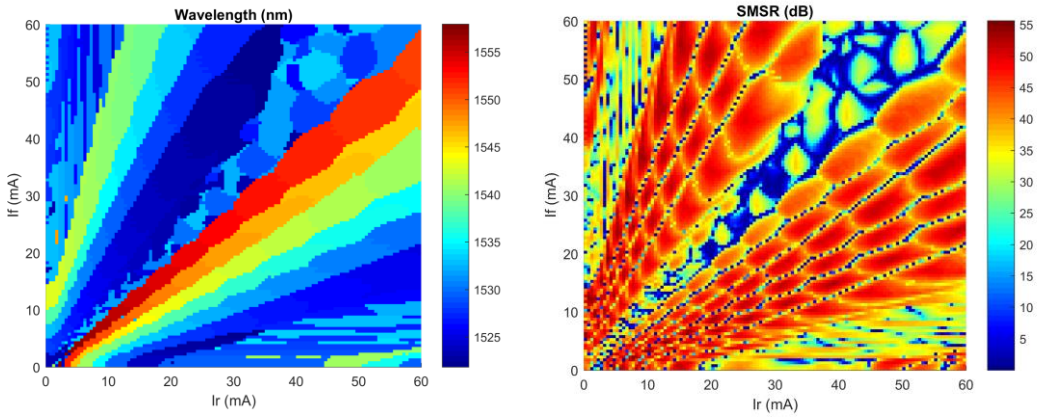

Fig.2-9 Measured static tuning map of MGY lasers versus front (If) and back (Ir) grating currents

The phase noise of the MGY laser was measured and compared with the results of the SGDBR laser. The same amount of current (90 mA) was applied on the gain section of both lasers, and the same operating conditions were applied on both lasers with 7 mA for one of the grating reflector and the other passive sections were terminated. The measurements were performed by using a coherent phase noise measurement technique. From the captured data, the FM-noise spectra of the MGY laser and the SGDBR laser were obtained and plotted in Fig.2-10. It should be noted that a 3 GHz low-pass filter was used in the analysis to suppress the additive white Gaussian noise (AWGN) from the receivers. It can be seen from Fig.2-10, the MGY laser presents an overall worse phase noise performance compare to the SGDBR. The high frequency (~1 GHz) white noise of the SGDBR is around several hundred KHz while the MGY laser shows over 1MHz. The SGDBR laser also shows less 1/f noise at low frequency (< 100 MHz) which makes it more suitable for wavelength conversion systems.

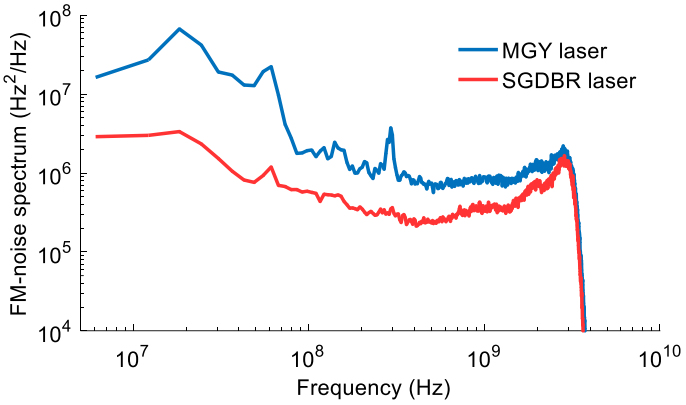

Fig.2-10 Measured FM-noise spectra of the MGY laser and SGDBR laser with the same injected condition: 7 mA for one of the grating reflector and other passive sections are terminated.

The phase noise of the tunable laser is strongly dependent on the injection currents on each section, the linewidth varies between several 100's kHz to several MHz with different injected currents. The output wavelength and phase noise of the SGDBR laser as a function of the injected currents in the front section were measured and shown in Fig.2-11, with 90 mA current on the gain section, 0 mA current on the phase and back section. The white noise and carrier noise are represented by the high frequency linewidth and low frequency linewidth, which are calculated from the FM-noise

spectrum by the simple equation: $\Delta\nu = \pi \cdot S_0$ [25]. The high frequency linewidth is related to the FM noise level in the frequency range beyond 500 MHz, whereas the low frequency linewidth contributed by the passive tuning sections is extracted by the mean value of the FM-noise in the frequency range under 50MHz. It can be observed from Fig.2-11, by changing the currents into a grating section, the entire reflection comb of the grating section shifts in wavelength and the laser wavelength jumps not only to an adjacent longitudinal mode, but can also jump by several nm to another super-mode at a wavelength where the reflection peaks of the Vernier-tuned gratings have re-aligned. By increasing the currents on the grating section, the low frequency linewidth and high frequency linewidth were found to present an opposite trend. The low frequency linewidth usually increases until the wavelength jump occurs, while the high frequency linewidth increases until the mode jump occurs. As most low frequency phase noise can be compensated by the DSP, the operation points of the SGDBR laser with less high frequency noise are preferred to perform data transmission experiments. According to these linewidth measurements results, two wavelengths of the SGDBR laser were chosen to switch between for the later wavelength conversion experiment. The 1548.68 nm wavelength of the SGDBR which is represented by the black point A shown in Fig.2-11, is chosen by applying 90 mA current on the gain section while the other passive tuning sections are terminated. The 1553.70 nm wavelength (point B) is chosen by increasing the current on the front section to 3.4 mA.

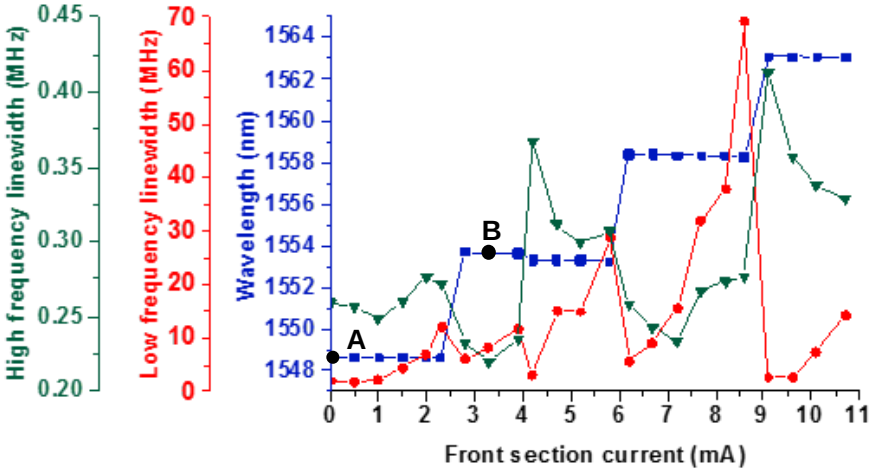

Fig.2-11 Measured high frequency linewidth (green triangles), low frequency linewidth (red dots) and output wavelength (blue squares)with different currents on the front section of the SGDBR laser, with 90 mA current on the gain section, 0 mA current on the phase and back section.

The switching performance of the SGDBR laser and the MGY laser were also investigated. Throughout the measurements, the currents on the gain section of the SGDBR laser and the MGY laser were set to 90 mA. The same switching signal was applied to the front grating section of the SGDBR laser and to the left grating section of the MGY laser. The other sections of the SGDBR laser and the MGY laser were terminated. Fig.2-12 shows the frequency offset between the tunable laser and the local oscillator at the coherent receiver, as a function of time after a switch for the Y-branch (MGY) and SGDBR laser. Fig.2-13 shows the linewidth change as a function of time after a switch for the Y-branch (MGY) and SGDBR laser. The sampling rate of the digital scope was set at 50 GSa/s, which gave a time resolution of 20 ps.

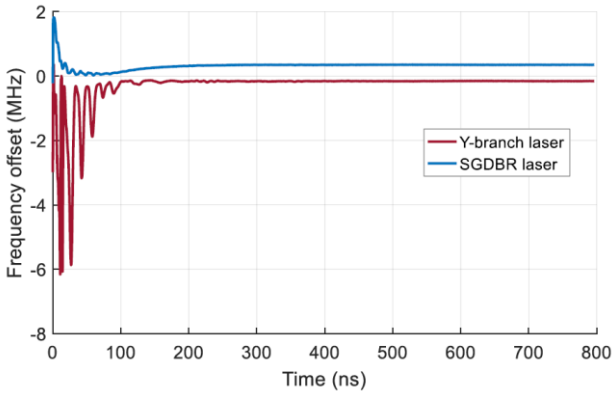

Fig.2-12 Frequency offset as a function of time after a switch for the Y-branch (MGY) and SGDBR laser

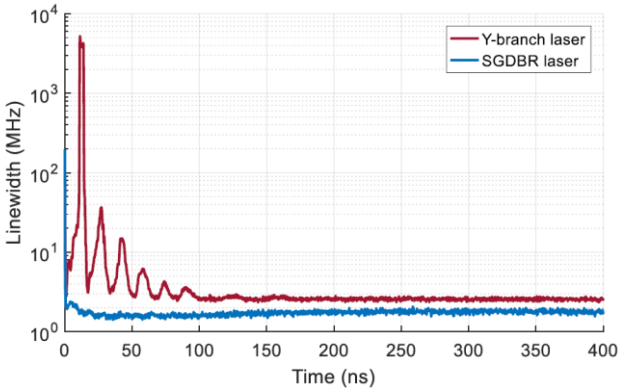

Fig.2-13 Dynamic linewidth change as a function of time after a switch for the Y-branch (MGY) and SGDBR laser

It can be seen from these figures that the reconfiguration time (defined as the time

it takes for the laser to be stable again after the switch) of both lasers is under 100 ns, and it takes longer time for the MGY laser to be stable compare with the SGDBR laser due to the impedance mismatch between the switching signal generator and the MGY section. It is also noted that the switching speed is limited by the rise time of the switching signal from the signal generator. Overall, the SGDBR outperforms MGY laser and is more suitable for use in the wavelength conversion experiments.

2.3.2 Fast reconfigurable wavelength conversion experiment

Fig. 2-14 depicts the schematic of the experimental setup of SOA-based wavelength conversion of QPSK and PM-QPSK (blue dashed) signals using a SGDBR laser as one of the pump sources. A narrow linewidth external cavity laser (ECL) was used as the signal source and it was modulated with QPSK data at 12.5-Gbaud using an IQ modulator. The optical QPSK signal was generated by programming the arbitrary waveform generator (AWG) with two uncorrelated pseudo-random bit sequences (PRBS) of 2^7-1 bits periodicity. The AWG operated at 25 GSa/s which gave 2 Sa/Symbol for the 12.5-Gbaud signal. The two PRBS signals were amplified by using the radio frequency amplifiers (RF) to drive the IQ modulator.

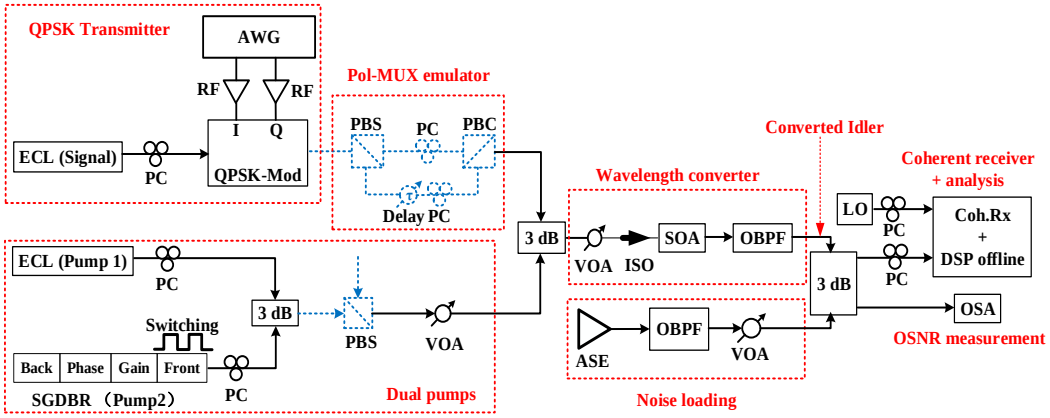

Fig.2-14 Schematic of the reconfigurable SOA-based wavelength conversion of QPSK and PM-QPSK (blue dashed) signals employing a SGDBR pump laser. PC: polarization controller, PBS: polarization beam splitter, PBC: polarization beam combiner, OBPF: optical band-pass filter, ISO: isolator, ASE: noise source, VOA: variable optical attenuator, OSA: optical spectrum analyzer, LO: local oscillator, Coh.Rx: coherent receiver.

For the wavelength conversion of QPSK signal, the generated optical QPSK signal was then coupled with two pumps (one SGDBR laser and one narrow linewidth ECL)

and sent into the SOA-based wavelength converter. For the wavelength conversion of PM-QPSK signal scheme, the PM-QPSK signal was generated by using a Pol-Mux emulator, consisting of a polarization beam splitter (PBS) at its input, a passive stage with a delay of 4.88 ns (61 symbols), two polarization controllers and a polarization beam combiner (PBC) to combine the polarization tributaries. The output of the two pumps were passed through polarization controllers, combined and polarization aligned using a 3 dB coupler and a PBS. For both schemes, the power of the signal and the pumps at the input of the SOA are -10 dBm and 0 dBm respectively for optimum conversion efficiency [26]. The signal wavelength underwent wavelength conversion through non-degenerate FWM in the SOA operating at 500 mA bias current.

The wavelength converted idler was filtered out by using a tunable optical bandpass filter (OBPF). The optical signal to noise ratio (OSNR) of the idler was changed by adding amplified spontaneous emission (ASE) from an EDFA that passed through a 2 nm bandwidth tunable optical bandpass filter. The filtered idler was then passed through a 3 dB splitter with one arm sent to the OSA for measuring the OSNR, and the other arm was passed into the polarization diversity coherent optical receiver and captured by a real-time oscilloscope sampling at 50GSa/s for offline DSP processing. The received idler power at the input of the coherent receiver was maintained at -19 dBm. The data captured from the real-time scope was first resampled to 2 samples per symbol using a priori knowledge of the clock frequency. Then the constant modulus algorithm (CMA) [27-29] was utilized to enable polarization de-multiplexing for PM-QPSK signal. An m^{th} power frequency offset compensation method [30-32] was employed to compensate the frequency offset between the received signal and the local oscillator in the coherent receiver, with m=4 being the number of distinct phases in the QPSK symbol set. In order to make this algorithm operate correctly, it was necessary to ensure that the value of the absolute frequency offset is always less than Rs/(2M), where Rs is the symbol rate. A second order PLL is employed for the phase noise estimation and a training symbol based synchronization [33] was employed in order to carry out the BER calculation.

2.3.3 Results and discussion

The wavelength of the fast-tuning SGDBR pump laser was switched between two operating modes by applying a switching signal to the wavelength tuning sections. In order to benchmark the system performance, the BER performances when pump2 was tuned and fixed to the two wavelengths that pump2 would later be dynamically switched between, was initially measured. The wavelength and power of the signal and pump1 (ECL) were kept constant throughout. The input and output spectra of the SOA when the SGDBR laser was set at 1548.68 nm and 1553.70 nm are shown in Fig.2-15(a) and Fig.2-15(b), respectively, and it can be observed that the indicated idler of interest has changed wavelength position from Ch 1 (1541.395 nm) to Ch 2 (1538.684 nm). The conversion efficiency was about -17.6 dB as shown in Fig. 2-15 (a), and -24.2 dB in Fig.2-15 (b).

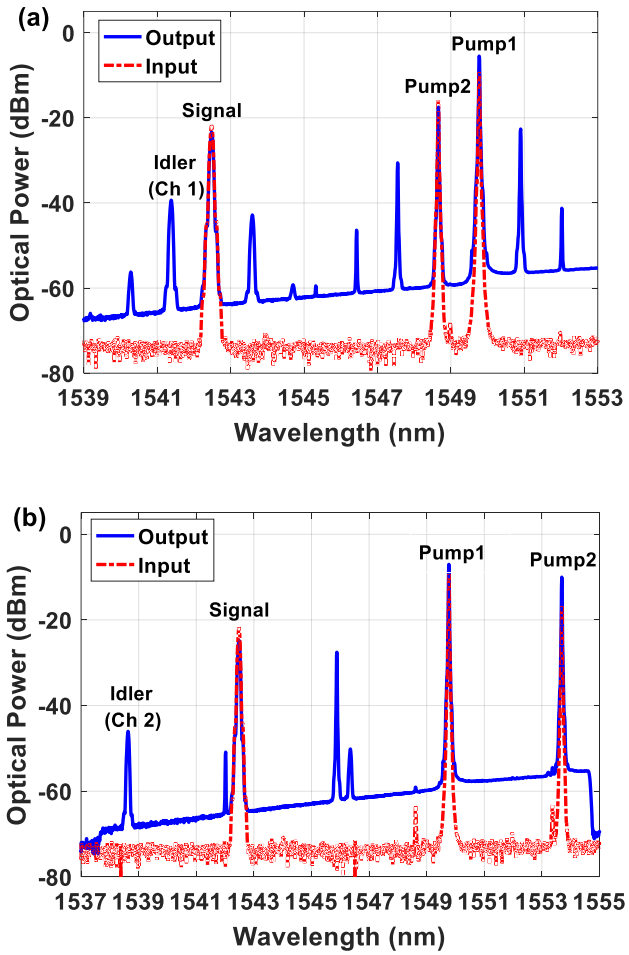

Fig.2-15 Input and output spectra of SOA showing the spectral locations of the signal (ECL), pump1 (ECL), pump2 (SGDBR) and converted idlers. (a) SOA input and output spectra when SGDBR is set at 1548.68 nm. (b) SOA input and output spectra when SGDBR is set at 1553.70 nm. The detected idlers are indicated.

BER performance as a function of OSNR at the receiver for the original signal, the signal after SOA and converted signals (idlers) for the QPSK and PM-QPSK signals at 12.5 GBaud are displayed in Fig. 2-16(a) and Fig. 2-16(b), respectively. It can be observed that the penalty between the original signal, the signal after SOA and wavelength converted idler is under 0.5 dB for both cases, indicating the quality of the wavelength conversion scheme and potential usefulness. The constellation diagrams of the wavelength converted idler for a received OSNR of 12 dB and 14.5 dB are also given in Fig. 2-16(a) and Fig. 2-16(b), respectively. The laser employed for the LO and pump1 have a linewidth of around 50 kHz and the linewidth of the 1548.68 nm and 1553.70 nm wavelengths of the SGDBR laser (employed as the second pump for FWM

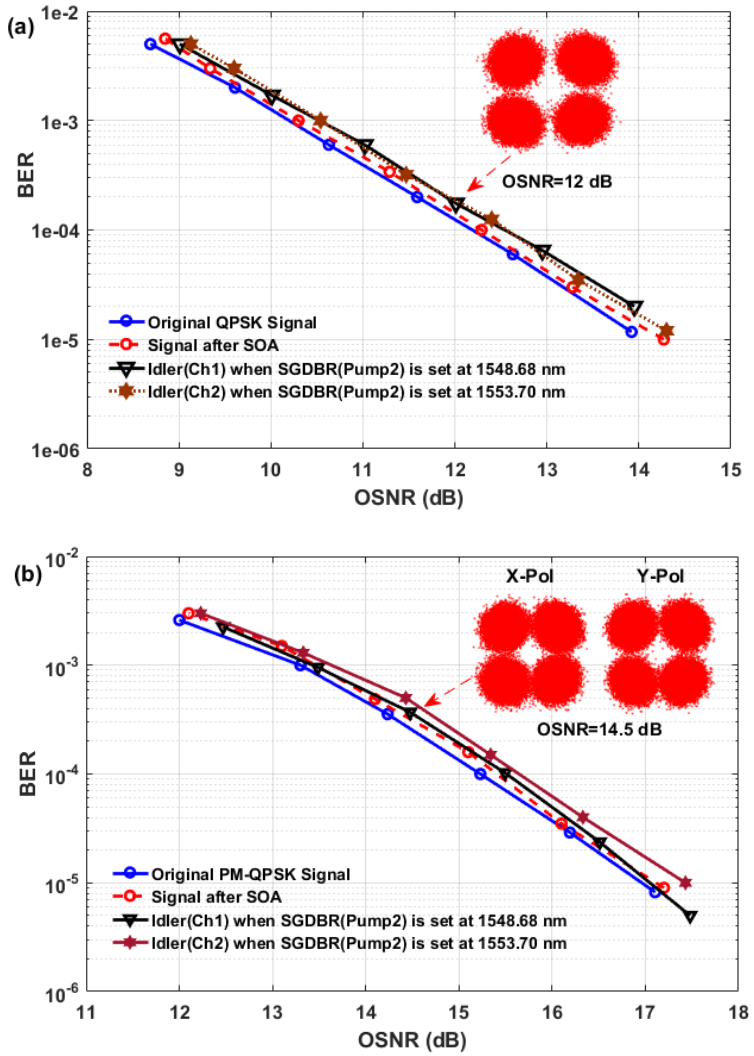

Fig.2-16 (a) BER versus OSNR curves for the input original signal, the signal after SOA, and the converted idlers for 12.5 GBaud QPSK signal . (b) BER versus OSNR curves for the input original signal, the signal after SOA, and the converted idlers for 12.5 GBaud PM-QPSK signal.

scheme) was measured to be 260 kHz and 210 kHz, respectively. The linewidth (from the high frequency phase noise region) of the idlers was measured to be around 370 kHz and 300 kHz as expected when the SGDBR was set to the two operating modes since the idler linewidth is the sum of the linewidths of the pumps and signal, and in this case the linewidth of the SGDBR pump laser dominates.

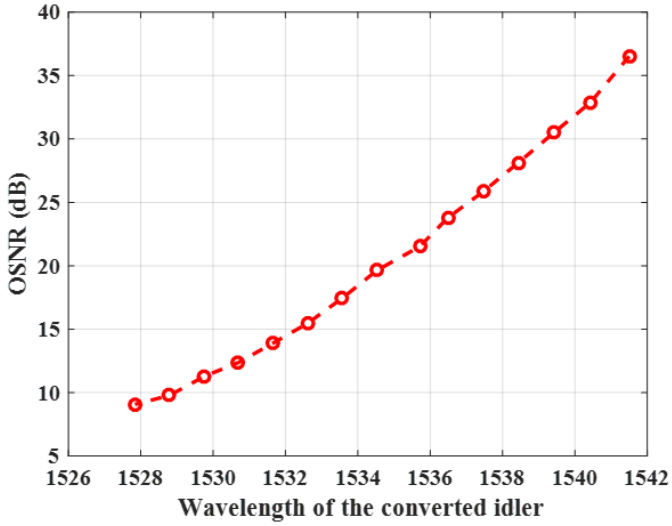

Fig.2-17 OSNR as a function of the wavelength of the converted idler.

To calculate the limitations of the wavelength conversion scheme, the OSNR of the idler as a function of the detuning between the two pumps was studied. The different wavelength converted idlers were filtered out by using an optical tunable band-pass filter. The OSNR measurement was then undertaken by using the OSA. In order to estimate the signal power and the noise floor correctly, the solution is to take two consecutive sweeps of the OSA with different resolution bandwidth (RBW) settings [34]. For the first sweep, OSA 0.2 nm RBW was used for the measurement of the signal power, and the second sweep measured the noise power by using 0.1 nm RBW setting. The output OSNR of the idler wavelength for the case with signal fixed at 1542.5 nm, pump1 fixed at 1549.8 nm, and the pump2 (SGDBR) tuned from 1548.7 nm to 1564.7 nm is displayed in Fig.2-17. Fig. 2-17 shows that a tuning range of around 14 nm can be achieved with more than 9 dB OSNR and ~11 nm tuning range can be achieved with more than 12 dB OSNR. By comparing the results in Fig. 2-16 and Fig. 2-17, we can find that ~14 nm tuning range can be achieved for the wavelength conversion of the QPSK data at 12.5Gbaud to get a BER value below the 7% FEC limit (3.8×10^{-3}) [35]. Around 11 nm tuning range can be achieved for the wavelength conversion of PM-

QPSK data to get a BER value below the 7% FEC limit.

In order to investigate the time-resolved BER [36,37] performance of the fast-reconfigurable wavelength converter, a square wave current with 500 kHz repetition rate was applied to the front section of the SGDBR to switch the wavelength converted idler between Ch1 (1541.395 nm) and Ch2 (1538.684 nm), with the other currents applied to the SGDBR laser held constant and the received OSNR set at 12 dB for the QPSK signal and 14.5 dB for the PM-QPSK signal. The time-resolved BER measurement was characterized for Ch1 by fixing the center frequency of the OBPF to Ch1 and adjusting the LO to the wavelength of Ch1. The process was then repeated for Ch 2.

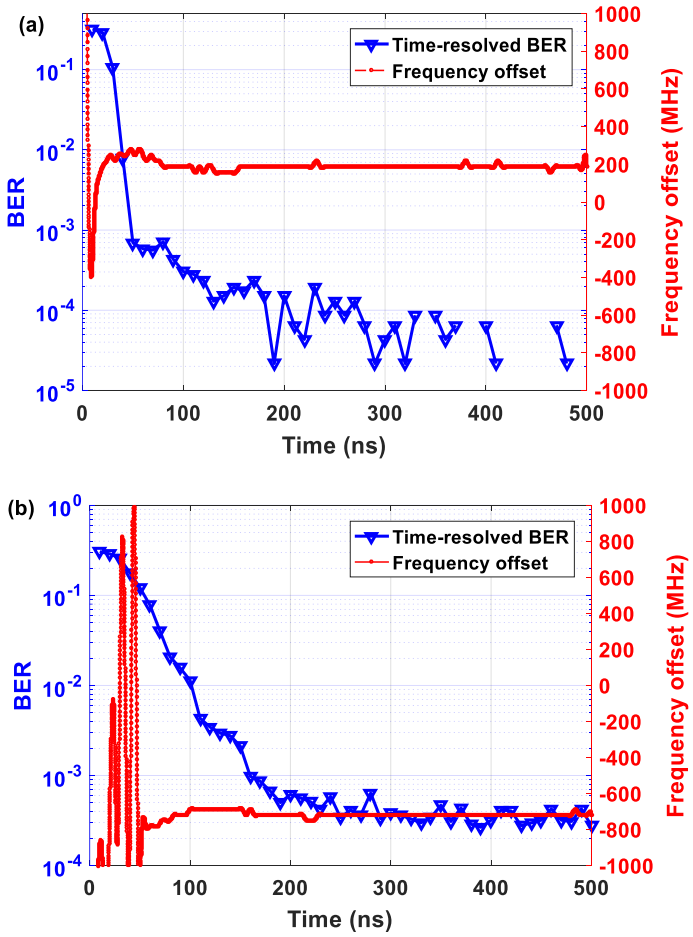

Fig.2-18 Time-resolved BER and frequency offset curves for (a) QPSK signal and (b) PM-QPSK signal at 12.5-GBaud, when the wavelength of the received signal (idler) is set at Ch1.

The results of wavelength conversion will be presented when pump2 is dynamically tuned between 1547.68 nm and 1553.7 nm. In order to accurately estimate the time-resolved BER performance after a switching event, a number of switching events were captured via multiple acquisitions using the real-time scope. Each data

point in the time-resolved BER curves corresponds to the probability of receiving an error in a 10 ns period. This means the BER is averaged over a block length of 125 symbols (10 ns), and data captured from 200 switching events was used for the calculation, with a total of 5×10^4 bits and 10^5 bits used for calculating each BER point in the time-resolved BER curves for QPSK and PM-QPSK signal at 12.5 GBaud. It can be seen from Fig.2-18(a) and Fig.2-18(b) that the reconfiguration time (time to have a BER better than the 7% FEC limit) after a switch is approximately 50 ns and 160 ns for QPSK and PM-QPSK signal, respectively. The red curves in Fig.2-18(a) and Fig.2-18(b) show the temporal frequency offset between the idler and the local oscillator in the coherent receiver, after a switching event. It takes around 100 ns for the frequency of the wavelength converted idler to fully stabilize after a switch.

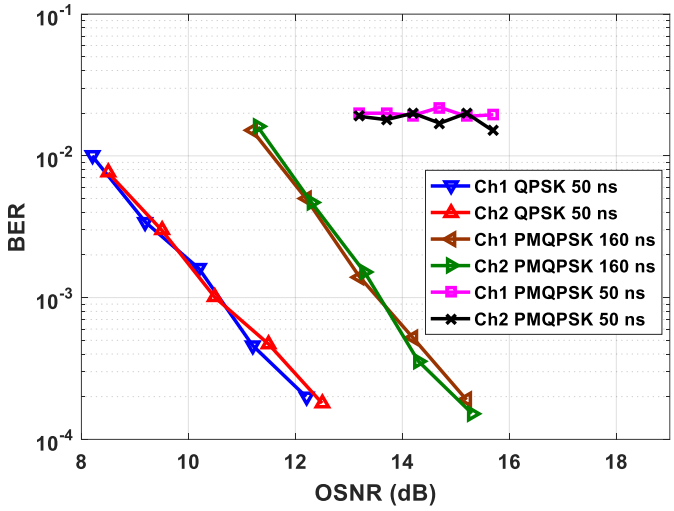

Fig.2-19 BER measurement as a function of OSNR in a switching environment with different waiting time after wavelength conversion when using QPSK and PM-QPSK decoding.

Fig.2-19 shows the BER measurement as a function of OSNR in a switching environment with different waiting time after the idler is switched to Ch1 and Ch2 when using QPSK and PM-QPSK decoding. The blue and red curves show the results for the data with a waiting time of 50 ns after switching when using QPSK decoding for Ch1 and Ch2, respectively. The brown and green curves are for a 160 ns waiting time when using PM-QPSK decoding for Ch1 and Ch2, respectively. The pink and black curves show the bad performance with a 50 ns waiting time using PM-QPSK decoding for Ch1 and Ch2, respectively. The required waiting time when using PM-QPSK decoding is longer than QPSK decoding mainly due to the longer convergence time associated with the CMA method used for de-multiplexing the dual-polarization packets.

It also can be seen that the BER versus OSNR performance in a switching scenario corresponds with the static performance shown in Fig.2-16(a) and Fig.2-16(b), which indicates that the incoming signal can be precisely and quickly converted to the required channel on a timescale of around 50 ns and 160 ns for the 12.5-GBaud QPSK and PM-QPSK signal by using the wavelength converter we present.

2.4 Conclusion

In this chapter, an SOA-based FWM wavelength conversion system using a fast switching tunable SGDBR laser and a narrow linewidth ECL as the pumps was studied by simulation and experiments. Different types of tunable laser were characterized and the SGDBR proved to be the best option among the tunable lasers for the use in fast reconfigurable wavelength converters. According to phase noise and polarization studies, the efficient and impairment free SOA-based wavelength converter based on FWM was designed. A rapidly reconfigurable SOA-based FWM wavelength conversion system using a fast switching tunable SGDBR laser as one of the pumps was demonstrated and the wavelength conversion of QPSK and Pol-Mul QPSK signals at 12.5-Gbaud, with total data rates of 25 Gbps and 50 Gbps, respectively, using the proposed scheme was experimentally studied. Wide tuning range (> 10 nm) and fast wavelength conversion time under 50 ns and 160 ns were achieved for the proposed reconfigurable wavelength conversion system for QPSK and PM-QPSK signals, respectively**.** The reconfiguration time was mainly affected by the combination of the switching time of the tunable pump laser and the CMA convergence time in DSP. The performance under the switching environment after the required reconfiguration time was the same as the static case when the wavelengths were fixed. The results show that it is feasible to develop fast reconfigurable wavelength converters for dynamic, adaptive and bandwidth efficient optical networks by using rapid switching tunable pump lasers in conjunction with fast tuning optical filters.

References

[1] G. Contestabile, L. Banchi, M. Presi, E. Ciaramella, Investigation of transparency of FWM in SOA to advanced modulation formats involving intensity phase and polarization multiplexing, J. Lightw. Technol., vol. 27, no. 19, pp. 4256-4261, Oct. 2009.

[2] N. Calabretta, All-optical label swapping of scalable in-band address labels and 160 Gb/s data packets, J. Lightw. Technol., vol. 27, no. 3, pp. 214-223, Feb. 2009.

[3] A. Anthur, R. T. Watts, J. O'Carroll, D. Venkitesh, L. P. Barry, Dual correlated pumping scheme for phase noise preservation in all-optical wavelength conversion, Opt. Express, vol. 21, no. 13, pp. 15568-15579, 2013.

[4] S. P. O Duill et al., All-optical Wavelength Conversion of Spectrally-Efficient Modulation Formats for Future Networks, (Invited) Proc. of Communication Systems Networks & Digital Signal Processing, pp. 28-33, 2014.

[5] H. Hu, R. M. Jopson, A. H. Gnauck, M. Dinu, S. Chandrasekhar, C. Xie, S. Randel, Parametric amplification wavelength conversion and phase conjugation of a 2.048-Tbit/s WDM PDM 16-QAM signal, J. Lightw. Technol., vol. 33, no. 7, 2015.

[6] S. T. Naimi, S. P. Ó Dúill, L. P. Barry, Simulations of the OSNR and laser linewidth limits for reliable wavelength conversion of DQPSK signals using four-wave mixing, J. Opt. Commun., vol. 310, no. 1, pp. 150-155, 2014.

[7] S. P. Ó Dúill, S. T. Naimi, A. P. Anthur, T. N. Huynh, D. Venkitesh, L. P. Barry, Numerical generation of laser-resonance phase noise for optical communication simulators, Appl. Opt., vol. 54, no. 11, pp. 3398-3406, 2015.

[8] A. P. Anthur, R. T. Watts, R. Zhou, P. Anandarajah, D. Venkitesh, L. P. Barry, Penalty-free wavelength conversion with variable channel separation using gain-switched comb source, Opt. Commun., vol. 324, pp. 69-72, 2015.

[9] A. P. Anthur, R. T. Watts, S. P. O'Duill, R. Zhou, D. Venkitesh, L. P. Barry, Impact of nonlinear phase noise on all-optical wavelength conversion of 10.7 GBaud QPSK data using dual correlated pumps, IEEE J. of Quantum Electron., vol. 51, no. 4, pp. 9100105, 2015.

[10] B. Filion, W. C. Ng, A. T. Nguyen, L. A. Rusch, S. LaRochelle et al., Wideband wavelength conversion of 16 Gbaud 16-QAM and 5 Gbaud 64-QAM signals in a semiconductor optical amplifier, Opt. Express, vol. 21, no. 17, pp. 19825-19833, 2013.

[11] G. Contestabile, Y. Yoshida, A. Maruta, K-I. Kitayama, Coherent wavelength conversion in a quantum dot SOA, IEEE Photon. Tech. Lett., vol. 25, no. 9, pp. 791-794, 2013.

[12] L. Krzczanowicz, M. J. Connelly, 40 Gb/s NRZ-DQPSK data all-optical wavelength conversion using four wave mixing in a bulk SOA, IEEE Photon. Technol. Lett., vol. 25, no. 24, pp. 2439-2441, 2013.

[13] S. T. Naimi, S. P. Ó Duill, and L. P. Barry, All Optical Wavelength Conversion of Nyquist-WDM Superchannels Using FWM in SOAs, J. Lightwave Technol., vol. 33, no. 19, pp. 3959-3967, 2015.

[14] K.Shi, Y. Yu, R. Zhang, W. Liu, L. P. Barry ”Static and dynamic analysis of side-mode suppression of widely tunable sampled grating DBR (SG-DBR) lasers”, J. Opt. Commun., vol. 282, no. 1, 2009.

[15] S. T Naimi, S. P. O Duill, and L.P. Barry, “Detailed Investigation of the pump phase noise tolerance for the wavelength conversion of 16-QAM signals using FWM,” IEEE/OSA J. Opt. Commun. Netw, vol. 6, no. 9, pp. 793–800, 2014.

[16] S. P. O Duill and L. P. Barry, “Improved reduced models for single-pass and reflective semiconductor optical amplifiers,” J. Opt. Commun., vol. 334, no. 1, pp. 170–173, 2015.

[17] D. Marcuse, “Computer simulation of FSK laser spectra and of FSK-to-ASK conversion,” J. Lightwave Technol., vol. 8, no. 7, pp. 1110–1122, 1990.

[18] S. P. Ó Dúill, S. T. Naimi, A. P. Anthur, T. N. Huynh, D. Venkitesh, L. P. Barry, Simulations of an OSNR limited wavelength conversion scheme, IEEE Photon. Technol. Lett., vol. 25, no. 23, pp. 2311-2314, 2013.

[19] Mishra, Arvind K., Time-resolved linewidth measurements of a wavelength switched SG-DBR laser for optical packet switched networks, Proc. OFC, USA, paper OTuC4. 2008.

[20] M. Seimetz, Laser linewidth limitations for optical systems with high-order modulation employing feed forward digital carrier phase estimation, Proc. OFC, San Diego, USA, paper OTuM2, 2008.

[21] Z. Jialin, Z. Huijuan, L. Fan, and Y. Yonglin, Numerical Analysis of Phase Noise Characteristics of SGDBR Lasers, J.Sel. Top. Quantum Electron., vol. 21, no. 6. pp. 1502009, 2015.

[22] S. Camatel and V. Ferrero, Narrow linewidth CW laser phase noise characterization methods for coherent transmission system applications, J. Lightw. Technol., vol. 26, no. 17, pp. 3048–3054, 2008.

[23] Kazuro Kikuchi, Characterization of semiconductor-laser phase noise and estimation of bit-error rate performance with low-speed offline digital coherent receivers, Opt. Express, vol. 20, no. 5, pp. 5291-5302 2012.

[24] T. N. Huynh, A. T. Nguyen, W. C. Ng, L. Nguyen, L. A. Rusch, and L. P. Barry, "BER Performance of Coherent Optical Communications Systems Employing Monolithic Tunable Lasers With Excess Phase Noise," J. Lightw. Technol., vol. 32, no. 10, pp. 1973-1980, 2014.

[25] J. P. Tourrenc et al., Low-frequency FM-noise-induced lineshape: A theoretical and experimental approach, J. Quantum Electron., vol. 41, pp. 549–553, 2005.

[26] Baveja, Prashant P., Drew N. Maywar, and Govind P. Agrawal, Interband four-wave mixing in semiconductor optical amplifiers with ASE-enhanced gain recovery, IEEE J. Sel. Top. Quantum Electron., vol. 18, no. 2, pp. 899-908, 2012.

[27] L. Liu, Z. Tao, W. Yan, S. Oda, T. Hoshida, J. C. Rasmussen, Initial tap setup of constant modulus algorithm for polarization de-multiplexing in optical coherent receivers, Proc.OFC, San Diego, USA, 2009 .

[28] K. Kikuchi, Performance analyses of polarization demultiplexing based on constant-modulus algorithm in digital coherent optical receivers, Opt. Express, vol. 19, no. 10, pp. 9868–9980, 2011.

[29] A. Leven, N. Kaneda and Y. Chen, A real-time CMA-based 10 Gb/s polarization demultiplexing coherent receiver implemented in an FPGA, Proc. OFC, San Diego,

USA, 2008.

[30] R. Maher, D. S. Millar, S. J. Savory, and B. C. Thomsen, Widely Tunable Burst Mode Digital Coherent Receiver With Fast Reconfiguration Time for 112 Gb/s DP-QPSK WDM Networks, J. Lightwave Technol. vol. 30, no. 24, pp. 3924-3930, 2012.

[31] J. E. Simsarian, J. Gripp, A. H. Gnauck, G. Raybon, and P. J. Winzer, FastTuning 224-Gb/s Intradyne Receiver for Optical Packet Networks, Proc. OFC, San Diego, USA, 2010.

[32] T. Nakagawa, M. Matsui, T. Kobayashi, K. Ishihara, R. Kudo, M. Mizoguchi, Y. Miyamoto, Non-data-aided wide-range frequency offset estimator for QAM optical coherent receivers, Proc. OFC, Los Angeles, USA, 2011.

[33] Y. Mori, C. Zhang, K. Igarashi, K. Katoh, and K. Kikuchi, Unrepeated 200-km transmission of 40-Gbit/s 16- QAM signals using digital coherent receiver, Opt. Express, vol. 17,no. 3, pp. 1435–1441, 2009.

[34] J. Dupre, J. Stimple, Making OSNR measurements in a modulated DWDM signal environment,http://www.keysight.com/upload/cmc_upload/All/SLDPRE_2_OSNR_ Measure.pdf.

[35] L. E. Nelson, Y. Pan, M. Birk, R. Isaac, C. Rasmussen, M. Givehchi, and B. Mikkelsen, "WDM Performance and Multiple-Path Interference Tolerance of a Real-Time 120 Gbps Pol-Mux QPSK Transceiver with Soft Decision FEC," in National Fiber Optic Engineers Conference, paper NTh1I.5, 2012.

[36] J. A. O'Dowd et al., Time resolved bit error rate analysis of a fast switching tunable laser for use in optically switched networks, J. Opt. Commun. Netw., vol. 4, no. 9, pp. A77-A81, 2012.

[37] F. Smyth et al., 10.7Gbd DQPSK packet transmission using a widely tunable slotted Fabry-Perot laser, Proc. ECOC, Torino, Italy, 2010.

Chapter 3

Quantum Dash Passively Mode-Locked Lasers for Coherent Wavelength Conversion System

3.1 Introduction

In chapter 2, a fast reconfigurable SOA-based wavelength converter employing fast switching sampled-grating distributed Bragg reflector (SGDBR) lasers was demonstrated to achieve the wavelength conversion of a QPSK data signal with a reconfiguration time of 10's of nanoseconds. Although the fast tunable DBR lasers can achieve ns tuning time, they present many disadvantages such as relatively large phase noise. When the FWM process is used for wavelength conversion of advanced modulation format signals, the phase noise transfer from the pump to the converted signal can have a deleterious effect on signal quality and cause a performance penalty [1]. One method to overcome the phase noise transfer issue is to use phase noise correlated pumps in a non-degenerate FWM scheme, as was demonstrated in [2-6], by using a frequency comb source based on a laser gain-switching technique. However, the optical frequency combs from gain-switched lasers have limited bandwidth. The mode-locked laser (MLL) based comb sources provide spectral flatness and excellent phase correlation between adjacent modes. With the potential for integration in photonic integrated circuits (PICs), MLL can be a suitable candidate for FWM-based wavelength conversion. A demonstration of wavelength conversion using pumps derived from a quantum dash passively mode-locked laser (QD-PMLL) was shown for direct detection signal in [7].

In this chapter, an all-optical wavelength conversion system based on FWM in semiconductor optical amplifiers for QPSK and 16-QAM signals using tunable dual-correlated pumps provided by the combination of a QD-PMLL and a programmable tunable optical filter is demonstrated. Detailed characterization of a QD-PMLL is firstly demonstrated, including the optical spectrum, FM noise spectrum and RIN

measurements. Secondly, the phase noise transfer issue in a dual-pumping FWM-based wavelength conversion scheme is discussed. The effects of additional phase noise transfer to the wavelength converted idler due to non-ideal correlation between the comb lines of the QD-PMLL is investigated. Finally, studies of the wavelength conversion of QPSK and 16-QAM signals at 12.5 Gbaud using the proposed scheme find that the bit error rate (BER) performance is below the 7% forward error correction (FEC) limit (BER of 3.8×10^{-3}) over a range of pump spacing exceeding 300 GHz for QPSK signals, and conversion of 16-QAM signals was limited by the wavelength conversion scheme though was nonetheless below the 20% FEC limit (BER of 2×10^{-2}).

3.2 Mode-locked lasers

Mode locked lasers have attracted a lot of interest due to their applications in many fields such as Wavelength Division Multiplexing (WDM) optical communication systems [8], radio over fiber (RoF) and superchannel transmission systems [9]. Mode locking is a technique for the generation of ultrashort optical pulses with picosecond or femtosecond durations. When a laser is mode locked or said to be phase locked, the longitudinal modes of the laser will constructively interfere with one another, producing a train of optical pulses. In the frequency domain, several axial resonator modes will oscillate with a fixed correlated phase. The frequency separation between the modes (FSR) can be given by FSR=c/2L, where c is the speed of light and L is the length of the laser cavity. Two common mode-locking mechanisms–active and passive mode locking are discussed here.

The laser resonator of an actively mode-locked laser contains the gain medium and an active element (for example, electro-optic modulator), which periodically modulates the resonator losses causing the round trip phase changes to being synchronized with the resonator round-trips [10,11]. The pulse duration will finally achieve a balance between pulse shortening effect from the modulator and pulse broadening effects caused by the limited gain bandwidth.

In passive mode-locked lasers, a nonlinear passive element, such as a saturable absorber is placed in the laser resonator. The saturable absorber behaves differently

depending on the intensity of the light passing through it [12]. It will selectively absorb low intensity light, and transmit high intensity light until it gets saturated. The passive mode locking method does not need an external driving signal and allows us to generate shorter optical pulse compare to active mode locking because by using the saturable absorber, we can modulate the resonator losses much faster than with an electro-optic modulator [11].

Passive mode locking can also be obtained using the Kerr effect within a laser cavity instead of using an absorber. The nonlinear interactions among the modes can be improved by using a quantum dash material for the laser [13]. Compared to quantum well structure, the quantum dash lasers (QD-PMLLs) [14-17] can achieve lower threshold, broader gain spectra, lower optical confinement factors, and lower linewidth enhancement factors. The QD-PMLL discussed in this chapter combines a broadened gain spectrum of the quantum dash material with passive mode-locking via FWM [14, 18] and allows for the generation of flat optical frequency combs.

3.3 Characterization of mode-locked lasers

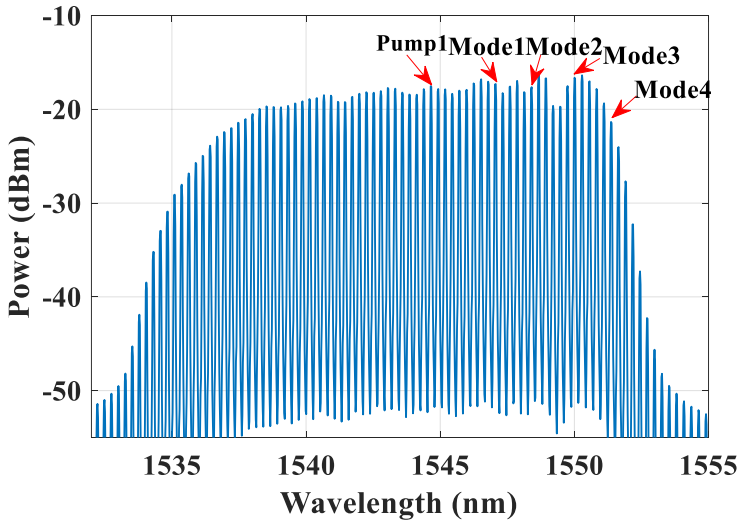

Fig.3-1 The optical spectrum of the QD-PMLL.

The QD-PMLL used in this work was grown by a gas source molecular beam epitaxy on an S-doped <0 0 1> InP substrate. The laser chip was mounted on a temperature-controlled copper base maintained at 25℃ for probe testing. Fig. 3-1 illustrates the spectrum of the QD-PMLL operating at a center wavelength around 1543

nm, with a free spectral range (FSR) of 33.6 GHz, under a bias current of 300 mA. The lasers exhibit the characteristic square-shaped emission spectrum with a spectral 3dB bandwidth larger than 10 nm. To employ a QD-PMLL to generate the pumps for a wavelength conversion system, its amplitude and phase noise properties are of paramount importance. Four modes of the QD-PMLL were selected randomly and individually filtered out and sent to the phase noise and relative intensity noise (RIN) measurement setups [19]. The spectral density of the frequency noise (FM-noise spectrum) of each of the selected modes is shown in Fig. 3-2. The FM-noise spectra exhibit a typical 1/f noise component at low frequencies and a dominant white FM noise at larger frequencies exceeding 100 MHz. The 1/f noise at low frequency is mainly came from the electronic devices connected to the laser. The increase of the noise at frequency above 1 GHz is mainly caused by the Gaussian noise from the measurement setup. The intrinsic optical linewidth can be obtained from the flat FM-noise component at large frequencies (> 100 MHz), which corresponds to 2~3 MHz. The FM noise spectra of each comb tone demonstrates similar levels of phase noise, though there is a slight increase when moving from Mode 1 to Mode 4 which is on the edge of the overall comb spectrum.

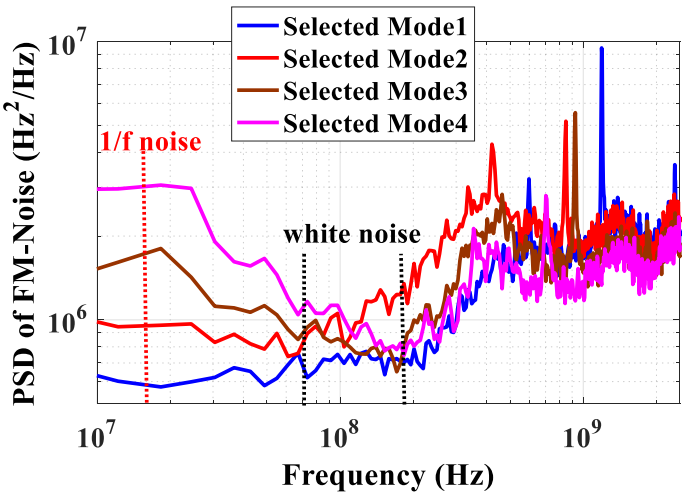

Fig.3-2 The FM noise spectra of selected modes.

The RIN measurement setup is showed in Fig.3-3. The selected modes were filtered out by a tunable bandpass filter and sent into a 10 GHz bandwidth APD photodiode. A bias tee was used after the APD, the DC bias part of the bias tee was

connected to a multi-meter for the shot noise measurement, and the RF signal was amplified by a high bandwidth RF amplifier. The received signal was finally captured by the electrical spectrum analyzer (ESA). The RIN of each individual mode and the entire emission spectrum was characterized and illustrated in Fig. 3-4. All modes possess considerable intensity noise at frequencies below 2 GHz, but lower intensity noise at higher frequencies. However, the measured RIN of the entire emission spectrum is reasonably low (~ -130 dB/Hz). This disparity indicates the presence of mode-partition noise (MPN) in these devices and has been presented in previous works [20]. For wavelength conversion systems, the amplitude noise of the QD-PMLL may potentially induce nonlinear phase noise during FWM which will be transferred to the idler.

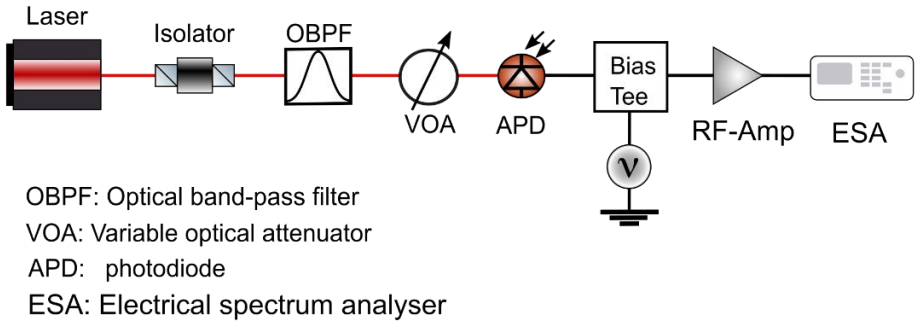

Fig.3-3 RIN measurement setup

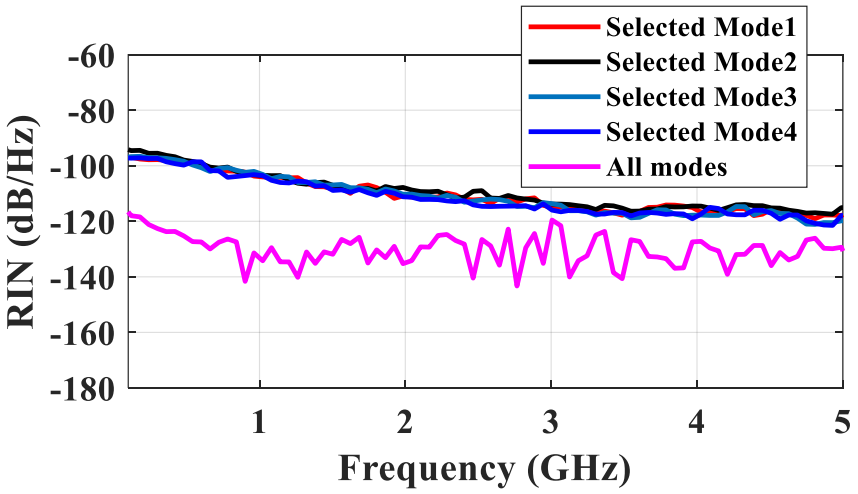

Fig.3-4 RIN for selected modes and all modes

3.4 Phase noise and FWM

Consider two pumps with electric field intensities given by, $\vec{E}_{p1}$ and $\vec{E}_{p2}$, mixing with a signal having an electrical field intensity of $\vec{E}_s$, generating an idler through FWM with a field $\vec{E}_i$. Let the phase of the mixing pumps and the signal be represented as, ω_{p1}, ω_{p2} and ω_s respectively. The frequency and the phase of the idler are related to the mixing frequencies by,

$$\omega_i = \omega_{p2} - \omega_{p1} + \omega_s \tag{3.1}$$

$$\phi_i = \phi_{p2} - \phi_{p1} + \phi_s \tag{3.2}$$

Unless both pumps have correlated phase noise, the phase noise of the idler is related to the phase noise of the mixing frequencies by the following relationship when the phase noise of the mixing frequencies is uncorrelated [21-24],

$$\triangle\sigma_i^2 = \triangle\sigma_{p1}^2 + \triangle\sigma_{p2}^2 + \triangle\sigma_s \tag{3.3}$$

Where $\triangle\sigma^2$ represents the variance of the phase noise. For white frequency phase noise, the linewidth and the phase error variance are linearly related [22]. Thus it can be observed from equation (3.3) that the phase noise of the idler will be the sum of the phase noise of the mixing frequencies.

When the two pumps have correlated phase noise, the phase error variances of the idler can be given by [2],

$$\triangle\sigma_i^2 = \triangle\sigma_{p1}^2 + \triangle\sigma_{p2}^2 + \triangle\sigma_s^2 - 2\,\mathrm{cov}(\triangle\phi_{p2,}\,\triangle\phi_{p1}) \tag{3.4}$$

Where $\triangle\phi_{p2,p1}$ represent the fluctuation in the phase of the pumps, and cov(x,y) represents the covariance of x and y.

When the dual pumps are correlated,

$$\mathrm{cov}(\triangle\phi_{p2,}\,\triangle\phi_{p1}) = \triangle\sigma_{p1}^2 = \triangle\sigma_{p2}^2 \tag{3.5}$$

By using equation (3.4) and equation (3.5), the phase error variances of the idler can be given by,

$$\Delta\sigma_i^2 = \Delta\sigma_s^2 \tag{3.6}$$

It can be seen that the phase noise of the idler will be the same as the phase noise of the signal. The dual-correlated pumping scheme can be used to eliminate the phase-noise transfer from the pump to the converted signal in a wavelength conversion system.

3.5 Wavelength conversion Experiment

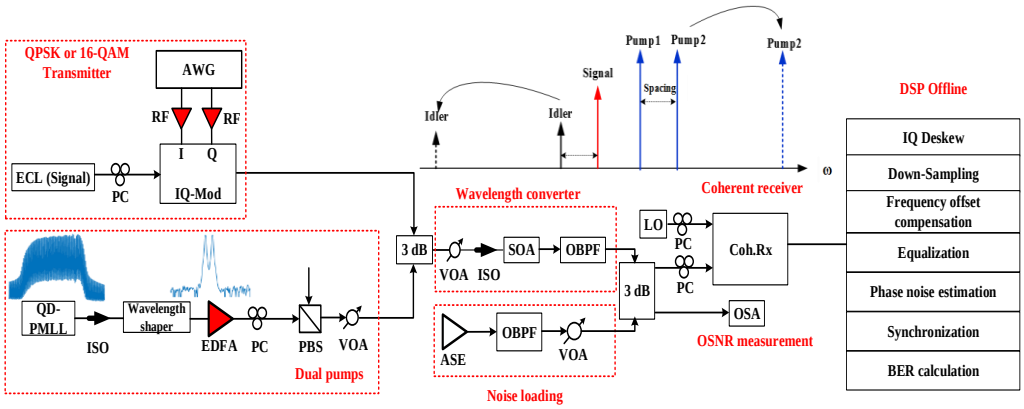

Fig. 3-5 Schematic of the reconfigurable SOA-based wavelength conversion of QPSK and 16-QAM signals employing a QD-PMLL as the pump lasers. PC: polarization controller, PBS: polarization beam splitter, OBPF: optical band-pass filter, ISO: isolator, ASE: noise source, EDFA: erbium-doped fiber amplifier, VOA: variable optical attenuator, OSA: optical spectrum analyzer, LO: local oscillator, Coh.Rx: coherent receiver.

Fig. 3-5 depicts the schematic of the experimental setup of SOA-based wavelength conversion of QPSK and 16-QAM signals using QD-PMLLs as the pump sources. A narrow linewidth external cavity laser (ECL) tuned to 1544.12 nm was used as the signal source and was modulated with QPSK and 16-QAM data at 12.5-Gbaud using an optical "I-Q" modulator. The optical modulator was driven by electrical signals generated within the arbitrary waveform generator (AWG) operated at 25 GSa/s which gave 2 samples per symbol for the 12.5-Gbaud signal. The generated optical QPSK (or 16-QAM) signal was coupled with pumps derived by selecting two modes from the QD-PMLL using a programmable optical filter (Finisar WaveShaper 1000S). The pumps were amplified using an EDFA and then passed through a polarization controller

and polarization beam splitter to align the polarization state of the pump to that of the data signal. The signal and pumps were then sent into the SOA-based wavelength converter. For the wavelength conversion of the QPSK (16-QAM) signal, the power of the signal and the pumps at the input of the SOA were set at -10 (-12) dBm and 0 (+4) dBm. The signal wavelength undergoes wavelength conversion through non-degenerate FWM in the SOA (CIP XN-OEC-1550) operating at 500 mA bias current. The nonlinear SOA is designed for large conversion efficiency (CE), and the wavelength converter system was optimized to yield a CE > 0 dB over a pump detuning range of several nm. The wavelength converted idler was filtered out by using a 0.1 nm bandwidth tunable optical bandpass filter (OBPF). The filtered idler was then passed through a 3 dB splitter with one arm sent to the OSA for measuring the OSNR, and the other arm was passed into the polarization diversity coherent optical receiver and captured by a real-time oscilloscope sampling at 50 GSa/s for offline DSP processing. The power of the local oscillator (LO) was set to be 16 dBm. The input power of the idler and the original signal to the coherent receiver was maintained at -19 dBm using a power monitor and an optical attenuator. In the DSP module, a timing deskew was first implemented to compensate for the timing mismatch between the four outputs of the coherent receiver. The data was then resampled to 2 samples per symbol using a priori knowledge of the clock frequency. An m^{th} power frequency offset compensation method was employed to compensate the frequency offset between the received signal and the LO. For QPSK data, a constant modulus algorithm (CMA) with 21-taps was employed for equalization. The CMA learning parameter is $\mu=8\times10\text{-}4$. For 16-QAM data, the CMA was used for pre-convergence using 10000 samples of the data, then a multi-modulus algorithm (MMA) was employed for steady-state operation. The 2^{nd} order decision-directed digital phase-locked loop (DD-PLL) was employed for the phase noise estimation [25] with $\rho= 0.02$ and $\gamma= 0.005$, as this has been proven to be a better technique to track the carrier phase of the lasers with excess FM noise such as the 1/f noise associated with the QD-PMLLs. A training symbol based synchronization was employed in order to carry out the BER calculation.

3.6 Results and discussion

The two pumps were selected from the QD-PMLL by using the programmable optical filter. The wavelength of pump1 was fixed at 1544.70 nm as shown in Fig. 3-1, and the spacing between pump1 and pump2 was changed by selecting other modes of the QD-PMLL to tune the wavelength of the converted idler and achieve different wavelength detuning. Fig.3-6 shows a typical input (red color) and output (blue color) spectra of SOA for the wavelength conversion experiment showing the spectral locations of the signal, pump1, pump2 and converted idlers. The maximum OSNR for the original signal after SOA is about 30 dB, the maximum OSNR of the idler is ~ 25 dB. In addition the conversion efficiency is better than 0 dB.

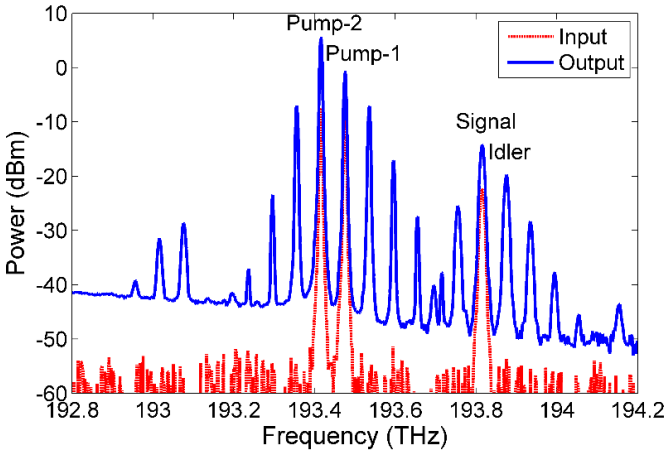

Fig.3-6 Typical input and output spectra of SOA for the wavelength conversion system showing the spectral locations of the signal, pump1, pump2 and converted idlers.

Fig. 3-7 shows the linewidths of the converted idlers as a function of the spacing of the two pumps. The intrinsic optical linewidth can be obtained from the flat FM-noise component at large frequencies (> 100 MHz). Because FM-noise is obtained by using the delayed self-heterodyne method [26], the linewidths are calculated from the FM-noise spectrum by the simple equation: $\Delta\nu = \pi \cdot S(f)/2$. The lowest linewidth is around 350 kHz when using two adjacent modes (with 33.6 GHz pump spacing) from the QD-PMLL, and the largest linewidth is around 2.4 MHz when the pump spacing is 302.4 GHz. The linewidths of the idlers are lower than the linewidths of the individual QD-PMLL modes (shown in Fig. 3-2) because of the phase noise cancellation when

pumps with correlated phase noise are used in the FWM process [6]. The linewidth of ECL is ~30 kHz and the increase in linewidth of the idler as the separation between comb lines from the QD-MLL increases is due to a loss in the correlation between the lines with increased spectral separation [19].

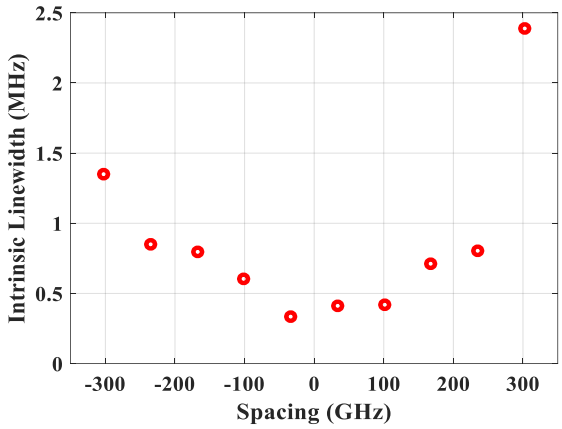

Fig. 3-7 Linewidth of converted idler as a function of pump spacing.

The results of the wavelength conversion of the QPSK signal at 12.5 Gbaud are shown in Fig. 3-8 which presents the BER versus OSNR curves for the wavelength converted idlers when pumps with different spectral separation are used. Only three groups of data, with pump spacing of 33.6 GHz (1×FSR), 235.2 GHz (7×FSR) and 302.4 GHz (9×FSR) are shown and compared with the original QPSK signal after SOA, which presents the same performance as the B2B QPSK signal (not shown).

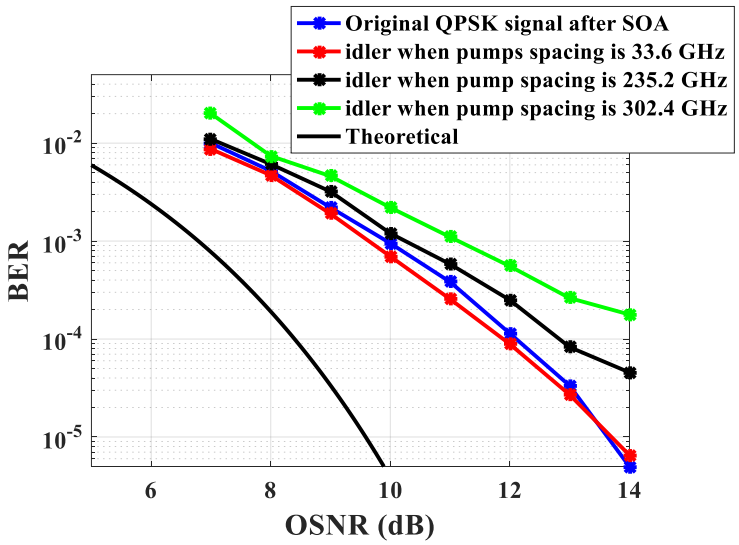

Fig. 3-8 BER as a function of OSNR at receiver for the signal after SOA and wavelength converted signal (idler) for 12.5 GBaud QPSK signal

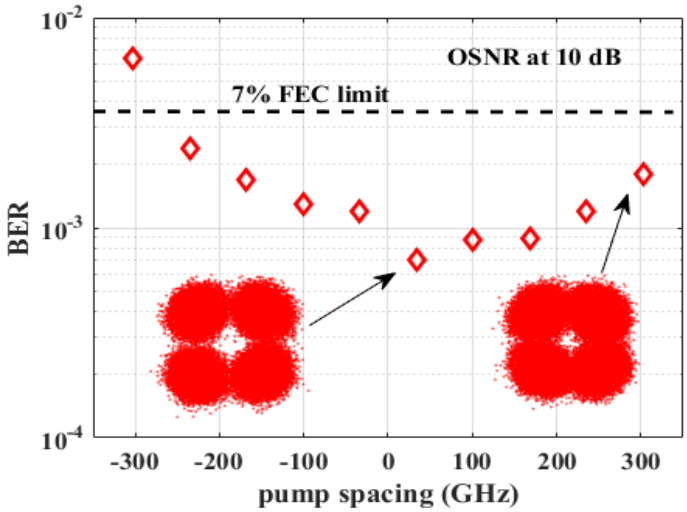

Fig. 3-9 BER measurement as a function of pump spacing for wavelength conversion of 12.5 GBaud QPSK signal

There is no penalty between the curves for the original QPSK signal after SOA and the converted idler when pump spacing is 33.6 GHz, and both OSNR penalty and BER increase with the pump spacing. The degradation in performance is because the phase noise correlation of the comb lines from the QD-PMLL will decrease with the increase of pump spacing, resulting in increased phase noise transfer from the pumps to the idler and hence increased OSNR penalties for the QPSK signal. Fig.3-9 shows the BER measurement for the wavelength conversion of 12.5 GBaud QPSK signal at different pump spacing when OSNR is kept at 10 dB. It can be observed that BER below 7 % FEC limit (BER = 3.8×10^{-3}) can be achieved over the range of approximately ±300 GHz pump spacing. The effect of the 1/f noise at low frequency from the mode-locked laser can be one of the reasons for the non-circular constellation diagram shown in Fig.3-9. Although the effect of the 1/f noise can be significantly suppressed by using 2nd order PLL, it is difficult to fully compensate for it. In addition, the non-circular constellation can be also caused by the nonlinear phase noise generated during the four-wave-mixing process in the SOA.

Fig. 3-10 shows the BER versus OSNR curves for the wavelength conversion of 12.5 Gbaud 16-QAM signals. The green line presents the performance of the B2B system. The blue line presents the BER versus OSNR for the wavelength converted idler when using QD-PMLL as the pumps with 33.6 GHz pump spacing.

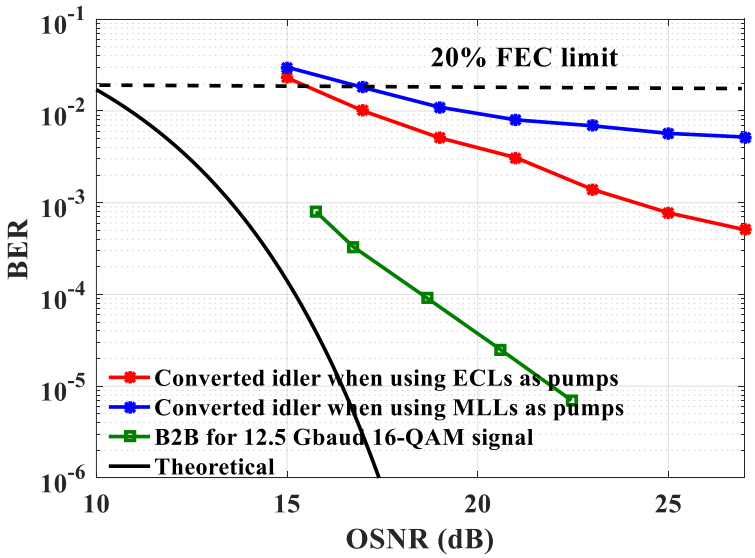

Fig. 3-10 BER versus OSNR performance of the back-to-back system and wavelength converted signal (idler) for 12.5 GBaud 16-QAM signals.

The performance of the wavelength conversion of 16-QAM signal when using two low linewidth ECLs as the pump lasers are displayed by the red line in Fig. 3-10 for comparison. A large OSNR penalty between the converted idler (employing ECL's as pumps) and the B2B performance is observed in Fig. 3-10. This is due to the nonlinear distortions introduced by the SOA on the wavelength converted signal, and the ASE noise added by the SOA which will cause more degradation in the multi-level 16-QAM signals than for the QPSK system which has a single amplitude level. For the wavelength conversion of the 16-QAM signal, the pump to signal power ratio was increased to about 16 dB to saturate the SOA gain more strongly in order to overcome the nonlinear distortions on the 16-QAM idler introduced by the SOA, this in-turn reduces the OSNR of the idler. It can be observed that the BER for the converted idler when using the QD-PMLL as the pumps is larger than 3.8×10^{-3}. However, with a 20% overhead FEC (BER = 2×10^{-2} threshold) employed, only a 17 dB OSNR is needed for the wavelength conversion of the 16-QAM signal. A 2 dB OSNR penalty can be observed between the curves when using QD-PMLL and ECL's as the pumps at the BER of 2×10^{-2}. The 2 dB penalty is mainly due to the larger phase noise of the converted idler when using the QD-PMLL as the pump lasers.

3.7 Conclusion

In this Chapter, an all-optical SOA-based wavelength conversion system using tunable dual-correlated pumps derived from the combination of a QD-PMLL with a programmable tunable optical filter was demonstrated. The properties of the QD-PMLL were analyzed by characterizing the phase noise and the RIN. Then the performance of wavelength conversion of QPSK and 16-QAM signals at 12.5 GBaud using the proposed scheme was investigated, with total data rates of 25 Gbps and 50 Gbps, respectively. For the wavelength conversion of QPSK signal, BER below 3.8×10^{-3} was achieved at the OSNR of 10 dB with different pump spacing, tunable over a range of ~±300 GHz. For the wavelength conversion of 16-QAM system, BER below 2×10^{-2} was achieved at the OSNR of 17 dB. These results show the potential use of a QD-PMLL in a dual correlated pumping wavelength conversion system that employs advanced modulation formats.

This work demonstrates that the phase noise of the laser modes is only partially correlated, with increasing de-correlation as the mode separation increases. This leads to additional phase noise transfer from the pumps to the idler during the FWM process and degradation of the BER performance of the wavelength conversion system. From a systems perspective the wavelength conversion system employing QD-PMLLs may thus only be suitable for use with QPSK at higher baud rates (e.g. > 20 Gbaud), and with a small wavelength conversion range (<1 nm). The jitter of the MLL can essentially be eliminated by using injection locking technique [19], thus ensuring no phase noise transfer to the idler, and successful wavelength conversion of higher order formats such as 16-QAM and above, with a large wavelength conversion range (several nm). The mode injection locking has been used to reduce the phase noise of a single frequency laser. Injection locking can be achieved by using the active mode locking solution, which a narrow linewidth laser will be used as a master laser and fed into the slave laser [27]. Another solution is to use the self injection locking technique that the output of the laser itself will be fed back to lock the laser. These methods can both significantly reduce the phase noise of the laser.

References

1. S. P. O'Duill, S .T. Naimi, A. P. Anthur, T. N. Huynh, D. Venkitesh and L. P. Barry. "Simulations of an OSNR-limited all-optical wavelength conversion scheme," IEEE Photon. Technol. Lett., vol. 25, no. 23, pp. 2311-2314, Dec. 2013.
2. A. P. Anthur, Regan T. Watts, Kai Shi, John O' Carroll, Deepa Venkitesh, and Liam P. Barry, "Dual correlated pumping scheme for phase noise preservation in all-optical wavelength conversion," Opt. Express, no.21, 15568-15579, 2013.
3. L. F. Tiemeijer, P. I. Kuindersma, P. J. A. Thijs, G. L. J. Rikken, "Passive FM locking in InGaAsP semiconductor lasers", IEEE J. Quantum Electron., vol. 25, pp. 1385-1392, June 1989.
4. J. Renaudier, G. H. Duan, P. Landais, and P. Gallion, "Phase correlation and linewidth reduction of 40 GHz self-pulsation in distributed Bragg reflector semiconductor lasers," IEEE J. Quantum Electron. 43, 147-156, 2007.
5. Sepideh T. Naimi, Seán P. Ó Dúill, and Liam P. Barry, "Detailed Investigation of the Pump Phase Noise Tolerance for Wavelength Conversion of 16-QAM Signals Using FWM," J. Opt. Commun. Netw. 6, 793-800, 2014.
6. A. P. Anthur, R. T. Watts, R. Zhou, P. Anandarajah, D. Venkitesh and L. P. Barry. "Penalty-free wavelength conversion with variable channel separation using gain-switched comb source," Opt. Commun., vol. 324 pp. 69-72, Aug. 2014.
7. Y. Ben M'Sallem, A. Shen, F. Lelarge, F. Pommereau, D. Make, S. LaRochelle, and Leslie Ann Rusch," Quantum-dash mode-locked lasers for tunable wavelength conversion on a 100 GHz frequency grid," IEEE J. of Opt. Commun. and Netw., vol. 4, No. 9, pp. A69-A76, 2012.
8. J. N. Kemal et al., "WDM transmission using quantum-dash mode-locked laser diodes as multi-wavelength source and local oscillator", Proc. Int. Conf. Opt. Fiber Commun. OSA, 2017.
9. R. Rosales et al., "Quantum dash mode locked lasers as optical comb sources for OFDM superchannels" in Eur. Conf. Optical Communication, Amsterdam, the Netherlands, Sep. 2012.

10. M. DiDomenico, “Small-signal analysis of internal (coupling type) modulation of lasers”, J. Appl. Phys., vol. 35, no. 10, pp.2870, 1964.
11. H. A. Haus, “Mode-locking of lasers”, IEEE J. Sel. Top. Quantum Electron., vol.6 , no.6, pp.1173, 2000.
12. R. Paschotta, “Passive mode locking with slow saturable absorbers”, Appl. Phys. B, vol.73, no.7, pp. 653, 2001.
13. R. Rosales, K. Merghem, A. Martinez, A. Akrout, J.-P. Tourrenc, A. Accard, F. Lelarge, A. Ramdane, " InAs/InP quantum-dot passively mode-locked lasers for 1.55μm applications ", IEEE J. Sel. Topics Quantum Electron., vol. 17, no. 5, pp. 1292-1301, Sep./Oct.2011.
14. F. Lelarge, B. Dagens, J. Renaudier, R. Brenot, A. Accard, F., Dijk, D. Make, O. L. Gouezigou, J.-G. Provost, F. Poingt, J. Landreau, O. Drisse, E. Derouin, B. Rousseau, F. Pommereau, and G.-H. Duan, “Recent advances on InAs/InP quantum dash based semiconductor lasers and optical amplifiers operating at 1.55 μm,” IEEE J. Sel. Top. Quantum Electron., vol.13, pp.111-124, 2007.
15. V. Vujicic, A. Anthur, V. Panapakkam, R. Zhou, Q. Gaimard, K. Merghem, F. Lelarge, A. Ramdane, and L. Barry., "Tbit/s optical interconnects based on low linewidth quantum-dash la-sers and coherent detection." in Conference on Lasers and Electro-Optics, paper SF2F.4, 2016.
16. J. Müller, J. Hauck, B. Shen, S. Romero-García, E. Islamova, S. Azadeh, S. Joshi, N. Chimot, A. Moscoso-Mártir, F. Merget, F. Lelarge, and J. Witzens, “Silicon photonics WDM transmitter with single section semiconductormode-locked laser,” Adv. Opt. Techn., vol.4, pp.119-145, 2015.
17. A. Moscoso-Mártir, A. Tabatabaei-Mashayekh, J. Müller, J. Nojić, R. Setter, M. Nielsen, A. Sandomirsky, S. Rockman, E. Mentovich, F. Merget, A. Garreau, F. Lelarge, and J. Witzens, "8-channel WDM silicon photonics transceiver with SOA and semiconductor mode-locked laser," Opt. Express, vol.26, pp.25446- 25459, 2018.
18. Z.G. Lu, J.R. Liu, S. Raymond, P.J. Poole, P.J. Barrios, and D. Poitras, “312-fs pulse

generation from a passive C-band InAs/InP quantum dot mode-locked laser," Opt. Express, vol.16, pp.10835-10840, 2008.

19. A. P. Anthur, V. Panapakkam, V. Vujicic, K. Merghem, F. Lelarge, A. Ramdane and L. P. Barry. "Correlation coefficient measurement of the mode-locked laser tones using four-wave mixing," Appl. Opt., vol. 55, no. 16, pp. 4441-4445, Jun. 2016.
20. V. Vidak, C. Calo, R. Watts, F. Lelarge, C. Browning, K. Merghem, A. Martinez, A. Ramdame and L. P. Barry. "Quantum dash mode-locked lasers for data centre applications," IEEE J. Sel. Topics Quantum Electron., vol. 21, no.6, pp. 53-60, 2015.
21. R. Hui and A. Mecozzi, Phase noise of four wave mixing in semiconductor lasers, Applied Physics Lett., vol. 60, no. 20, pp. 2454-2456, 1992.
22. Kazuro Kikuchi, Characterization of semiconductor-laser phase noise and estimation of bit-error rate performance with low-speed offline digital coherent receivers, Opt. Express, vol. 20, no. 5, pp. 5291-5302, 2012.
23. A. P. Anthur, R. T. Watts, J. O'Carroll, Deepa Venkitesh, and L. P. Barry, "Effect of phase noise on all-optical wavelength conversion of DQPSK data using FWM," National Communication Conference, India , 2013.
24. J. Zhou, R. Hui, and N. Caponio,"Spectral linewidth and frequency chirp of four-wave mixing components in optical fibers," IEEE Photon. Technol. Lett. 6, 434–436, 1994.
25. T. N. Huynh, A. T. Nguyen, W. C. Ng, L. Nguyen, L. A. Rusch and L. P. Barry. "BER Performance of Coherent Optical Communications Systems Employing Monolithic Tunable Lasers With Excess Phase Noise," J. Lightwave Technol., vol. 32, no. 10, pp. 1973-1980, May 2014.
26. Tam N. Huynh, Lim Nguyen, and Liam P. Barry, "Phase Noise Characterization of SGDBR Lasers Using Phase Modulation Detection Method With Delayed Self-Heterodyne Measurements," J. Lightwave Technol., no.31, pp. 1300-1308, 2013.
27. R. Hui, A. D'Ottavi, A. Mecozzi, and P. Spano, "Injection locking in distributed feedback semiconductor lasers," IEEE J. Quantum Electron., vol.27, no.6, 1688–1695, 1991.

Chapter 4

Reduction of nonlinear distortion in wavelength conversion system by post-compensation based on machine learning clustering

4.1 Introduction

A lot of work has been undertaken on four-wave mixing (FWM) based wavelength conversion with advanced signal modulation formats such as 16-QAM and 64-QAM by using nonlinear fibers, waveguides, and semiconductor optical amplifiers (SOAs) [1-4]. Nonlinear distortion of the wavelength converted signal caused by gain saturation effects in the SOA can significantly degrade the signal quality and cause difficulties for the practical wavelength conversion of signal data with advanced modulation formats. Variations of digital back-propagation (DBP) have been introduced to overcome the nonlinear effects in SOA-based WC systems. More specific, a numerical inverse SOA has been implemented in WC using DBP, where the dynamic gain equation is typically solved using the Runge-Kutta 4th-order method [5-6]. However, DBP is sensitive to SOA parameters and the performance can be affected by changes in the condition of the wavelength conversion system, and the computational complexity of DBP is quite high, forbidding its implementation in real-time signal processing. Recently, supervised/unsupervised machine learning for non-blind/blind nonlinear cancellation of fiber-induced nonlinearities have been implemented in long-haul coherent optical networks [7]. In particular, unsupervised machine learning clustering such as K-means and fuzzy-logic are attractive as they are completely blind and do not require training-data that limits signal capacity [7].

In this chapter, the wavelength conversion of 16-QAM and 64-QAM signals in an SOA-based wavelength converter using degenerate FWM that incorporates machine learning clustering based nonlinearity compensation (NLC) to improve the tolerance to

nonlinear distortion is demonstrated. Machine learning clustering based NLC is performed using K-means and Density-based spatial clustering of applications with noise (DBSCAN). Results reveal that the machine learning clustering based NLC has a clear benefit due to its ability of tackling the combination of non-circularly-symmetric Gaussian noise and nonlinearity.

4.2 Machine learning clustering algorithms

4.2.1 k-means clustering

The most well-known, K-means (exclusive/hard clustering) is based on an iterative, data-partitioning process, assigning n observations to exactly one of k clusters defined by centroids, where k is chosen before the algorithm starts. Using the minimum Euclidean distance, the centroids of the clusters (centers of constellation points) are moved to the densest points/symbols [8]. The Fig.4-1 shows the structure of the k-means algorithm. Initially, the standard k-means algorithm selects k points at random as cluster centers and then proceeds by alternating between two steps:

Step 1 (assignment**)**: Assign objects to their closest cluster center according to the Euclidean distance function.

Step 2 (centroids update**)**: Calculate the centroid or mean of all objects in each cluster.

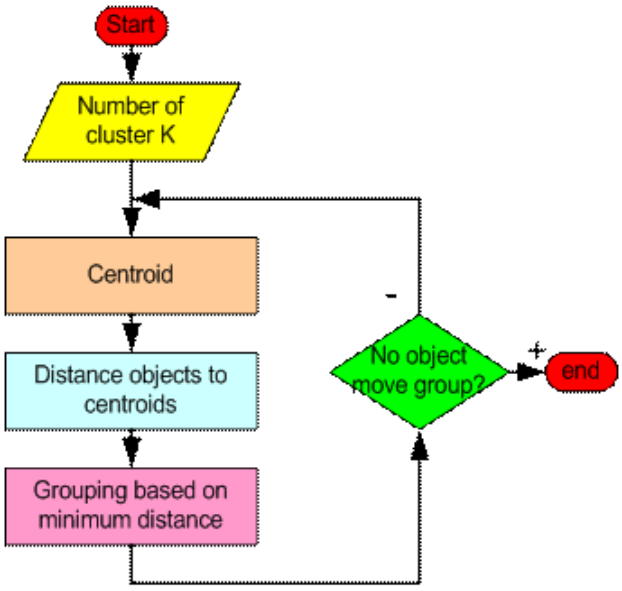

Fig.4-1 K-means algorithm

Repeat steps 1 and 2 until the same points are assigned to each cluster in consecutive rounds. K-Means is relatively an efficient method, however, we need to specify the number of clusters, in advance and the final results are sensitive to initialization and often terminates at a local optimum. Unfortunately there is no global theoretical method to find the optimal number of clusters. A practical approach is to compare the outcomes of multiple runs with different k and choose the best one based on a predefined criterion. In general, a large k probably decreases the error but increases the risk of overfitting.

4.2.2 Density-based spatial clustering of applications with noise (DBSCAN)

Two novel modified algorithms are developed, both using DBSCAN [9] to associate the received points into their respective clusters. Received constellation points that cannot be clustered are defined as "un-clustered" noisy points. However, instead of performing linear equalization on these points which leads to underestimating the system performance, here we propose to use K-means clustering (method-(1)), or the minimum distance between an un-labelled point and the clustered points (method-(2)).

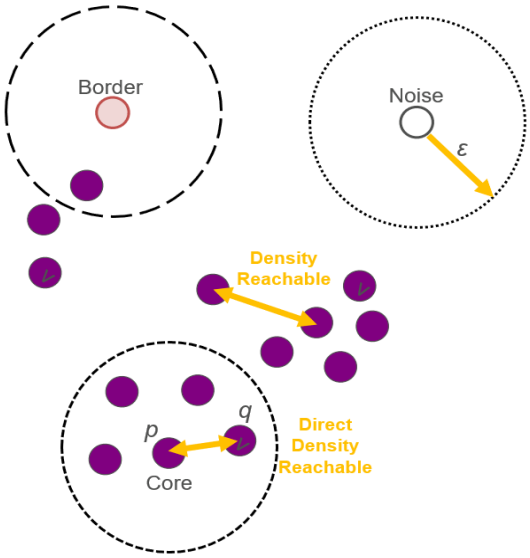

Fig. 4-2: Example of DBSCAN when the number of Min. Points is 4.

In density-based clustering the algorithm makes an assumption that clusters are dense regions in space separated by regions of lower density [10, 11]. A dense cluster

is a region which is "density connected", i.e. the density of points in that region is greater than a minimum [12]. Since these algorithms expand clusters based on dense connectivity, they can find clusters of arbitrary shapes [12]. DBSCAN is an example of a density-based clustering algorithm that deals with stochastic-noisy data. DBSCAN searches for dense areas and expands these recursively to find arbitrarily shaped clusters. The two main parameters of DBSCAN are the ε ('Epsilon') and the 'minimum points'. The ε defines the radius of the "neighborhood region" while the 'minimum points' define the minimum number of constellation points (symbols) that should be contained within that neighbourhood. DBSCAN arbitrarily selects a point from our received coherent digital signal, until all points of the signal have been visited. If the predefined number of 'minimum points' is within the radius-ε, then we consider all these points to be part of the same cluster. The clusters are then expanded by recursively repeating the neighbourhood calculation for each neighbouring point. However, for the unallocated constellation points, if the number of points in the ε-neighbourhood is less than a predefined threshold, the points are designated to be "noisy" and not assigned to a particular cluster. These noisy data in conventional DBSCAN are not further processed. Here we propose to apply as a 2^{nd} stage clustering only for these noisy points: method-(1) K-means, and method-(2) the minimum distance between an unlabelled point and the clustered points. A schematic diagram for conventional DBSCAN is depicted in Fig. 4-2 when the number of minimum points is 4. In Fig. 4-2 we make the following assumptions [13]:

a. **Epsilon neighbourhood (Nε):** A set of all constellation points (symbols) within a distance 'ε'.
b. **Core point:** A constellation point whose Nε contains at least a 'minimum point' (including itself).
c. **Direct Density Reachable:** A point q is directly density reachable from a point p, if p is core point and $q \in$ Nε.
d. **Density Reachable:** Two constellation points are density reachable if there is a chain of 'direct density reachable' points that link these two points.

e. **Border Point:** A constellation point that is 'direct density reachable' but not a core point.

Noise: Constellations points not belonging to any point's Nε.

The steps related to the conventional and modified DBSCAN are listed below, where the algorithm converges until all symbols have been allocated to a cluster or labelled as 'noisy' only if conventional DBSCAN is considered (i.e. step 5 below: 1st loop) [11,12]:

1. Randomly select a constellation point *p* (referred to Fig. 4-2) in the constellation map.
2. Retrieve all constellation points directly density-reachable from *p* that satisfy the condition of the radius ε limits.
3. If the constellation point *p* is a core point, a cluster is formed. Search recursively and find all its density connected points and assign them to the same cluster as *p*.
4. If *p* is not a core point, the DBSCAN algorithm "scans" for the rest of the unvisited constellation points.
5. **DBSCAN 1st loop:** Points that are un-clustered are labelled as zero points ("noisy points") where linear equalization is performed only for these points; and then the conventional DBSCAN algorithm stops.
6. **DBSCAN 2nd loop (*the extra novel step*):**

i. ***Method-(1)***: A K-means clustering algorithm is activated for the "noisy points" using the Lloyd's algorithm [8,9]:

a. Assignment: Allocate each observation to the cluster whose mean has the least squared Euclidean distance ("nearest" mean).

b. Update: Calculate the new means to be the centroids of the observations in the new clusters. K-means converges when assignments do not change. New selected symbols are located in the centroids of each cluster.

ii. ***Method-(2)***: The minimum distance between the unlabelled "noisy points" and the clustered points is calculated where all updated symbols are located in the new centroids per cluster.

4.3 SOA-based wavelength conversion experiment setup

Fig. 4-3 depicts the schematic diagram of the experimental setup of the SOA-based wavelength conversion of the 10 GBaud 16-QAM and 5 GBaud 64-QAM signals. A narrow linewidth (<100 kHz) external cavity laser (ECL) tuned to 1549.5 nm is used as the signal source and was modulated with data using an optical I-Q modulator. The optical modulator is driven by electrical signals generated by the arbitrary waveform generator (AWG), operating at 20 GSa/s, with two uncorrelated pseudo-random bit sequences (PRBS) of 2^{15}-1 bits periodicity. An ECL with linewidth under 100 kHz is used as the pump source and fixed at 1550 nm, the pump power is set at 10 dBm for both 16-QAM and 64-QAM experiments. The signal and pump are combined by using a 3 dB coupler and sent into the SOA-based wavelength converter. The signal undergoes wavelength conversion through degenerate FWM in the SOA operating at 450 mA bias current. The SOA device used in the experiment is a nonlinear SOA that operates over C-band with a typical small signal gain of 20 dB, a saturation power of +9 dBm, and noise figure of 10 dB. After the FWM process in the SOA, the converted idler is then filtered out by using a tuneable optical bandpass filter (OBPF). For performance evaluation, the OSNR of the idler is changed by adding amplified spontaneous emission (ASE) from a fiber amplifier that is passed through a 2 nm bandwidth OBPF.

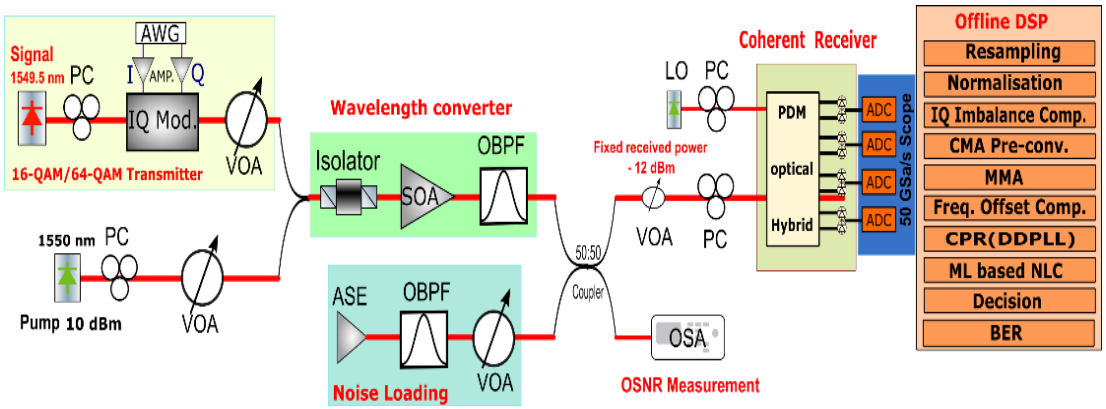

Fig. 4-3 Experimental setup for the SOA-based wavelength conversion of the 10 GBaud16-QAM and 5 GBaud 64-QAM signals. PC: polarization controller, VOA: variable optical attenuator, OBPF: optical band-pass filter, LO: local oscillator, CMA/MMA: constant/multi-modulus algorithm, CPR: carrier phase recovery, DDPLL: decision-directed phase-locked loop.

The filtered idler is then split in a 3 dB coupler with one arm sent to the optical spectrum analyser (OSA) for the OSNR measurement, and the other arm passed into the coherent receiver and captured by a real-time oscilloscope sampling at 50 GSa/s for offline DSP. The data is first resampled to 2 samples per symbol using a priori knowledge of the clock frequency. Then the constant modulus algorithm (CMA) combined with multi-modulus algorithm (MMA) is utilized for signal equalization. An M^{th} power frequency offset compensation method is employed to compensate the frequency offset between the signal and the LO in the coherent receiver. The decision-directed phase-locked loop (PLL) method is employed for the carrier phase recovery, and the NLC using machine learning clustering algorithms are placed before the hard decision and bit-error-rate (BER) calculation.

4.4 Results and discussion

Fig. 4-4 shows the input and output spectra of the SOA showing the locations of the signal, pump and idler. Note that the conversion efficiency (CE) is changed from -7.5 dB to - 9 dB as we increase the signal power from -11 dBm to 1 dBm as shown in Fig.4-5. The CE is defined by the ratio of the power of the idler and the power of the input signal. The decrease of the CE with the increase of the input signal power shown in Fig. 4-5 is mainly due to the saturation of the gain in the SOA. It is ensured that the OSNR and the received power of the idler at the input to the coherent receiver is constant. The performance of the proposed machine learning clustering based NLC are compared by Q-factor measurement. The Q factor is related to BER by $Q = \log_{10}[\sqrt{2}erfc^{-1}(2BER)]$.

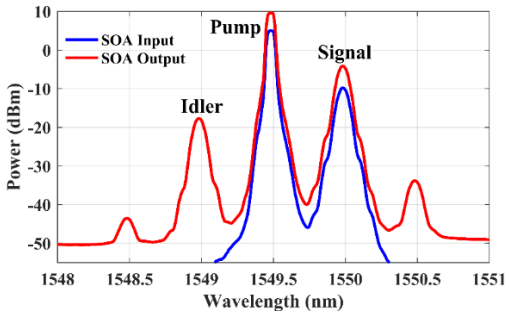

Fig.4-4 Input/output spectra of SOA showing spectral locations of signal, pump and converted idler.

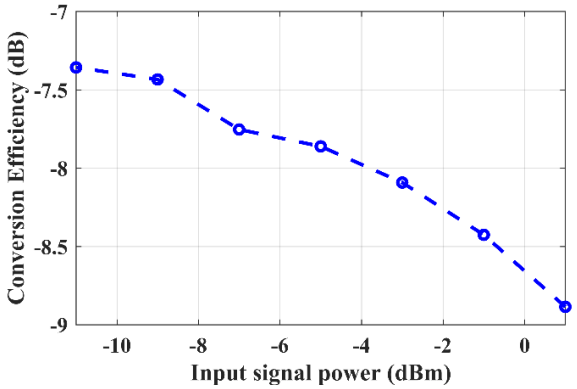

Fig.4-5 Conversion efficiency (CE) changed as a function of input signal power.

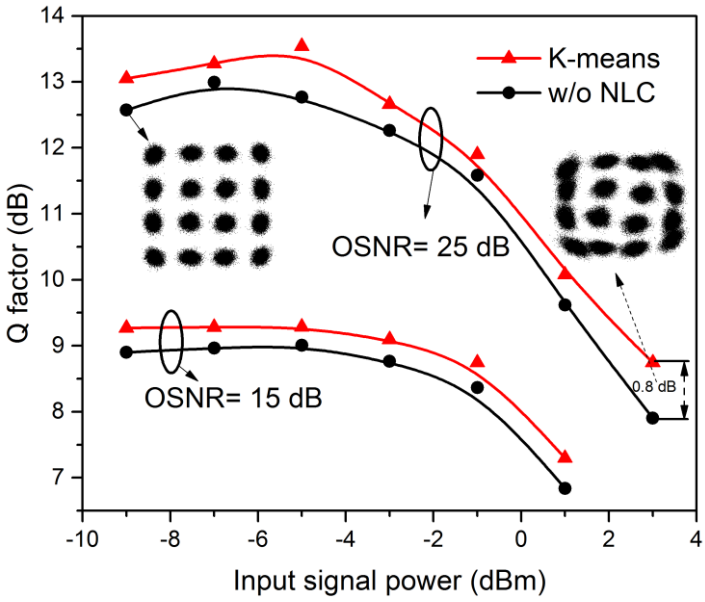

Fig. 4-6 Q factor vs. signal power for 10GBaud 16-QAM wavelength conversion without (w/o) NLC; with K-means and Fuzzy logic algorithms in different OSNR situations (25 dB and 15 dB).

Fig. 4-6 shows the Q factor versus the input signal power curves for 10 GBaud 16-QAM wavelength conversion without (w/o) NLC (circle-marked); with K-means (upward triangle-marked) algorithm when the OSNR at the receiver is set at 25 dB and 15 dB. The B-Spline algorithm is used for the curve fitting. The OSNR is measured using the same method described in Chapter 2. For 16 QAM wavelength conversion, we do not observe significant improvement mainly because the nonlinearity issue is not significant due to the strong pump. It can be seen from Fig. 4-6 that for the case with an OSNR of 25 dB, K-means algorithm improves the Q-factor by ~0.8 dB when the signal power is 3 dBm. The Q factor begins to decrease when the input signal power is

under -9 dBm due to the effect of the ASE noise from the SOA.

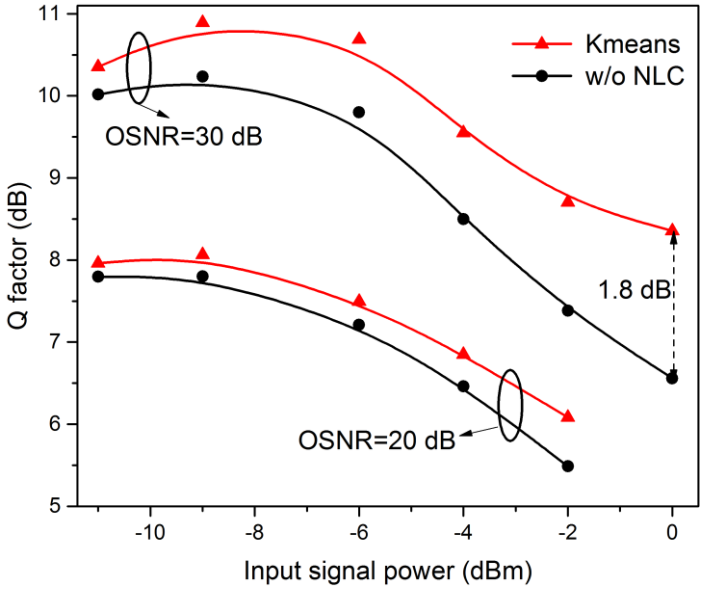

Fig. 4-7 Q factor versus input signal power curves for 5 GBaud 64-QAM wavelength conversion w/o NLC; with K-means and Fuzzy logic algorithms in different OSNR situations (30 dB and 20 dB).

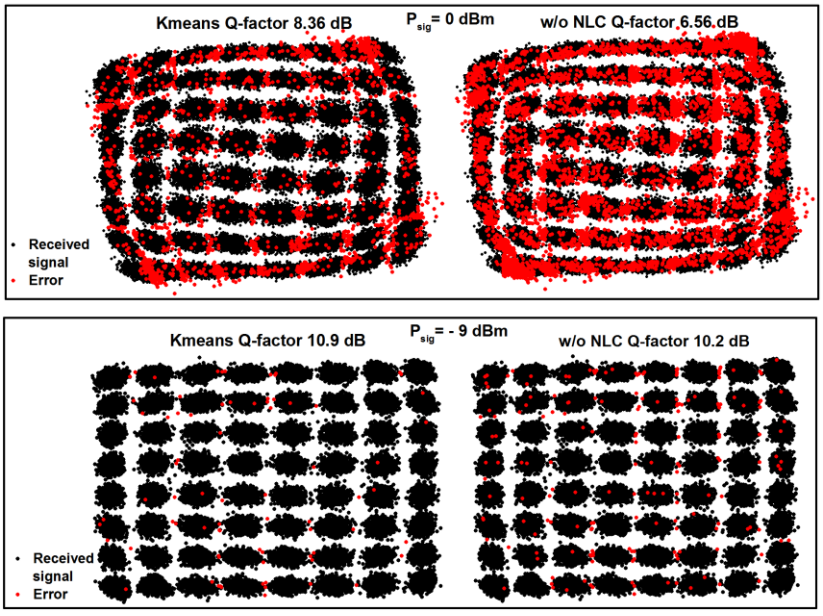

Fig.4-8 Received 64-QAM constellation diagrams with input signal power of 0 dBm and -9 dBm for K-means and w/o using NLC (OSNR= 30 dB).

For the case with an OSNR of 15 dB, in general the K-means can give ~0.5 dB Q-factor improvement. The Q factor improvement for 64-QAM wavelength conversion is more significant than the 16-QAM, because the 64-QAM is more sensitive to

nonlinearities in the system. K-means algorithm can improve the Q-factor by ~1.8 dB (OSNR=30 dB) when the signal power is 0 dBm as shown in Fig.4-7. The constellation diagrams for the wavelength conversion of 64-QAM signals (OSNR =30 dB), with input signal power of 0 dBm and -9 dBm are shown in Fig.4-8. The nonlinear distortion is more serious with a 0 dBm input signal power, and the number of counting errors (red dotted) are shown and compared between the cases when K-means is used and w/o NLC algorithm is used. It is obvious that the number of errors has been reduced by using the K-means algorithm. For the case with -9 dBm signal input power, the nonlinear effect is not significant, the K-means can still slightly reduce the number of errors caused by the ASE noise from the SOA and the small effect from nonlinear distortion.

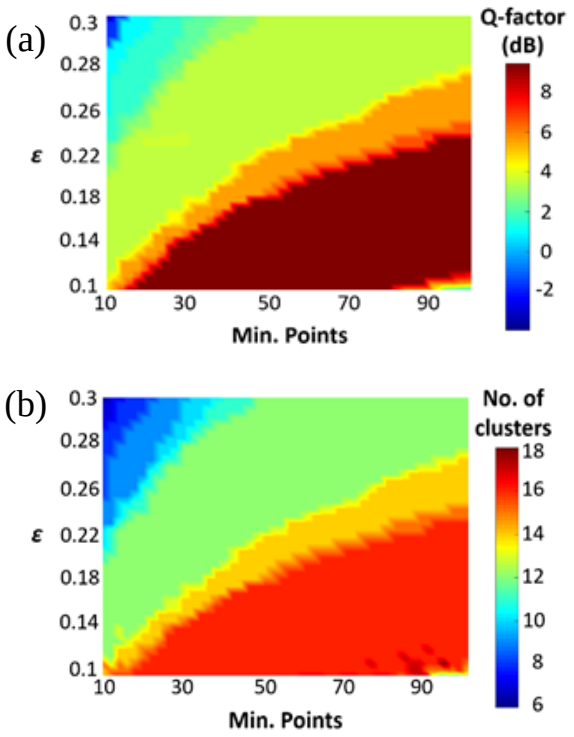

Fig. 4-9: Example of evolution of the minimum constellation points with ε for DBSCAN method-(2) in terms of (a) Q-factor and (b) the output number of clusters for 16-QAM WC at optimum -5 dBm of input signal power at the SOA with 25 dB of OSNR.

In order to test the DBSCAN algorithm, a 10 Gbaud 16-QAM signal is injected at the input of the SOA at -5 dBm of optical power. Two parameters are needed to optimize the DBSCAN algorithm to produce the highest Q-factor, namely ε and the minimum

number of constellation points (min. points). The calculated Q-factor while scanning for ε and the minimum points is shown in Fig. 4-9(a) for DBSCAN method-(2). The highest Q-factor can be found for $0.1 < \varepsilon < 0.22$ and when the minimum number of points is less than 90. It should be noted however, that the optimization DBSCAN process is more time consuming for 64-QAM. In Fig. 4-9(b), we also demonstrate that the output number of clusters after using DBSCAN are highly affected by the aforementioned parameters.

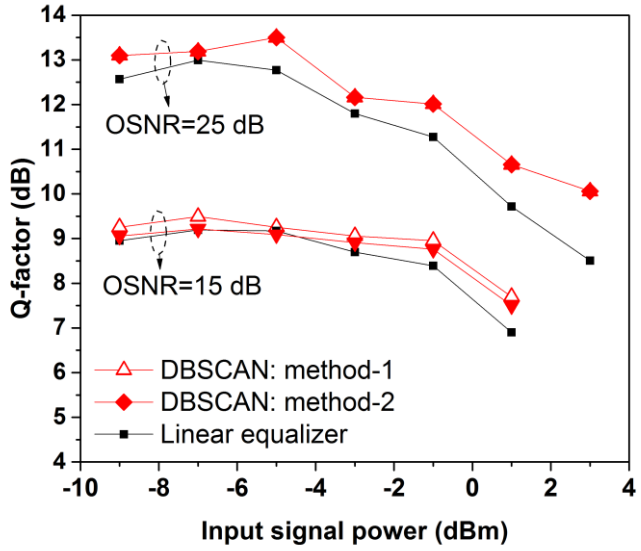

Fig. 4-10: Q-factor vs. input signal power at the SOA for DBSCAN in 16-QAM WC.

In Fig. 4-10, the performance of the clustering algorithms is compared in 16-QAM WC at 15 and 25 dB of OSNR, while in Fig. 4-12 results are presented for 64-QAM WC at 30 and 20 dB of OSNR. DBSCAN optimization is performed for every power level in Fig. 4-10 and Fig.4-12. Fig. 4-11 depicts the received constellation diagrams clustered using DBSCAN method-(2) at 3 dBm of input signal power at the SOA (OSNR=25 dB). The left constellation diagram in Fig.4-11 presents the output from the 1st loop of DBSCAN, in which the "noisy" constellation points are clearly indicated by the black circles. From Fig. 4-10, it is evident that the DBSCAN performance benefit is significant over linear equalization; up to ~1.6 dB improvement in Q-factor, when the OSNR is high (25 dB). All clustering algorithms have similar Q-factor except at 1 dBm of input signal power and low OSNR (15 dB), where DBSCAN method-(2)

slightly outperforms the other cases. However, in Fig. 4-12 DBSCAN shows better potential in compensating nonlinearities at high OSNR (30 dB).

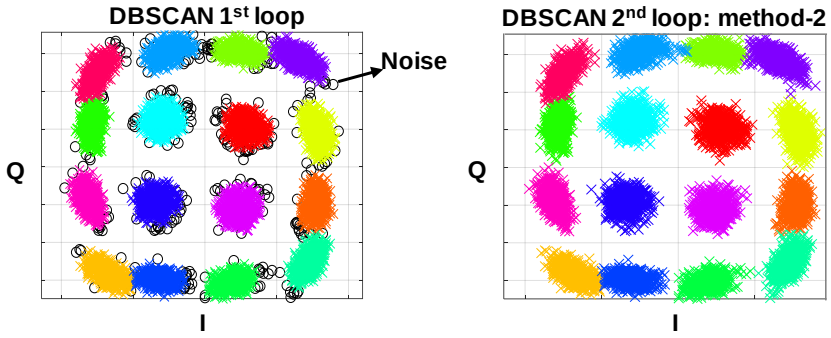

Fig.4-11: Received constellation diagrams for DBSCAN 1st loop with noise (upper diagram) and 2nd loop with method-(2) (lower diagram) at 3 dBm of input signal power (OSNR=25 dB).

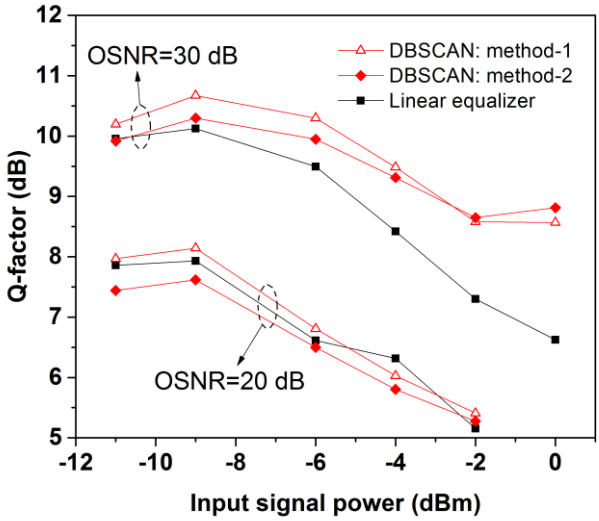

Fig. 4-12: Q-factor vs. SOA input power for clustering in 64-QAM WC.

The larger performance benefits in 64-QAM over 16-QAM signifies that DBSCAN is more effective for higher-order modulation formats (~0.8 dB Q-factor improvement over linear equalization at optimum power). On the other hand, DBSCAN method-(2) outperforms method-(1) only at high OSNR and high input powers. This occurs because nonlinear distortion is more severe at high input signal powers, causing more rotation of the outer-ring clusters and Gaussian-circular shapes are no longer maintained. This is justified in the received constellation diagrams of Fig. 4-13 at 0 dBm of input power: Method-(1) which involves K-means hard (exclusive) clustering cannot handle well the

rotated non-circular shaped outer-ring clusters, resulting in more errors compared to the soft-clustering ability of method-(2). It should also be noted that method-(1) is more effective for lower signal powers below -3 dBm. On the contrary, since at lower signal powers nonlinearity is not dominant, the clusters maintain their Gaussian-circular shape. This enables the hard clustering of K-means and DBSCAN method-1 to be more effective than soft-clustering (method-(2)).

Overall, DBSCAN can reduce the nonlinearity and improve the Q-factor at optimum and higher powers/OSNR in 64-QAM, which is the key for future-proof WCs, requiring higher-order modulation formats.

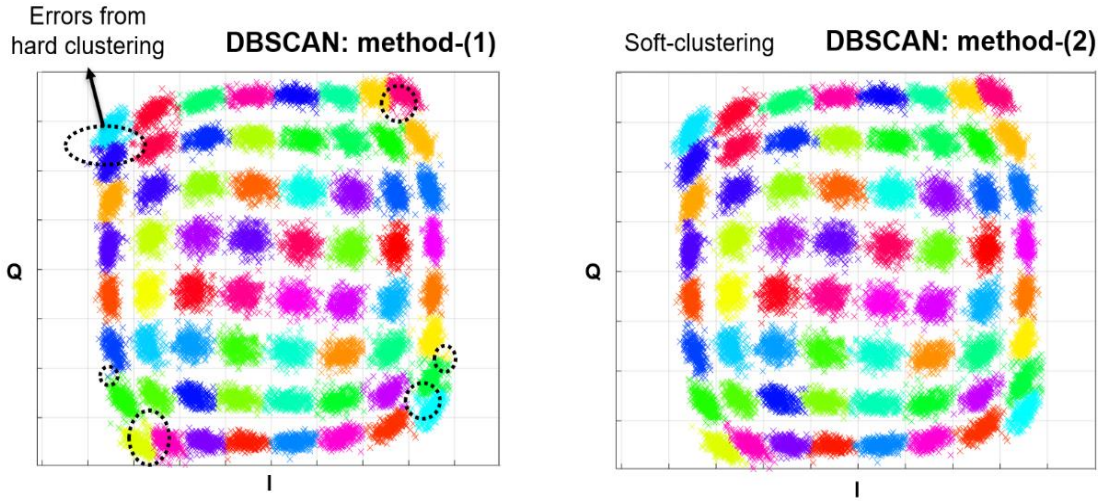

Fig. 4-13: Received constellation diagrams for DBSCAN (a) method-1 and (b) method-2 at 0 dBm SOA power (OSNR= 30 dB).

4.5 Conclusion

In this chapter, wavelength conversion of 10 GBaud 16-QAM and 5 GBaud 64-QAM signals in an SOA-based single pump configuration that incorporates machine learning clustering based blind-NLC is presented to improve the tolerance to nonlinear distortion induced from wavelength conversion. The use of NLC can effectively improve the Q-factor performance by increasing the tolerance to the nonlinear distortion and ASE noise from the SOA. The best Q factor improvement we achieve with K-means is ~1.8 dB for the 64-QAM wavelength conversion with an OSNR of 25dB. K-means can be used to tackle the combined effects of non-circularly-symmetric

Gaussian noise and nonlinearity, and be potentially employed in real-time systems due to its low complexity.

The DBSCAN-based NLC for 10 Gbaud 16-QAM and 5 Gbaud 64-QAM SOA-based WC systems using degenerate FWM was also demonstrated. Two novel modified DBSCAN algorithms were proposed, in which the “un-clustered” noisy constellation points (symbols) were processed using K-means (method-(1)) or the minimum distance between an unlabelled point and the clustered points (method-(2)). DBSCAN showed better potential in compensating SOA nonlinearities at high OSNR and for 64-QAM. However, at optimum -9 dBm of input signal power in 64-QAM, method-(1) had the best performance outperforming linear equalization by ~0.8 dB in Q-factor. The soft-clustering ability (density-based) of DBSCAN method-(2) was useful at high OSNR and high input signal powers at the SOA because the high nonlinearity causes rotation of the outer-ring clusters. In such rotated non-circular shaped clusters, method-(1) was not effective because it involves K-means hard clustering (center-based). On the other hand, since at lower signal powers the impact of nonlinearity is relaxed and the clusters maintain a Gaussian-circular shape, method-(1) outperformed method-(2). DBSCAN might be sensitive to parameter change, however, results have indicated that it is a robust soft-clustering algorithm (method-(2)) for combating the nonlinear distortion induced from the SOA in WC systems.

References

1. Guo-Wei Lu, Takahide Sakamoto, and Tetsuya Kawanishi, "Wavelength conversion of optical 64QAM through FWM in HNLF and its performance optimization by constellation monitoring," Opt. Express, vol.22, pp.15-22, 2014.
2. Francesco Da Ros, Metodi P. Yankov, Edson P. da Silva, Minhao Pu, Luisa Ottaviano, Hao Hu, Elizaveta Semenova, Søren Forchhammer, Darko Zibar, Michael Galili, Kresten Yvind, and Leif K. Oxenløwe, "Characterization and Optimization of a High-Efficiency AlGaAs-On-Insulator-Based Wavelength Converter for 64- and 256-QAM Signals," J. Lightwave Technol., vol.35, pp.3750-3757, 2017.
3. Benoît Filion, W. C. Ng, An. T. Nguyen, Leslie A. Rusch, and Sophie LaRochelle, "Wideband wavelength conversion of 16 Gbaud 16-QAM and 5 Gbaud 64-QAM signals in a semiconductor optical amplifier," Opt. Express, vol.21, pp.19825-19833 2013.
4. Sepideh T. Naimi, Seán P. Ó Dúill, and Liam P. Barry, "Detailed Investigation of the Pump Phase Noise Tolerance for Wavelength Conversion of 16-QAM Signals Using FWM," J. Opt. Commun. Netw., vol.6, pp.793-800, 2014.
5. B. Filion et al., “Postcompensation of Nonlinear Distortions of 64-QAM Signals in a Semiconductor-Based Wavelength Converter,” IEEE J. Lightw. Techn., vol. 34, no. 9, p. 2127, 2016.
6. Benoît Filion, An T. Nguyen, Leslie Ann Rusch, and Sophie LaRochelle, "Digital Post-Compensation of Nonlinear Distortions in Wavelength Conversion Based on Four-Wave Mixing in a Semiconductor Optical Amplifier," J. Lightwave Technol. , vol. 33, pp.3254-3264, 2015.
7. E. Giacoumidis et al., “Blind Nonlinearity Equalization by Machine Learning based Clustering for Single- and Multi-Channel Coherent Optical OFDM”, IEEE J. Lightw. Techn., vol. 36, no. 3, p. 721, 2018.
8. J. Zhang, W. Chen, M. Gao, and G. Shen, “K-means-clustering-based fiber nonlinearity equalization techniques for 64-QAM coherent optical communication

system", Opt. Exp., vol. 25, no. 22, p. 27570, 2017.

9. A.P.T. Lau, et al., "Signal Design and Detection in Presence of Nonlinear Phase Noise", IEEE J. Lightw. Techn., vol. 25, no. 10, p. 3008, 2007.
10. X. Lu, K. Wang, L. Qiao, W. Zhou, Y. Wang, N. Chi, "Non-linear Compensation of Multi-CAP VLC System Employing Clustering Algorithm-Based Perception Decision", IEEE Phot. J., vol. 9, no. 5, 2017.
11. M. Ester, H. P. Kriegel, J. Sander, and X. Xu, "A Density-Based Algorithm for Discovering Clusters in Large Spatial Databases with Noise", in Proc. International Conf. on Knowl. Discov. & Data Mining, Portland, Oregon, USA, p. 226, Aug. 1996.
12. J. Shen et al., "Real-Time Superpixel Segmentation by DBSCAN Clustering Algorithm", IEEE Trans. on Image Proc., vol. 25, no. 12, p. 5933, 2016.
13. R. Boada, R., Borkowski, and I. T. Monroy, "Clustering algorithms for Stokes space modulation format recognition', Opt. Exp., 23, vol. 12, p. 15521, 2015.

Chapter 5

Narrow Linewidth hybrid InP-TriPleX photonic integrated tunable lasers based on micro ring resonators

5.1 Introduction

Tunable semiconductor lasers, which can provide wide wavelength tuning range, high side-mode suppression ratio (SMSR), high output power, narrow linewidth and fast switching speeds are highly desirable for dense wavelength division multiplexing (DWDM) systems in current core networks and potentially in future optical access networks [1]. In DWDM networks, the use of coherent detection technology combined with advanced modulation formats is being employed to achieve higher spectral efficiencies to overcome the capacity limitations of current network implementations. While quadrature phase shift keying (QPSK) is now widely used in commercial optical networks, the use of more advanced modulation formats and constellation diagrams to increase the spectral efficiency are being investigated. Recent work has presented 256-QAM and 1024-QAM optical systems for access and core network applications [2], however, as the modulation format is increased the laser linewidth requirements become extremely stringent [3]. As outlined in the previous chapters, narrow linewidth tunable lasers are also a key requirement for future all-optical wavelength convertors based on FWM in SOA's, and the wavelength conversion of these advanced modulation formats will require very narrow linewidth tunable lasers.

Among various types of tunable lasers, the external cavity lasers (ECL) can exhibit narrow linewidth due to their long cavity length and indeed recent work [4] has demonstrated an ECL with linewidths below 10 kHz that are suitable for higher order modulation in coherent optical systems. Due to the complexity and footprint of the ECL's, distributed feedback (DFB) laser arrays and distributed Bragg reflector (DBR) type lasers are the preferred tunable laser options for commercial coherent transceivers employing QPSK transmission. However, the linewidth of these devices is typically several hundred kHz [5] which limits their use with higher order modulation formats.

A new structure of micro ring resonator external cavity laser (MRR-ECL) has recently been developed based on the TriPleX waveguide platform [6-8]. TriPleX technology is a photonic waveguide platform based on alternating silicon nitride (Si_3N_4) and silicon oxide (SiO_2) layers, fabricated with CMOS compatible equipment. It has very low optical waveguide losses over a wide wavelength range (from 405 nm to 2350 nm) and has shown its potential for application in a number of fields [9]. Waveguide losses as low as 0.1dB/m have been measured. The waveguide platform is mature and functionality is also captured by verified basic building blocks. This allows the TriPleX platform to be one of the three main platforms (next to InP and SOI) to offer the corresponding library and associated design kit in Multi Project Wafer (MPW) runs. The range of applications can be enhanced by hybrid integration of TriPleX with different material platforms, to include increased optical functionality [10], which may make these devices suitable for future coherent transceivers in optical networking applications.

In this chapter, the tuning map, the relative intensity noise (RIN), linewidth, and switching time of the MRR-ECL based on the TriPleX waveguide platform are characterized, before demonstrating its performance in a coherent transmission system. A detailed characterization of the laser linewidth was undertaken across the whole tuning range by using the delayed self-heterodyne (DSH) method. The results show that the device has a lowest linewidth of ~35 kHz and linewidth less than 80 kHz over the whole tuning range. This work demonstrates the switching time of the laser when it is switched between two adjacent modes and non-adjacent modes. Finally, the device is applied in coherent 16-QAM and 64-QAM transmission systems as the laser source, and achieves similar performance to a commercial external cavity laser source.

5.2 Laser design

The structure of the device is schematically shown in Fig. 5-1. The pigtailed hybrid laser assembly has two optimized optical interfaces: the InP coupled to the TriPleX photonic integrated circuit (PIC), forming the hybrid tunable laser cavity; and the TriPleX PIC coupled to the polarization maintaining (PM) fiber output. The

InP/InGaAsP seminconductor optical amplifier (SOA) chip is provided by the Fraunhofer Heinrich Hertz Institute (HHI).

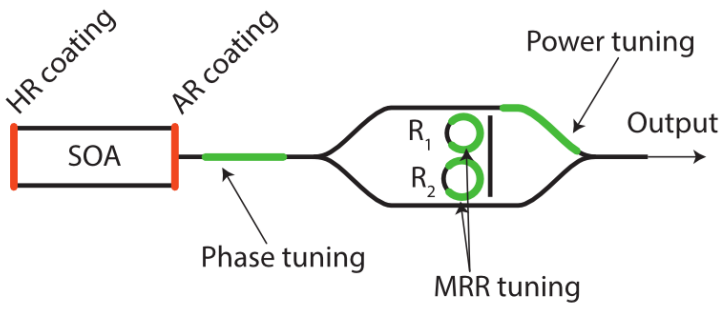

Fig. 5-1 Schematic diagram of a MRR-ECL [7].

The InP based SOA has a high reflective (HR) coated back-facet to reduce cavity losses, and a low reflectivity front facet to impose lasing on the external TriPleX cavity. The TriPleX waveguide circuit consists of two cascaded MRRs with slightly different radii, exploiting the Vernier effect to achieve wavelength tuning. The radii as well as the power coupling coefficients of the MRRs are chosen such that the free spectral range (FSR) of the mirror exceeds the 3 dB gain bandwidth of the SOA thereby suppressing the spectral side peaks of the mirror response to avoid lasing at undesired side modes. The result is a highly frequency selective feedback mirror enforcing single-frequency operation. The low propagation loss of the TriPleX waveguides allows for high quality resonators, resulting in several cm's of effective optical path length inside the cavity. In addition, by optimized on-chip spot-size convertors [9], very efficient coupling to a range of mode fields ranging from standard SM fiber (10 microns) to the modes of the InP gain section (3 microns) is achieved, resulting in low loss chip-to-chip coupling (<1dB) between the InP and the TriPleX. The resulting laser cavity has a large cavity photon lifetime enabling narrow spectral linewidth performance compared to typical DFB/DBR lasers. The phase section of the device can be used to tune the longitudinal mode to achieve fine tuning of the wavelengths, and the output power can be optimized by using the power tuning section. The device is subsequently packaged in a fiber pigtailed butterfly package (as shown in Fig 5-2) containing a thermistor and thermoelectric cooler (TEC) for accurate thermal control of the device. The footprint

of the MRR-ECL is comparable to conventional DFB and DBR lasers, but is smaller than conventional ECL. More details of the device including details on the radii of the rings and individual FSR can be found in [7, 9].

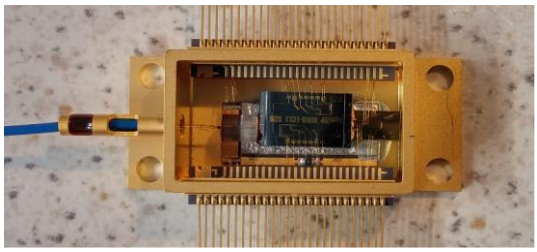

Fig.5-2 Photograph of fiber pigtailed hybrid tunable laser in a butterfly package containing a TEC and NTC for thermal control of the narrow linewidth laser cavity.

5.3 Laser characterization

The packaged MRR-ECL was mounted on a circuit board and the temperature was set at room temperature (23 ℃) using the laser diode thermoelectric cooler (TEC). The threshold current of the device was measured to be around 13 mA. Fig. 5-3 and Fig. 5-4 show the tuning map and side mode suppression ratio of the MRR-ECL as a function of the voltage applied at the two ring resonators. The current on the SOA was kept at 70 mA throughout the tuning map measurements. In Fig.5-3 and Fig. 5-4, the voltage on the two ring sections was tuned from 0 to 10 V. Coarse tuning can be achieved by adjusting the voltage to either of the rings independently and more precise wavelength tuning can be achieved by using both rings together.

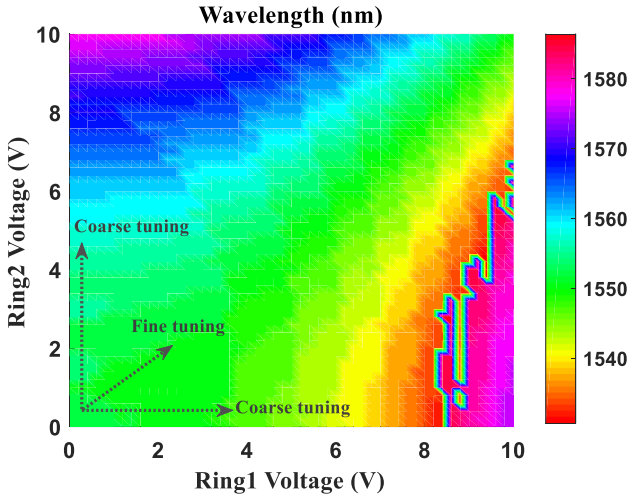

Fig. 5-3 Wavelength tuning map

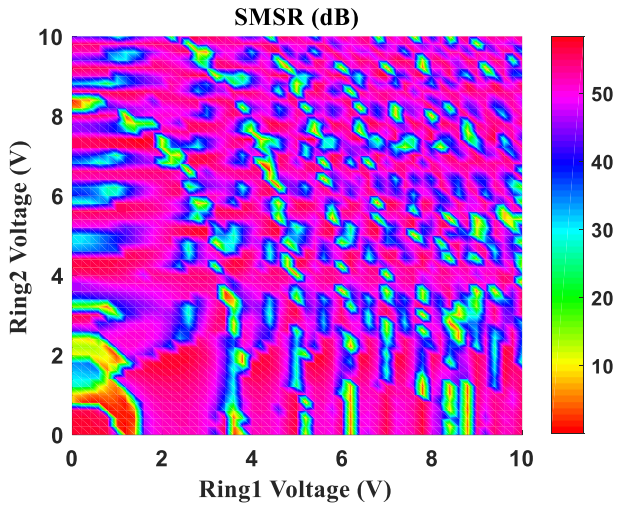

Fig. 5-4 Side mode suppression ratio (SMSR) of MRR-ECL versus voltage on the rings.

It can be seen from Fig.5-3 and Fig.5-4, the device has a tuning range of more than 50 nm (1530 nm~1580 nm) with a SMSR in excess of 50 dB across all wavelengths. High output power (~10 dBm) can be attained by increasing the current into the SOA to greater than 200 mA, and using the power tuning section to optimize output power. Fig. 5-5 shows the superimposed spectra of the laser covering the whole C-band from 1530 nm to 1580 nm with an output power of ~10 dBm on each wavelength achieved with 200 mA current applied to the SOA. The spectral flatness of the laser is under 3 dB.

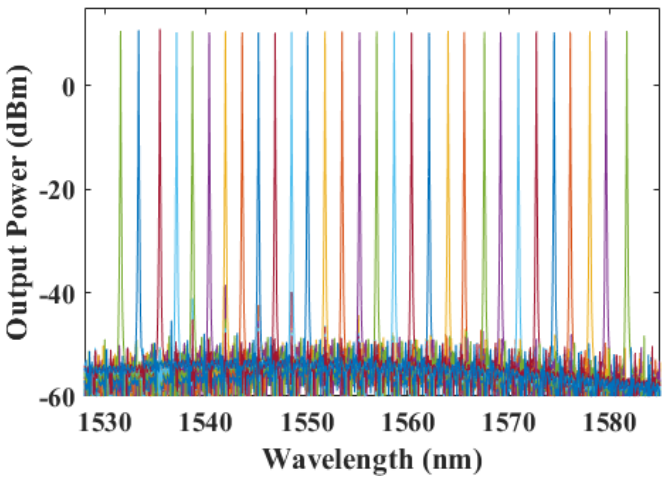

Fig.5-5 Superimposed laser spectra.

The relative intensity noise (RIN) was measured to be less -130 dB/Hz at 70mA current to the SOA as shown in Fig. 5-6 by using a basic RIN-measurement setup. The other sections of the laser were not used. The output of the laser was passed through an isolator and sent into a high speed (~40 GHz bandwidth) photodetector. A bias-tee was used to separate the DC and AC signal from the photodetector. The DC signal was measured to estimate the shot noise of the photodetector, and the AC signal was amplified and characterized by using an electrical spectrum analyzer.

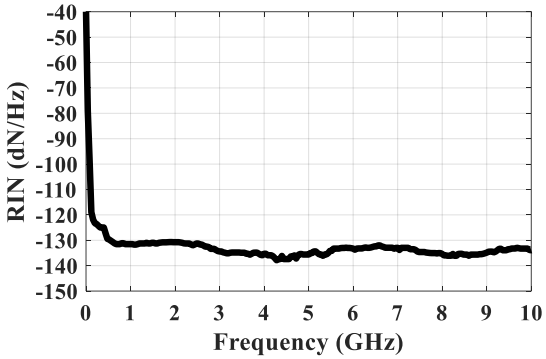

Fig. 5-6 RIN measurement

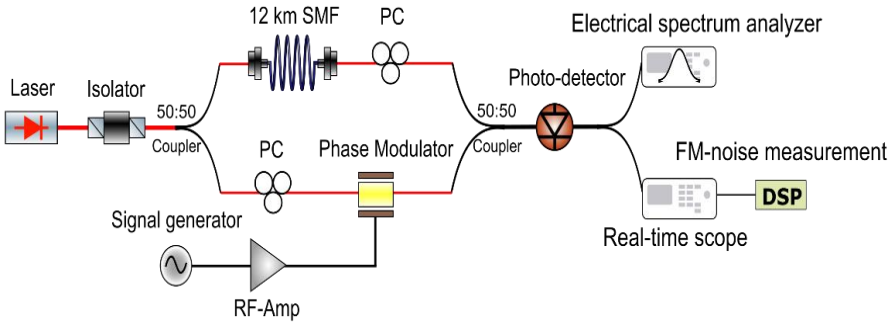

Fig. 5-7 Delayed Self-Heterodyne (DSH) Linewidth and FM-noise measurement setup

In order to characterize the phase noise of the laser, the delayed self-heterodyne method was used. The diagram of the measurement setup is shown in Fig. 5-7. The laser output was firstly divided into two parts, with one part of the light passed through a 12 km single mode fiber to introduce a sufficient time delay to de-correlate the signals in the two arms, while the other part was modulated by an optical phase modulator with a 2 GHz RF signal. A 10 GHz photodiode was used to detect the signal after the two optical signals were recombined by an optical coupler. Then the linewidth spectrum can be observed by using an electrical spectrum analyzer. To characterize the FM-noise of

the laser, a real-time scope operating at 10 GSa/s sampling rate was used to capture 400,000 data samples from the detected signal for off-line digital signal processing (DSP). By analyzing the data using the technique in [12], the full information of the laser phase noise can be recovered and the FM-noise spectrum can be obtained.

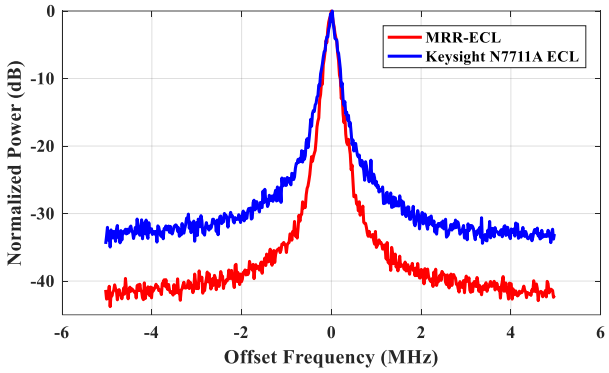

Fig. 5-8 Linewidth measurement

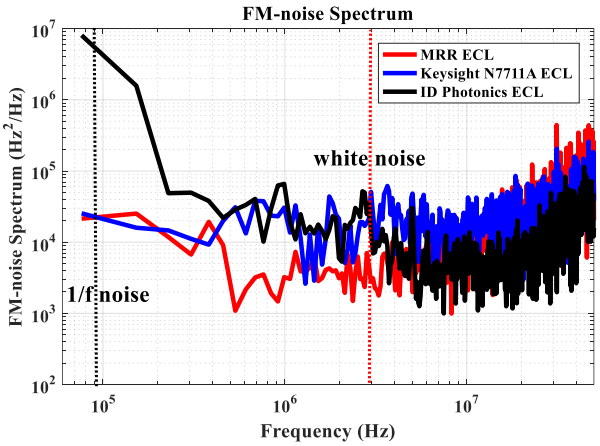

Fig. 5-9 FM-noise measurement

The linewidth of the MRR-ECL was characterized and compared with another commercial ECL (Keysight N771AA ECL). As presented in Fig.5-8 the full spectral width of the MRR-ECL at 20 dB down from the peak is around 800 kHz, which corresponds to a laser 3 dB linewidth of 40 kHz at an injection current of 70 mA to the SOA and no voltage applied to the ring resonators. The 20 dB linewidth of the Keysight N771AA ECL is around 1.2 MHz, which corresponds to a 3 dB linewidth of 60 KHz. It is noted that the linewidths measured with the DSH technique include contributions from the white noise and 1/f noise of the lasers characterized.

Fig.5-9 shows the phase noise measurement results for the MRR-ECL and two

commercial ECL's (Keysight N771AA ECL, and ID Photonics ECL). The power of the lasers were kept the same at ~5 dBm in this phase noise measurements. It is clear from Fig.5-9 that the MRR-ECL has the lowest white noise (corresponding to an intrinsic linewidth of less than 10 kHz) among the three types of lasers and a low frequency phase noise (1/f noise) that is lower than the ID Photonics ECL and compares well with the Keysight ECL. The ID photonics tunable laser used in this measurement is the PureSpectrumTM tunable narrow-linewidth laser (PS-TNL) manufactured by Teraxion. The white noise optical filtering technology based on ultra-narrowband muti-wavelength fiber Bragg grating (FBG) has been applied on this laser to reduce the white noise at high frequency (GHz). The white noise filtering system only shows its benefits at high frequency, however the worse phase noise performance of this PS-TNL at low frequency (1/f noise) is mainly caused by the filtering system.

Fig. 5-10 shows the linewidth of the MRR-ECL measured using the DSH technique, as a function of wavelength, with linewidth under 80 kHz over the whole tuning range. The current on the SOA section was kept at about 80 mA in this measurement. The lowest linewidth can be achieved at around 35 kHz at 1554 nm wavelength, with slightly larger linewidths observed when the laser was operated at higher wavelengths.

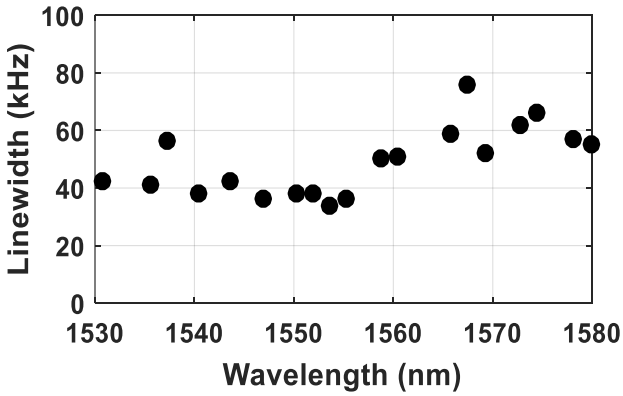

Fig. 5-10 Measured linewidth as a function of laser wavelength for MRR-ECL.

The linewidth of the tunable laser as a function of biasing current on the SOA, with no voltage applied on the other sections is shown in Fig. 5-11. The laser operates at ~1550 nm wavelength. The laser shows best linewidth performance (35 kHz) with a biasing current of 80 mA. And the highest linewidth (56 kHz) is observed with a biasing current of 190 mA. The linewidth measurements cannot be achieved when the SOA

current is kept at 100 mA, 150 mA, 160 mA and 170 mA due to the multi-wavelength operation of the laser. As stated before it should be noted that these linewidth values calculated from the DSH setup include frequency noise contributions from 1/f laser noise and the intrinsic white noise is lower than the values presented here.

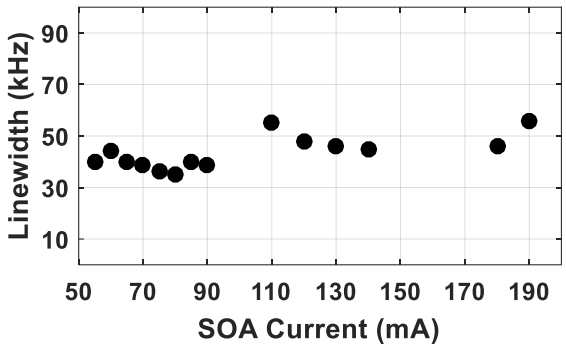

Fig. 5-11 Measured linewidth as a function of SOA injected current for MRR-ECL.

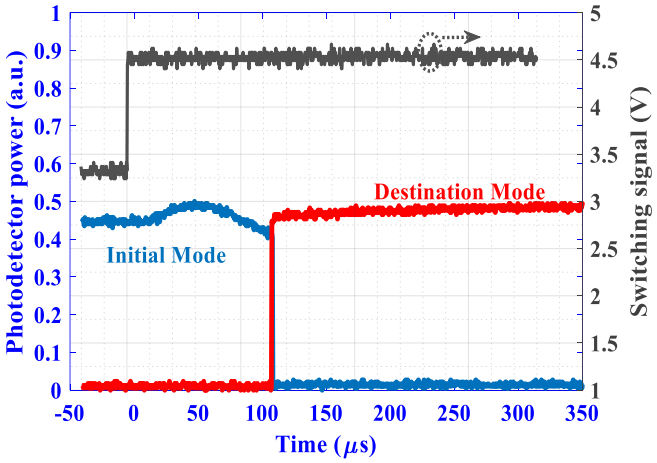

Fig. 5-12 Laser switching times between two adjacent modes

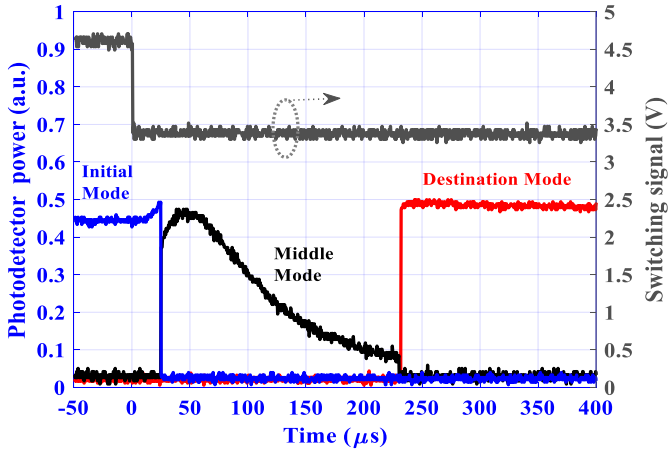

Fig. 5-13 Laser switching times between two non-adjacent modes

Finally, the tuning time of the laser was measured by applying a 100 Hz clock signal to one ring section to switch the laser between two adjacent modes and then non-adjacent modes, filtering out each mode with a 0.2 nm bandwidth optical bandpass filter, and then measuring the detected power in each wavelength as a function of time with a 10 GHz photodetector and a real time scope. In Fig. 5-12, the amplitude of the switching signal was switched from 3.3 V to 4.5V to tune the laser wavelength from initial mode (1553.51 nm) to destination mode (1555.23 nm). Fig. 5-12 shows the received power on the initial wavelength and the wavelength the laser is switched to, indicating it takes about 100 microseconds after the clock edge for the thermal tuning of the ring to induce the wavelength switch [13], but the actual switch between wavelengths occurs on a sub microsecond time scale. Fig. 5-13 shows the result when switching between two non-adjacent modes by switching the signal amplitude from 4.6 V to 3.4 V. In this scenario, there is a middle mode (1550.22 nm) between the initial mode (1556.94 nm) and destination mode (1553.51 nm). The laser initially switches from the initial mode (blue line) to the middle mode which is represented by the black coloured line in Fig.5-13, and it takes totally ~250 microseconds after the applied electrical switching signal for the laser to reach the destination wavelength (red line).

5.4 Coherent transmission experiment

In order to evaluate the performance of the TriPleX based MRR-ECL in an optical coherent system, the laser was utilized in a coherent setup as the signal source tuned to 1550 nm and was modulated with 16-QAM data at 12.5-Gbaud using an optical “I-Q” modulator. In order to further highlight the excellent linewidth and low phase noise properties of the device, the order of the modulation format was increased to 64-QAM and the baud rate was reduced to 5 Gbaud. For the coherent 64-QAM experiment, two wavelengths (1550.2 nm 1567.5 nm) of the MRR-ECL (with slight different linewidths) were used in the experiment. Fig. 5-14 shows the experimental setup used for the 12.5Gbaud 16QAM and 5 Gbaud 64-QAM coherent transmission. A commercial ECL (Keysight N7711A) was also used in the transmission experiments in order to compare with the performance of the MRR-ECL. The optical I-Q modulator was driven by two

electrical signals generated from an arbitrary waveform generator (AWG) which operated at 25 GSa/s, with data streams consisting of two uncorrelated pseudo-random bit sequences (PRBS) of 2^{15}-1 bits periodicity. The modulated optical signal was then passed through a 3 dB splitter with one arm sent to the OSA for measuring the OSNR, and the other passed into the coherent optical receiver and captured by a real-time oscilloscope sampling at 50 GSa/s. The optical signal to noise ratio (OSNR) was changed by adding amplified spontaneous emission (ASE) from an Erbium-doped fiber amplifier (EDFA) that is passed through a 2 nm bandwidth tunable optical bandpass filter. The received signal power at the input of the coherent receiver was maintained at −19 dBm. The local oscillator (LO) used in the setup was a commercial ECL laser with a typical linewidth of ~50 kHz.

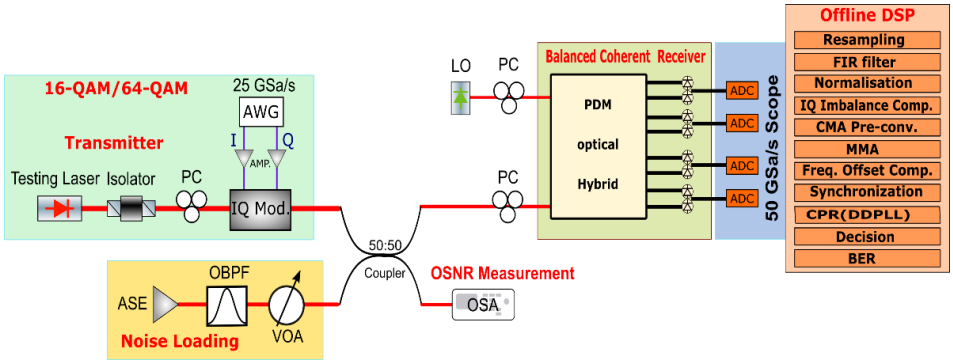

Fig. 5-14 Schematic of the experimental setup for 64-QAM coherent transmission.

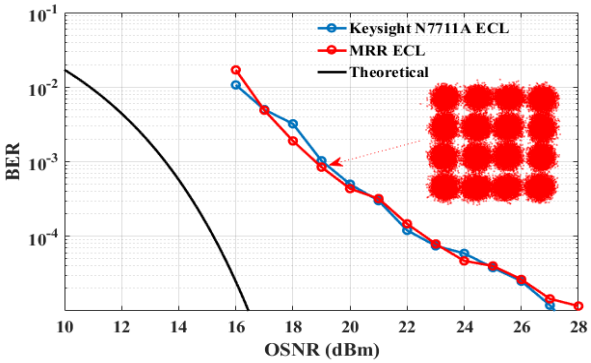

Fig. 5-15 BER versus OSNR curve for 16 QAM data signal at 12.5 Gbaud with constellation diagram for 12.5 Gbaud16-QAM at OSNR of 19 dBm

The required DSP functionality was performed offline. The data was first

resampled to 2 samples per symbol using a priori knowledge of the clock frequency. Then the constant modulus algorithm (CMA) combined with multi-modulus algorithm (MMA) was utilized for the equalization [14-16]. An M^{th} power frequency offset compensation method is employed to compensate the frequency offset between the signal and the LO in the coherent receiver [17]. The decision-directed phase-locked loop (DD-PLL) method was employed for the carrier phase recovery, and the synchronization is achieved by adding training symbols at the beginning of the data in order to carry out the BER calculation [18]. The performance of the MRR-ECL in terms of BER versus OSNR was verified to be comparable to a commercial ECL laser (Keysight N7711A) as shown in Fig.5-15, and the constellation diagram of the 12.5 Gbaud 16-QAM signal at an OSNR of 19 dB is presented in Fig. 5-15. These results indicate the excellent performance of this tunable laser in a coherent optical communication system.

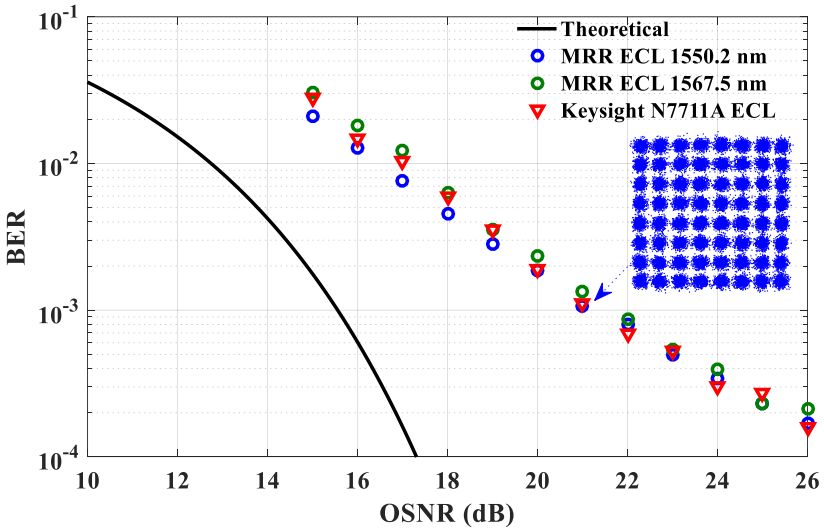

Fig. 5-16 OSNR versus BER curve for 64-QAM at 5 Gbaud

The results for the coherent 64-QAM system at 5 Gbaud when using the MRR-ECL laser at two operating wavelengths, and the commercial laser, are presented in Fig. 5-16. The BER is displayed as a function of received OSNR and the constellation diagram of the received 64-QAM signal when using MRR-ECL at 1550.2nm and an OSNR of 21 dB is presented in Fig. 5-16. It can be observed from Fig. 5-16 that the

OSNR penalty compared with the theoretical curve at a BER of 10^{-3} is about 5.5 dB, and the performance of the MRR-ECL in terms of BER versus OSNR in the case of coherent 64-QAM systems operating at 5 Gbaud was verified to be comparable to a commercial ECL laser. As the MRR-ECL is tuned from 1550.2 nm to 1567.5 nm, a small penalty in the BER performance (~0.5dB at a BER of 10^{-3}) can be observed due to the slightly increased linewidth at this wavelength. Nevertheless, these results indicate the excellent performance of the presented MRR-ECL in a coherent optical communication system with higher order modulation formats.

5.5 Conclusions

In this chapter, detailed characterization of a hybrid InP-TriPleX integrated tunable laser based on silicon nitride micro ring resonators has been presented. The performance of the MRR-ECL laser was investigated in the coherent transmission system for 12.5 Gbaud 16-QAM and 5 Gbaud 64-QAM signals, and the presented laser exhibits comparable performance with a commercial ECL laser. A tuning range of around 50 nm with high output power (~10 dBm), high SMSR (>50 dB), and narrow linewidth of under 80 kHz across the whole tuning range makes this a promising device for use in coherent communication systems employing higher order modulation formats.

Furthermore, the laser presents narrow linewidth and the ability to be switched in several hundred μs level, which makes the device suitable for potential integrated wavelength conversion system, especially given the ease of integration of the PIC. The MRR-ECL can be potentially integrated with SOA and micro ring resonators based optical tunable filters on the same chip in order to build a compact, stable and practical reconfigurable wavelength convertor for the future optical networks.

References

1. Klaus Grobe, Michael H. Eiselt, Stephan Pachnicke, and Jörg-Peter Elbers, "Access Networks Based on Tunable Lasers," J. Lightwave Technol., vol. 32, pp. 2815-2823, 2014.
2. R. Maher et al., “Constellation shaped 66 GBd DP-1024QAM transceiver with 400 km transmission over standard SMF,” , Proc. ECOC, Th.PDP.B.2, 2017.
3. M. Seimetz, “Laser linewidth limitations for optical systems with high-order modulation employing feed forward digital carrier phase estimation,” in Proc. OFC, paper OTuM2, Feb. 2008.
4. K. Kasai, M. Nakazawa, Y. Tomomatsu, and T. Endo, "Full C-band, Mode-Hop-Free Wavelength-Tunable Laser Diode with a Linewidth of 8 kHz and a RIN of -130 dB/Hz," in Proc. OFC, paper W1E.2, 2017.
5. M. Larson, Y. Feng, P. Koh, X. Huang, M. Moewe, A. Semakov, A. Patwardhan, E. Chiu, A. Bhardwaj, K. Chan, J. Lu, S. Bajwa, and K. Duncan, "Narrow linewidth high power thermally tuned sampled-grating distributed Bragg reflector laser," in Proc. OFC, paper OTh3I.4, 2013.
6. Y. Fan, J. P. Epping, R. M. Oldenbeuving, C. G. H. Roeloffzen, M.Hoekman, R. Dekker, R. G. Heideman, P. J. M. van der Slot and K.-J. Boller, "Optically integrated InP-Si3N4 hybrid laser," IEEE Photon. J., vol.8, no.6, 2016.
7. J. L. Zhao, R. M. Oldenbeuving, J. P. Epping, M. Hoekman, R. G. Heideman, R. Dekker, Y. Fan, K.-J. Boller, R. Q. Ji, S. M. Fu, and L. Zeng, “Narrow-linewidth widely tunable hybrid external cavity laser using Si3N4/SiO2 microring resonators”, in Proc. IEEE 13th International Conference on Group IV Photonics (GFP), Shanghai, China, pp. 24-25, 2016.
8. Y. Fan, R. Oldenbeuving, M. Hoekman, D. Geskus, R. G. Heideman, C. G. H. Roeloffzen, and K.-J. Boller, “290 Hz intrinsic linewidth from an integrated optical chip-based widely tunable InP-Si3N4 hybrid laser”, in Proc. Conference on Lasers and Electro-Optics, San Jose, USA, 2017.
9. C.G.H. Roeloffzen, M. Hoekman, E.J. Klein, L.S. Wevers, R.B. Timens, D.

Marchenko, D. Geskus, R. Dekker, A. Alippi et all., “Low loss Si3N4 TriPleX optical waveguides: technology and applications overview”, IEEE J. Sel. Topics in Quantum Electron., vol. 24, no. 4, 2018.

10. K. Wörhoff, R.G. Heideman, A. Leinse, M. Hoekman, “TriPleX: A Versatile Dielectric Photonic Platform,” Adv. Opt. Techn., vol.4, no.2, pp.189, 2015.
11. Yi Lin; Colm Browning; Roelof Bernardus Timens; Douwe H. Geuzebroek; Chris G. H. Roeloffzen; Dimitri Geskus; Ruud M. Oldenbeuving; René G. Heideman; Youwen Fan; Klaus J. Boller; Jialin Zhao; Liam Barry," Narrow linewidth hybrid InP-TriPleX photonic integrated tunable laser based on silicon nitride micro-ring resonators," in Proc. OFC, paper Th2A.14, 2018.
12. Tam N. Huynh, Lim Nguyen, and Liam P. Barry, "Phase Noise Characterization of SGDBR Lasers Using Phase Modulation Detection Method With Delayed Self-Heterodyne Measurements," J. Lightwave Technol., vol.31, pp.1300-1308, 2013.
13. R. M. Oldenbeuving, E. J. Klein, H. L. Offerhaus, C. J. Lee, H. Song, and K.-J. Boller, “25 kHz narrow spectral bandwidth of a wavelength tunable diode laser with a short waveguide-based external cavity,” Laser Phys. Lett., vol. 10, no. 1, 2013.
14. L. Liu, Z. Tao, W. Yan, S. Oda, T. Hoshida, and J. C. Rasmussen, "Initial Tap Setup of Constant Modulus Algorithm for Polarization De-multiplexing in Optical Coherent Receivers," Proc. OFC, pp. OMT2, 2009.
15. K. Kikuchi, “Performance analyses of polarization demultiplexing based on constant-modulus algorithm in digital coherent optical receivers,” Opt. Express, vol.19, pp.9868–9980, 2011.
16. A. Leven, N. Kaneda and Y. Chen, “A real-time CMA-based 10 Gb/s polarization demultiplexing coherent receiver implemented in an FPGA,” in Proc. OFC, paper OTuO2, 2008.
17. J. C. M. Diniz, E. S. Rosa, V. B. Ribeiro, J. C. R. F. Oliveira, and A. C. Bordonalli, "Wide-Range Frequency Offset Estimator for DSP-based Optical Coherent Receivers," IEEE Int. Micro. & Optoelectron. Conf., pp. 710-713, 2011.
18. Y. Mori, C. Zhang, K. Igarashi, K. Katoh, and K. Kikuchi, “Unrepeated 200-km

transmission of 40-Gbit/s 16- QAM signals using digital coherent receiver", Opt. Express, vol.17, pp. 1435–1441, 2009.

Chapter 6

Conclusions and Future work

Future optical networks need to be more reconfigurable in order to increase the switching efficiency and reduce the network latency. Wavelength converters will potentially play an important role in network nodes to avoid contention and to dynamically allocate wavelengths to ensure optimum use of fiber bandwidth. All-optical wavelength conversion can be employed to avoid the use of optical-to-electrical-to-optical (OEO) convertors and significantly reduce the power consumption of the transmission system. In this thesis, the SOA-based wavelength conversion system with the use of different tunable lasers including a sampled-grating distributed Bragg reflector (SGDBR) laser, a quantum dash passively mode-locked laser (QD-PMLL) and narrow linewidth external cavity lasers (ECLs) as the pump sources is demonstrated and investigated. The thesis investigates how these tunable lasers can be controlled to ensure that the incoming data packets can be converted to the required wavelength channel without degradation in signal performance. Other issues such as the phase noise transfer and the nonlinear distortion effect during the wavelength conversion process are also studied.

6.1 Main contributions of this thesis

The contributions of this thesis can be described as follows:

- Implementation of fast reconfigurable wavelength conversion system using a rapid switching SGDBR laser as the pump. The tuning maps (wavelength and SMSR), the linewidth and tuning speed of the SGDBR laser are characterized before the demonstration of the wavelength conversion of QPSK and Pol-Mul-QPSK signals at 12.5-Gbaud using the proposed scheme. The time-resolved bit error rate (TR-BER) is used to estimate the reconfiguration

time of the wavelength conversion system in a switching scenario. Below 50 ns and 160 ns reconfiguration time is achieved for the proposed wavelength conversion system for QPSK and PM-QPSK signals, respectively.

- Demonstration of all-optical SOA-based wavelength conversion system using lines from a single-section quantum dash passively mode-locked laser and detailed investigation of how the correlation between comb lines effects system performance. The tunable pumps are generated by the combination of the mode locked laser and a tunable optical filter. The phase noise and relative intensity noise (RIN) of the mode locked laser are measured, and wavelength conversion of 12.5 Gbaud QPSK and 16-QAM data over a range of pump spacings exceeding 300 GHz using the proposed scheme is achieved.
- Machine learning clustering based nonlinearity compensation is performed using K-means and Density-based spatial clustering of applications with noise (DBSCAN), to reduce the nonlinear distortion in SOA-based wavelength conversion system with 16-QAM and 64-QAM modulation format. Results show that the proposed novel machine learning algorithms can significantly improve the BER performance due to their ability to tackle the combination of non-circularly-symmetric Gaussian noise and nonlinearity.
- A novel tunable laser design using micro ring resonators (MRRs) is investigated. The tuning map, the RIN, linewidth, and switching time of the MRR-ECL based on the TriPleX waveguide platform are characterized. The laser is employed in coherent transmission systems using advanced modulation formats such as QPSK, 16-QAM and 64-QAM, and shows similar performance compare to commercial ECLs. The laser presents narrow linewidth, rapid tuning speed at several hundred μs level and can be potentially integrated with SOA and micro ring resonators based optical tunable filters, which make it suitable for a photonic integrated wavelength conversion solution.

6.2 Future research directions

- Firstly, the linewidth and stability of the quantum dash passively mode-locked laser can be improved by using the resonant external optical feedback [1]. The wavelength conversion of 64-QAM or more advanced modulation formats signals can thus be potentially achieved.
- Secondly, two tunable MRR-ECL lasers can be integrated and be used as the pump sources in a reconfigurable dual-pumping scheme wavelength conversion system. The integrated two pump lasers can offer narrow linewidth, large wavelength tuning range, fast switching speed and high stability for the wavelength convertors, which might be a solution for the future practical wavelength conversion system.
- Finally, real-time implementation of the K-means algorithms to compensate the nonlinear distortion in the wavelength conversion system. The real-time K-means can also be used for long-haul transmission system to compensate the distortion caused by the Kerr effect.

References

1. J. N. Kemal et al., "32QAM WDM transmission using a quantum-dash passively mode-locked laser with resonant feedback", Proc. OFC, 2017.

Appendix A: List of Published Papers

Journal papers

1. **Y. Lin**, E. Giacoumidis, S. O'Duill and L. Barry," DBSCAN-Based Clustering for Nonlinearity Induced Penalty Reduction in Wavelength Conversion Systems ", IEEE Photonics Technology Letters, vol. 31, no. 21, 2019.
2. S. O'Duill, **Y. Lin** and L. Barry, "Identifying the Contribution of Carrier Shot Noise and Random Carrier Recombination to Excess Frequency Noise in Tunable Lasers", Photonics from MDPI, vol.6, Issue 1, no.1, 2019.
3. E. Giacoumidis, **Y. Lin**, J. L. Wei. I. Aldaya, A. Tsokanos, and L. P. Barry, "Harnessing machine learning for fiber-induced nonlinearity mitigation in long-haul coherent optical OFDM", Future Internet, vol. 11, no. 2, 2019.
4. **Y. Lin**, C. Browning, R. B. Timens, D. H. Geuzebroek, C. G. H. Roeloffzen, D. Geskus, R. M. Oldenbeuving, R. G. Heideman, Y. Fan, K. J. Boller, J. Zhao, and L. P. Barry, " Characterization of hybrid InP-TriPleX photonic integrated tunable lasers based on silicon nitride (Si_3N_4 /SiO_2) microring resonators for optical coherent system ", IEEE Photonics Journal, vol. 10, no. 3, pp. 1-8, 2018.
5. F. Liu, **Y. Lin**, A. J. Walsh, Y. Yu, and L. P. Barry, "Doubly differential star-16-QAM for fast wavelength switching coherent optical packet transceiver," Optics Express, vol. 26, no. 7, pp. 8201-8212, 2018.
6. **Y. Lin**, A. P. Anthur, S. P. Ó Dúill, V. Panapakkam, Q. Gaimard, A. Ramdane and L. P. Barry, "Quantum Dash Passively Mode-Locked Lasers for Coherent Wavelength Conversion System", IEEE Photonics Technology Letters, vol. 30, no. 10, pp. 947-950, May 2018.
7. F. Liu, **Y. Lin**, Y. Yu, and L. P. Barry, " Parallelized Kalman Filters for Mitigation of the Excess Phase Noise of Fast Tunable Lasers in Coherent Optical Communication Systems," IEEE Photonics Journal, vol.10, no.1, pp. 1–11, 2018.

8. **Y. Lin**, A. P. Anthur, S. P. Ó Dúill, Y. Yu and L. P. Barry, "Fast reconfigurable SOA-based wavelength conversion of advanced modulation format data," Applied sciences, vol.7, no.10, Sep 2017.
9. F. Liu , **Y. Lin**, Y. Liu, A. P. Anthur , Y. Yu, and L. P. Barry, " Investigation into the phase noise of modulated grating Y-branch lasers," IEEE Journal of Selected Topics in Quantum Electronics, vol. 23, no. 6, Nov./Dec. 2017.

Conference papers

1. **Y. Lin**, E. Giacoumidis, S. O'Duill, A. P. Anthur, and L. P. Barry, "Reduction of nonlinear distortion in SOA-based wavelength conversion system by post-blind-compensation based on machine learning clustering," in Optical Fiber Communication Conference (OFC) 2019, paper Th2A.35.
2. C. Browning, A. Delmade, **Y. Lin**, D. H. Geuzebroek, and L. P. Barry, "Optical Heterodyne Millimeter-Wave Analog Radio-over-Fiber with Photonic Integrated Tunable Lasers," in Optical Fiber Communication Conference (OFC) 2019, paper W1I.4.
3. **Y. Lin**, C. Browning, R. B. Timens, D. H. Geuzebroek, C. G. H. Roeloffzen, D. Geskus, R. M. Oldenbeuving, R. G. Heideman, Y. Fan, K. J. Boller, J. Zhao, and L. P. Barry, "Narrow linewidth hybrid InP-TriPleX photonic integrated tunable laser based on silicon nitride micro-ring resonators," in Optical Fiber Communication Conference (OFC) 2018, paper Th2A.14.
4. C. Browning, M. Ruffini, **Y. Lin**, R. B. Timens, D. H. Geuzebroek, C. G. H. Roeloffzen, D. Geskus, R. M. Oldenbeuving, R. G. Heideman, Y. Fan, K. J. Boller, and L. P. Barry, "Optically switched 56 GBd PAM-4 using a hybrid InP-TriPleX integrated tunable laser based on silicon nitride micro-ring resonators," in Conference on Lasers and Electro-Optics, (CLEO) 2018, paper SW4C.5.

5. F. Liu, **Y. Lin**, A. J. Walsh, Y. Yu, and L. P. Barry, "Doubly Differential Two-level 8PSK for Enabling Optical Packet Switching in Coherent Systems," in Optical Fiber Communication Conference (OFC) 2018, paper W2A.35.
6. A. P. Anthur, S. O'Duill, **Y. Lin**, D. Venkitesh, and L. P. Barry, "Polarization dependent loss due to four-wave mixing," in European Conference on Lasers and Electro-Optics and European Quantum Electronics Conference 2017, paper CI_2_6.
7. **Y. Lin**, A. P. Anthur, F. Liu, S. O'Duill, Y. Yu, and L. P. Barry, "Fast Reconfigurable SOA-Based Wavelength Conversion of Pol-Mux QPSK Data Employing Switching Tuneable Pump Lasers," in European Conference on Lasers and Electro-Optics and European Quantum Electronics Conference 2017, paper CD_P_36.
8. F. Liu, **Y. Lin**, L. P. Barry, and Y. Yu, "Kalman Filter for Carrier Phase Recovery in Coherent Transmission Systems Employing Fast Tunable Lasers," in Asia Communications and Photonics Conference (ACP) 2017, paper Su3B.2.
9. **Y. Lin**, A. P. Anthur, S. O'Duill, S. T. Naimi, Y. Yu, and L. P. Barry, "Fast reconfigurable SOA-based all-optical wavelength conversion of QPSK data employing switching tunable pump lasers," in Optical Fiber Communication Conference (OFC) 2017, paper Th2A.46.
10. **Y. Lin**, S. T. Naimi, S. O'Duill, and L. P. Barry, "Novel Implementation of SOA-Based All-Optical Wavelength Conversion of DQPSK Signals Using Fast Switching Tunable Lasers," in Asia Communications and Photonics Conference (ACP) 2016, paper AF3H.2.